Use Authorization

In presenting this dissertation in partial fulfillment of the requirements for an advanced degree at Idaho State University, I agree that the Library shall make it freely available for inspection. I further state that permission to download and/or print my dissertation for scholarly purposes may be granted by the Dean of the Graduate School, Dean of my academic division, or by the University Librarian. It is understood that any copying or publication of this dissertation for financial gain shall not be allowed without my written permission.

Signature ________________________________

Date ____________________________________

Identification of Muscle Motor Point Location Based on Dempster Shafer Theory

By

Madhavi Anugolu

A Dissertation submitted in partial fulfillment of the Requirements for the degree of

Doctor of Philosophy

In

Engineering and Applied Science

IDAHO STATE UNIVERSITY

Fall 2014

To the Graduate Faculty:

The members of the committee appointed to examine the dissertation of MADHAVI ANUGOLU find it satisfactory and recommend that it be accepted.

Dr. Marco P. Schoen, Advisor

Dr. Alba Perez, Committee Member

Dr. Alex Urfer, Committee Member

Dr. Craig Rieger, Committee Member

Dr. Jim Creelman, GFR

I dedicate this dissertation to

My Parents A.Y. Prasad and A. Indira devi

for their love and support

ACKNOWLEDGEMENT

This dissertation work represents my four years of research experience that I had here at ISU, Measurement and Control Engineering Research Center (MCERC). I utilized this opportunity and gained a lot of experience in various fields.

I would like to extend my deepest gratitude to my advisor, professor, **Dr. Marco P**. **Schoen**, an invaluable mentor. He was and remains my best role model as a person, mentor and as a professor. Without his continuous help, motivation and support this dissertation would not have been possible.

I would also like to thank my other committee members **Dr. Alba Perez,** for serving as my committee member and giving her valuable suggestions. **Dr. Craig Rieger,** for his great support and his inspiring words. **Dr. Alex Urfer,** who was always willing to help, offered his advices and insight throughout my work and last but not least **Dr. Jim Creelman** for his help with the experiments and serving as my GFR.

A special thanks to **Chandu** (Dr. Potluri), for inspiring me to opt for a PhD. I am very grateful and blessed to know him. I am indebted to him for supporting me personally and academically in every possible way for the completion of my PhD.

Finally, and importantly, I thank my entire family (Parents, sister, brother, uncles and their families) for supporting me throughout all my studies at the University. Without their financial help, unconditional support and unlimited patience this research would not have been possible.

Above all I would like to thank almighty god for giving me the strength, knowledge and health and resolve to be here today.

Table of Contents

List of Figures

List of Tables

Abstract

The spatial locations of sEMG sensors are fixed due to the prosthetic socket contact fittings. However, the daily use of upper extremity prosthetics causes relative motion between the skin and the prosthetic sockets. These motions result in a degeneration of functionality over the time, due to a mismatch of motor point locations and sEMG sensor placement. This work presents a novel approach to automatically track motor point locations using an array sEMG sensor. Currently, there exists no theory that defines how to automatically locate motor points locations from using only surface EMG electrodes. This work proposes a novel technique for identifying motor point locations based on the Dempster Shafer Theory (DST) of evidence. The concept behind the DST is given by the combination of evidences obtained from different sources. Using these evidences, the DST models the conflict between the obtained information. The DST approach requires information extracted from the given data. For this work, the sources of evidences are chosen from the Kullback Information Criterion (KIC) and a Fuzzy inference system. The KIC is obtained from identifying the dynamical relationship between the sEMG signals and its corresponding finger forces of the prosthetic device. The fuzzy logic inference system also uses the sEMG signal and corresponding force signals as input output, and the membership functions are created from the sEMG entropy, relative error and the correlation between the sEMG and force signals. The proposed technique is applied on the data obtained from set of test subjects. In particular, the sEMG signals and its corresponding skeletal muscle force signals from the Flexor Digitorum Superficialis are acquired. The acquired sEMG signals are rectified and filtered using a Discrete Wavelet Transforms (DWT) with a Daubechies 44. For the

system identification, an Output Error (OE) model structure is assumed to obtain the dynamic relation between the sEMG signal and finger force signal. The results based on statistical data for 10 subjects show the potential of the proposed theory and approach for affectively identifying the motor point locations using an array sEMG sensor

Chapter 1: Introduction

1.1 Problem Statement

According to the information provided by the National Center for Health Statistics, there will be 50,000 new amputations every year in the USA. Some of the reasons are cardiovascular diseases, diabetes mellitus, trauma, tumor etc., [1].The recent wars in Afghanistan and Iraq substantially increased the number of amputees; “at least 251,102 people have been killed and 532, 715 people have been seriously wounded,” [2]. About 57% of them are trans-radial amputees, [2-5]. About 80% of amputees use prosthetic devices [6], around 30-50 % of amputees are using myoelectric controlled devices [7] and 30-50% of disabled people do not use prosthetic hands regularly for many reasons [1]. The statistical breakdown of causes of upper extremity amputations is seen in Figure 1.1[8]

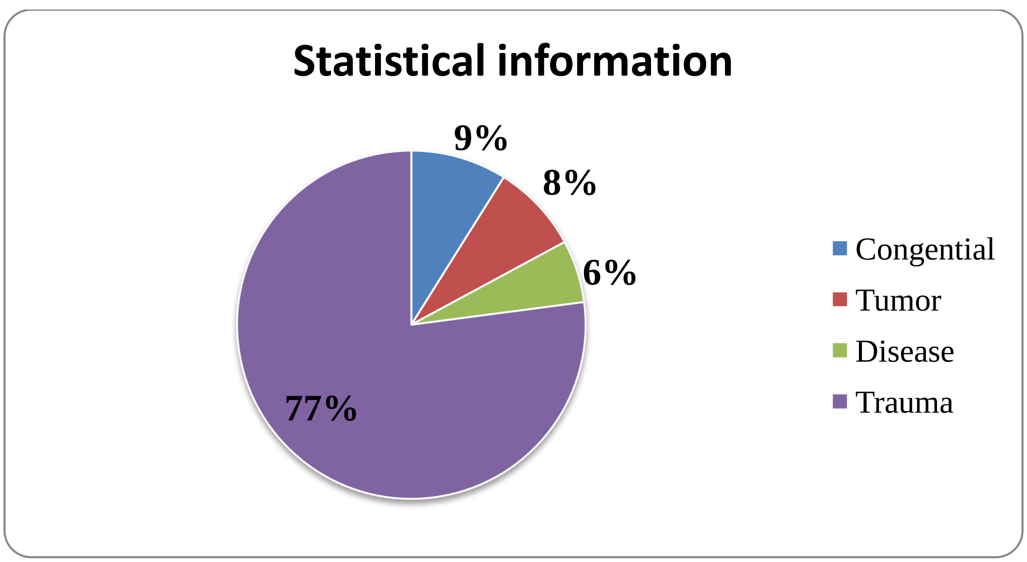

Figure 1.1: Percentages of upper extremity amputations based on etiology.

The general definition of an amputation is the removal of the body extremity. It can be classified into two categories: (a) Lower extremity amputation and (b) Upper extremity body amputation. For this work, we focus on the upper extremity amputation. The amputation can be differentiated depending upon the amputation location. The Table1.1 provides the typical forms of upper limb amputation.

Table 1.1: Types of upper extremity amputation

No.	**Type of Amputation**	**Description**	**Pictorial Information[9]**
1	Partial hand amputation	This amputation is removal of the fingers	
2	Metacarpal amputation	This is the amputation of the whole hand with the wrist in contact	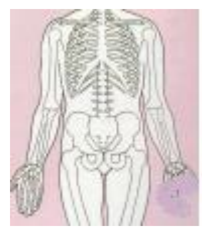
3	Wrist disarticulation	This amputation is the removal of the hand at the wrist joint	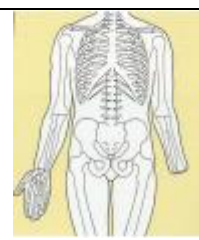

4	Below elbow amputation (transradial)	This amputation is the removal of the hand below the elbow joint	
5	Elbow disarticulation	This amputation is the removal of the forearm at the elbow joint	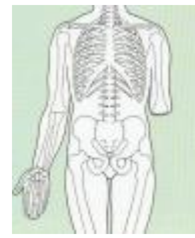
6	Above elbow amputation (transhumeral)	This amputation is the removal of the arm above the elbow joint	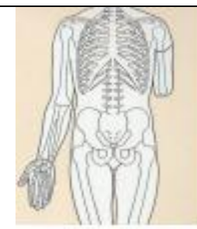
7	Shoulder disarticulation	This amputation is the removal of the whole hand	

Besides the type of amputation and its etiology, the loss of limb psychologically affects the amputee, which may lead to low self-esteem and social isolation. In addition, phantom limb pain and sensation increases the struggle when trying to perform daily activities. To overcome these factors, an appropriate fitting and functioning prosthetic device can help the amputee regain as much function as possible. Because upper extremity amputations are increasing due to numerous causes, the need has spurred research and development toward the development a prosthetic hand that closely mimics the functions of the human hand. However, it is a challenging task to design a prosthetic device which can mimic normal limb function because of the complexity associated with the human hand and its multi-faceted dynamics during function involving force, activation, fatigue and its nonlinear EMG activation and dynamics.

The National Science Foundation started the research in the field of prostheses after World War II[10]. Since then it has been an ongoing research field with many innovations.

Upper limb prosthetics devices can be either passive or active. The passive devices are meant for only cosmetic purpose. The active devices can be mainly classified into two types:

(a) Body-Powered Prosthetics

(b) Electric-Powered Prosthetics

Table 1.2 provides information about the above mentioned prosthetics types

Table 1.2: Comparison between body-powered and electric-powered prosthetics

Features	**Body-Powered Prosthetics**	**Electric-Powered Prosthetics**
Cost	Relatively low	High
Weight	Heavier	Light
Power	Mechanical appearance	Battery powered
Ease of use	Difficult	Easy

The major development in case of electrical powered prosthetics it that they can be controlled using feedback from myoelectric, pressure, or strain gauge signals, or the combination of any of these [11]. In this work, the focus is on myoelectric prosthetic devices and the related research. A myoelectric prosthetic device is an externally powered artificial limb which uses the excitation of existing muscle tissue in the residuum for the control. The myoelectric prosthesis serves both the passive (cosmetic) and active (functional) purposes. The added advantage of the myoelectric prosthesis is that it can be custom made according to the user requirements that fits to the existing residual limb. With the advancements in technology, many commercial and research, based myoelectric prosthetic devices have evolved in recent years. Some examples are Otto bock, iLimb from touch bionics, Utah arm form motion control and Bebionic V2 from RSL Stepper and the recent DEKA from the DARPA [12]. All the available commercial devices have predefined tasks. Even though there are numerous prosthetics available, there is no device at an affordable cost with sensory or vibrotactile feedback [13]. A detailed review of the existing research done in the field of sensory feedback is provided in Chapter 5.

Myoelectric technology uses residuum socket electrodes to capture signals from the muscle contacts on the skin, use advanced signal processing techniques and employ the processed signals to activate the prosthetic device. The most commonly available prosthetics are based on the electromyogaphic signals. The Electromyography (EMG) is measuring the electrical potential of the muscle groups when activated electrically or neurologically.

The EMG can be used either for clinical or kinesiological applications. The most commonly widespread techniques to capture the EMG signals are needle electrodes and surface electrodes. In general, for clinical research, the EMG signals will be captured by using needle electrodes, which is a painful invasive technique [14]. The EMG signals obtained from the needle electrodes have proven to be of much diagnostic value [15-17]. The one main drawback of the former technique is that its invasiveness in the approach and it also requires a trained professional. This motivated the researchers in the field of EMG to develop an alternative methodology based on non-invasive technique which can provide the information of the underlying muscles. The surface Electromyography (sEMG) signals are made up of the motor unit action potentials (MUAP's) of different muscle fibers and varying sizes. The factors that affect the MUAP are the type of the electrodes, filtering properties of the electrodes, etc. [18]. The MUAP occurrence frequency depends on the muscle contraction levels [19]. The parameters that characterize the motor unit are motor unit conduction velocity (MUCV), motor unit size and depth.

1.2 Purpose of the Study

The anatomical characteristics of the muscle can be studied from the detailed information of the motor unit action potential [20]. In case of sEMG based prosthetics, data acquisition and analytics plays an important role to characterizing the anatomy. Some of the properties and problems of recorded signals are addressed in [21].They are:

a.) The amplitude of the sEMG signal varies depending on the size of the muscle that is measured and its position relative to the electrode.

b.) Due to muscle fatigue, a subjective change in the perception of the force produced during a finger action, or due to external influences related to electromagnetic pollution, and amplitude changes.

c.) The most challenging property of surface based EMG signal measurement with respect to a robust classification is that it changes with arm posture. This is because the underlying muscles, especially towards the wrist, change their position relative to the electrodes on the skin when the hand is rotated.

To date, various investigations have focused on different methods related to the challenges of EMG capturing, filtering and adapting these features for the use of operating a prosthetic hand.

1.3 Motivation

Previous research and studies have shown that most of the applications that use surface Electromyography signals are implemented by computers. So, data acquisition and quality of the acquired data plays a major role. In case of invasive methods, a concentric needle will be inserted through the skin surface into the superficial layers of the muscle. Besides of the advantages of needle electrodes to acquire a good data set, there are some disadvantages as listed in Table 1.3.

Table 1.3: Advantage and disadvantages of needle and surface EMG electrodes

Electrode type	Advantages	Disadvantages
Needle Electrodes	• Precise information • Able to record single muscle group activity • Deeper muscle can be accessible	• Requires certified personnel to acquire the data • Detection area may not be the representation of the

		entire muscle
sEMG	• Easy to apply • Doesn't require any certification • Less discomfort	• Can only be applicable for superficial muscles • Cross-talk issues

The sEMG data is acquired by placing the sensors on the surface of the skin. The sEMG data passes through several tissue layers before reaching the skin surface. The raw signals will be contaminated with signals from different muscle groups, which lead to cross talk. The sEMG sensor placed right above the motor point collects the least amount of the interference and hence can lead to better information about the particular muscle group.

A motor unit is made up of the motor neuron and all the muscle fibers driven by it. The motor point is the entry point of the main nerve that supplies that muscle. In order to identify the motor point location associated with the finger movement, a specialized instrument called RICHMAR HV 1000 (Details are explained in Chapter 3) was used. It uses a wet probe with variable voltage level for stimulation. Some subjects are reluctant to go through the process. Hence, one goal of this work is to investigate ways to identify the motor point without giving any discomfort to the test subjects. The approach proposed in this work of identifying the motor point is presented in the Hypothesis section.

Over the past few decades, different approaches were proposed to identify the motor point form the surface Electrography signals. The research done so far is presented here.

In 2003, Chauvet E, et al., [22] proposed an iterative algorithm, which is based on a fuzzy logic technique to automatically decompose electromyography signals into motor unit action potential trains. First, the proposed algorithm was tested using simulated EMG signal comprising of six different motor units and added external white noise. Later, it was tested on the EMG signals captured by a high spatial resolution sEMG device. Even though it failed to identify the same number of MUAP's as the experienced neurophysiologist, it can be considered as a good contribution in the field of non-invasive physiology. A study was conducted by Holobar A, et al., [23] to compare the resulted obtained by using high-density surface electromyography at isometric low-level force tasks and the Bipolar intramuscular EMG signals. The Convolution Kernel Compensation (CKC) technique was proposed and tested on the simulated EMG signals and compared them with intramuscular signal decomposition to validate the accuracy of the non-invasive recordings decomposition. The same authors extended their work to implement this approach in the real-time in 2013 [24]. All the aforementioned techniques and most of the research done in the identification of the motor unit is based on the EMG decomposition process [25-28]. The novelty in the present work is that it is based on the System Identification technique.

1.4 Research Hypotheses

The aim of the current study is to identify the motor point from the proposed novel approach based on Dempster-Shafer theory. The concept behind the DST is given by the combination of evidences obtained from different sources. Using these evidences, DST models the conflict between the obtained information. The DST approach requires that at least two evidences were extracted from the given data. For this work, the sources of evidences were chosen from the Kullback Information Criterion (KIC) and a Fuzzy inference system. The KIC was obtained from identifying the dynamical relationship between the sEMG signals and its corresponding finger forces of the prosthetic device. The fuzzy logic inference system also uses the sEMG signal and corresponding force signals as input output, and the membership are chosen from the sEMG entropy, relative error and the correlation between the sEMG and force signals. The theoretical concepts of the Dempster-Shafer Theory, KIC and Fuzzy logics were addressed in detail in Chapter 5. This concept can be generalized to any other data.

Chapter 2:

Physiological Anatomy

A human hand can be defined as the most distal part of the upper extremity. Human hands are used for both power and precision grips. The human hand consists of palm and five digits as shown in Figure 2.1. The connection between the hand and the forearm is the wrist. The posterior part of the hand is called the dorsum of the hand [29].

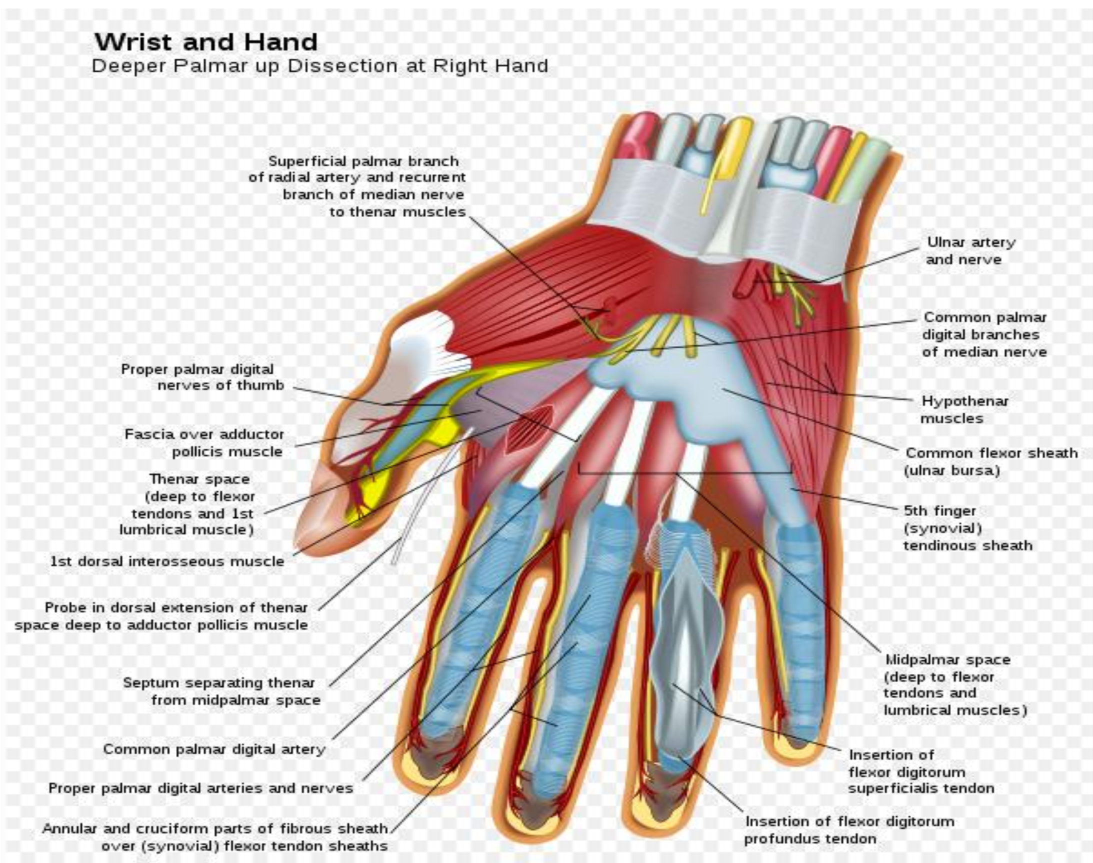

Figure 2.1: Deeper Palmar up Dissection at Right Hand [29].

2.1 Bony Skeleton of the Upper Limb

The upper limb shown in Figure 2.2 is composed of three major segments, namely the forearm, upper arm and the hand, which are connected by movable joints. The upper limb is appended to the trunk of the body by the pectoral girdle. This appendicular skeleton carries out normal manipulative movements.

2.1.1 Pectoral (Shoulder) Girdle

The pectoral girdle consists of clavicles anteriorly and scapulae posteriorly. The pectoral girdles with their associated muscles form the shoulders. The girdles are very light and are responsible for the greater degree of mobility exhibited by the upper limbs. The clavicles are the collar bones, which are slender and long double curved bones attached to the sternum medially and scapulae laterally. The Scapulae are the shoulder blades, which are thin and triangular flat bones. Scapulae articulate with the humerus of the arm forming the shoulder joint and the thorax[30].

2.1.2 Upper Limb

The skeleton of the upper limb is made of thirty separate bones arranged in three segments – upper arm, forearm and the hand shown in Figure 2.2. The upper arm includes humerus and the forearm is comprised of the radius and ulna. The hand consists of twenty seven bones, eight carpals in the wrist, five metacarpals in the palm and fourteen phalanges in five fingers[31]. Each finger has three phalanges with the exception of the thumb, which has only two.

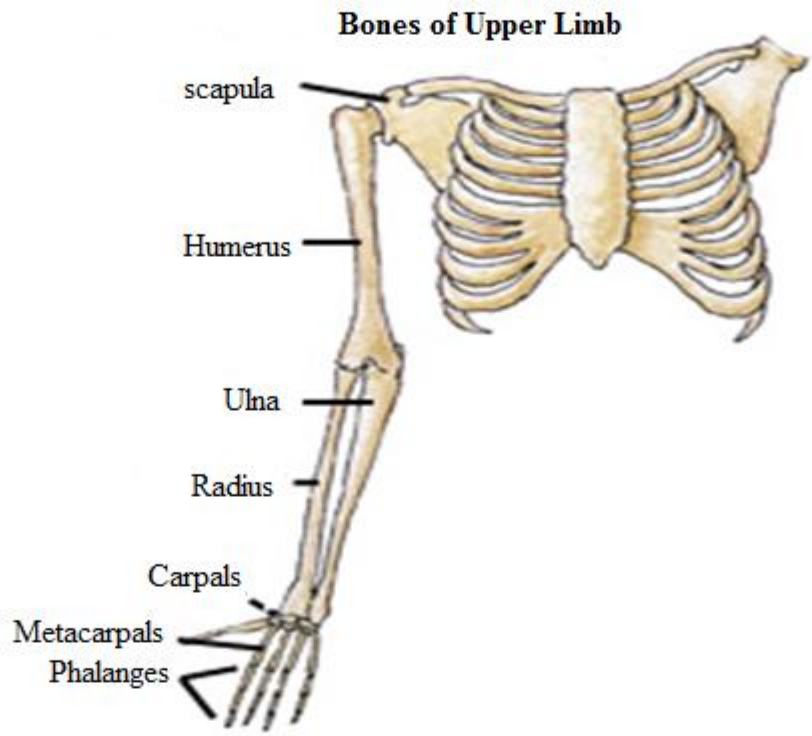

Figure 2.2: Bones of the upper limb[32].

The upper arm and the forearm bend at the elbow in the hinge joint (elbow joint). The elbow joint is not as flexible as the shoulder joint, but is more stable. The elbow joints permit movements like flexion, extension, supination and pronation. The radius and ulna articulate with the carpal bones in the hand. The carpal bones further articulate with the metacarpals and phalanges, thus resulting in many more joints in the hand. All these joints are responsible for the greater range of flexibility, stability and mobility of the upper limb. Wide and diverse functions are made possible with these many joints, like lifting up heavy weights and fine movements such as picking up small needles, writing and skilled movements etc.

2.2 Muscles of Upper Limbs and Their Functions

2.2.1 Muscles Crossing the Shoulder Joint: Arm Movements

Nine muscles cross the shoulder joint and insert on the humerus. The pectoralis major, latissimus dorsi, and the deltoid muscles aid in the arm movements. Supraspinatus, infraspinatus, teres minor and subscapularis muscles together referred to as rotator cuff muscles, help in the angular and rotational movements of the arm and also prevent dislocations of the humerus. Thus they act as synergists and fixators. The other two muscles are the teres major and the coraco-brachialis which help in adducting and flexing the arm [33].

The anterior compartment muscles of the shoulder joint, the pectoralis major, the coracobrachialis and the anterior fibers of the deltoid flex the arm and lift it anteriorly. The muscles posterior to the shoulder joint, latissimus dorsi and the posterior fibers of the deltoid and teres major, help in extension of the arm. Middle fibers of the deltoid muscle help in arm abduction. The main adductors of the arm include pectoralis major anteriorly and latissimus dorsi posteriorly. All these muscles contribute to the rotational and angular movements of the humerus.

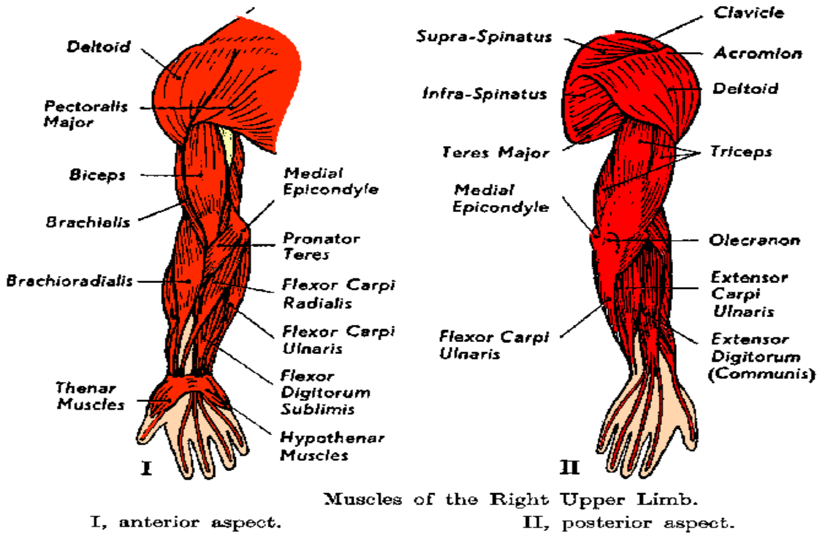

Figure 2.3: The Skeletal Muscular System and Muscles of the Upper Extremities [33].

2.2.2Muscles Crossing the Elbow Joint: Flexion and Extension of the Forearm

The arm muscles cross the elbow joint and insert into the radius and ulna. As the elbow joint is a hinge joint, all the movements are confined to extension and flexion. The posterior group of muscles, triceps brachii and the anconeus, help in extension of the forearm. The anterior arm muscles, brachialis, biceps brachii and brachioradialis help in flexion of the forearm [33].

2.2.3 Muscles of the Forearm: Movements of the Wrist, Hands and Fingers

The forearm muscles are categorized into two groups, those that move the wrist and those that cause the movements of the fingers and thumb. The forearm muscles arise from the humerus in the arm and cross the elbow and the wrist joints. Therefore, the actions are mainly confined to the movements of flexion and extension of the fingers and abducting and adducting the wrist joint.

Like the arm muscles, the forearm muscles are divided into anterior and posterior groups and perform the same functions. The anterior groups of muscles act as flexors, except for the pronator teres and the pronator quadratus which pronate the forearm. The posterior group of muscles acts as extensors, except the supinator muscle along the biceps brachii which supinates the forearm. These muscles are further categorized into superficial and deep muscle layers. All the forearm muscles are fleshy at the origin and end as slender tendons at the wrist and the fingers, thus making the hand and wrist less bulky, enabling fine movements.

The anterior superficial group of muscles of the forearm includes the pronator teres, flexor carpi radialis, Palmaris longus, flexor carpi ulnaris and the flexor digitorumsuperficialis. The deep anterior group includes flexor pollicislongus, flexor digitorumprofundus and the pronator quadratus.

The posterior superficial group of muscles includes the brachioradialis, extensor carpi radialislongus, extensor carpi radialis brevis, extensor digitorum, and extensor carpi ulnaris. The deep posterior group includes supinator, abductor pollicislongus, extensor pollicis brevis and longus and extensor indicis[33].

2.2.4 Intrinsic Muscles of the Hand: Fine Movements of the Fingers

These muscles entirely lie in the palm and are not located on the dorsal side. They aid in moving the fingers. The powerful movements of the fingers are done by the fore-arm muscles whereas fine movements are taken care by these small muscles.

These muscles of the palm are divided into three groups, thenar muscles, hypothenar muscles and the muscles of the palm. The thenar muscles are the abductor pollicis brevis, flexor pollicis brevis, opponenspollicis and the abductor pollicis, which help in the movements of the thumb. The hypothenar muscles include abductor minimi, flexor minimi brevis and opponensdigitiminimi, which move the little finger. The thenar and the hypothenar muscles help in flexing, abducting and opposing the fingers. The midpalmar muscles are the lumbricals, palmar and dorsal interossei, which help in extending the fingers at the joints and also act as adductors and abductors [33].

2.3 Movements of the Upper Limb

Movements of the upper limbs include medial and lateral rotations, supination and pronation, abduction and adduction, flexion and extension, circumduction, opposition, and radial and ulnar deviations. Flexion, extension, abduction and adduction are the angular movements that increase or decrease the angle between the bones.

2.3.1 Flexion and Extension

Flexion is a movement of bending at the joint, to reduce the angle. Extension is a movement to straighten at a joint, or to increase the angle as shown in Figure 2.4(a). Flexion and extension are the main movements at the elbow joints, though they occur at all the shoulder, wrist and phalangeal joints.

2.3.2 Pronation and Supination

Pronation and Supination are the movements aided by the muscles acting on the forearm. Supination is to rotate the forearm to make the palm face forwards. Pronation is to rotate the forearm as to make the palm face backwards as shown in Figure 2.4.

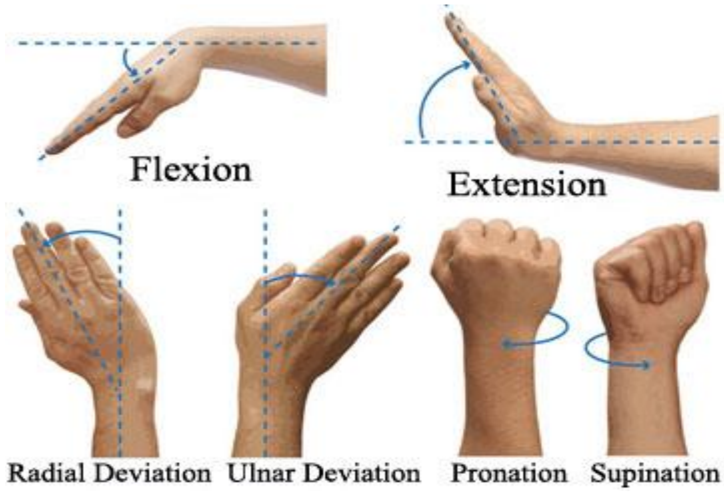

Figure 2.4: Flexion, Extension, Radial Deviation, Ulnar Deviation, pronation And Supination of the hand [34].

2.4. Nerve Supply of Upper Limbs

The nerve supply to the upper limbs include the sensory and the motor innervation. The nerves have both the sensory and motor functions responsible for sensations and movements correspondingly.

The motor nerves include five terminal nerves and many collateral nerves of the brachial plexus. The terminal nerves include musculocutaneous, axillary, radial, median and ulnar nerves. They innervate all the muscles of the upper limbs and are responsible for all the movements and primary actions of flexion, extension, medial and lateral rotations, supination, extension and abduction and adductions at all the joints, see Figure 2.5.

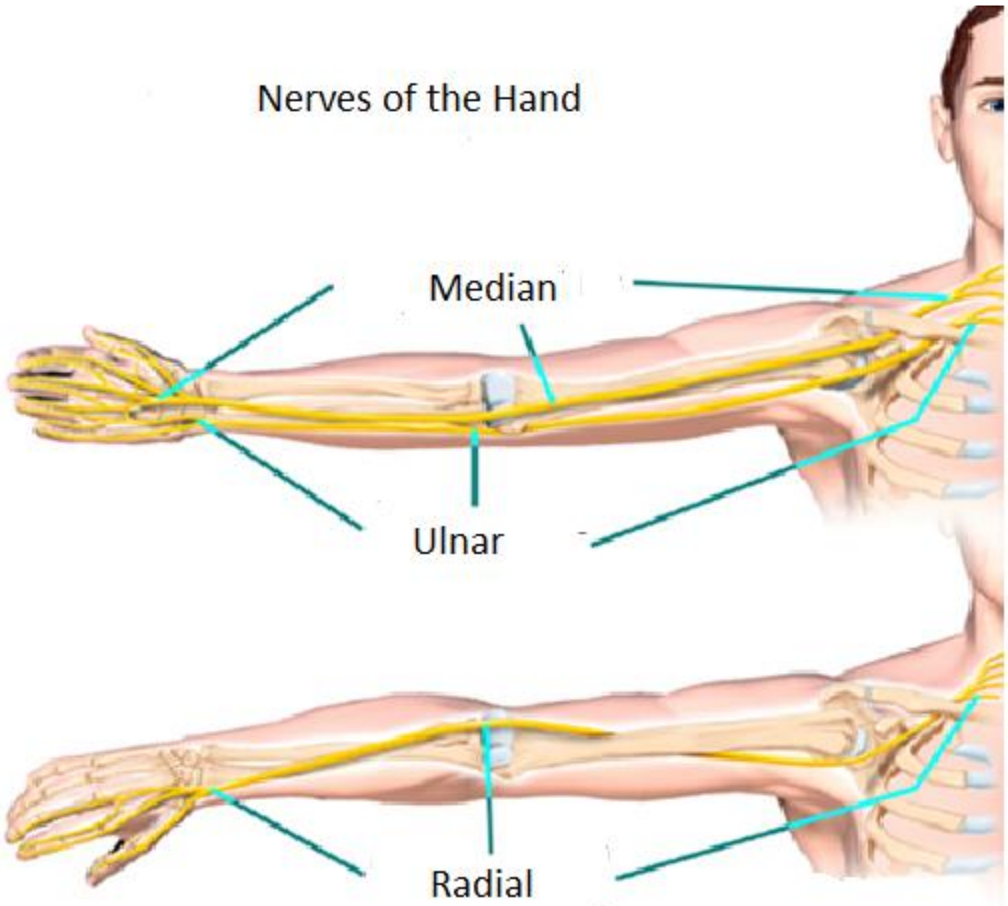

Figure 2.5: Nerves of the hand [35].

Chapter3: Experimental Design

This chapter gives an insight into the experimental design implemented for this work. In particular the acquisition of the sEMG signal and its corresponding force signals is addressed. This chapter is subdivided into two section i.e., equipment used and the experimental set-up.

3.1 EMG Equipment

The following block diagram represents the data acquisition procedure utilized in this work.

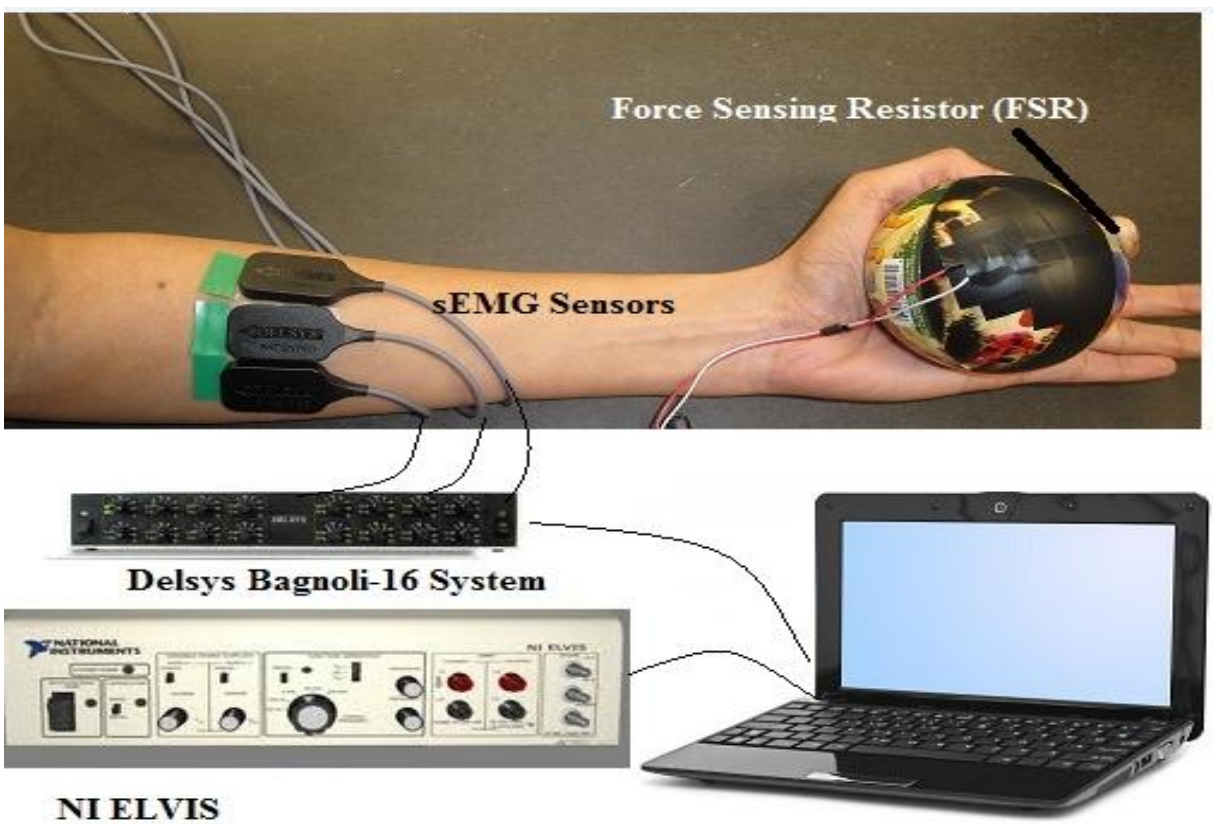

Figure 3.1 : Experimental design set-up

The following subsections present a brief description of the equipment utilized in this work.

3.1.1 Simulator (RICH-MAR HV 1000)

In order to identify appropriate EMG electrode attachment points, the subject's anterior forearms were cleaned with isopropyl alcohol swabs. A wet probe point stimulator was used at the forearm superficial musculature (flexor digitorum superficialis) and the dispersion pad on the left forearm was used to identify the specific motor point areas on the right forearm that stimulate the greatest full flexion activation of the ring finger (fourth digit).

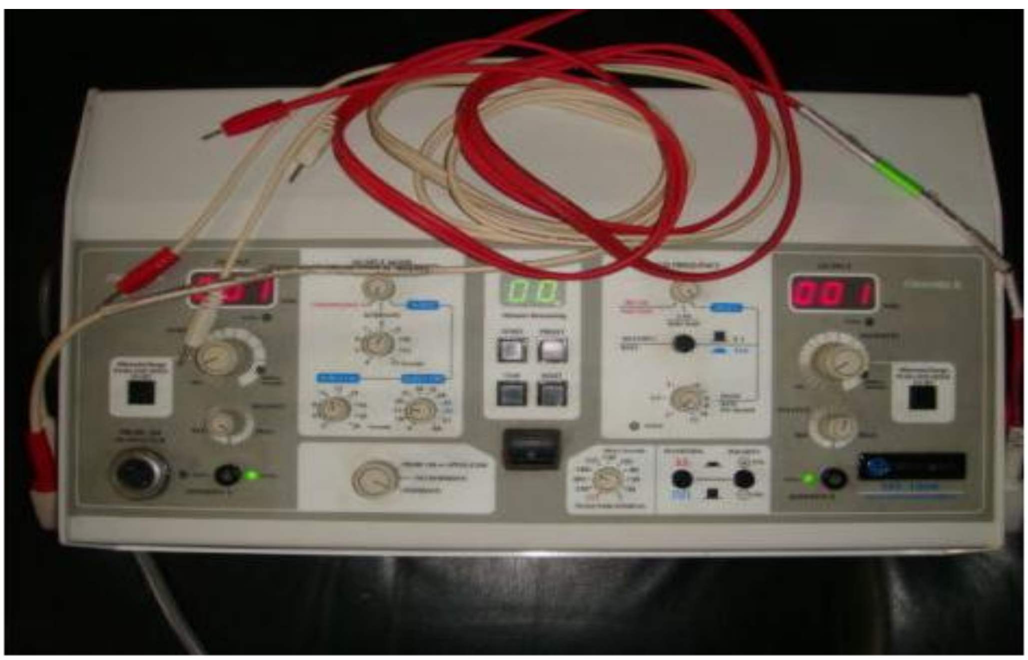

Figure 3.2: Simulator (Rich-Mar HV 1000).

The point simulator voltage was progressively increased and its probe was passed along the skin surface of the musculature until the largest motion of the finger was observed. Using this technique, three points were marked on the forearm. Figure 3.2 depicts the point simulator used [36].

3.1.2 SCB-68: I/O Connector Block for DAQ Devices

Shown in Figure 3.3 is the SCB-68 connector box. SCB -68 is an I/O connector box with 68-pin connectors. This box acts as an interface between the DAQ boards and the computer.

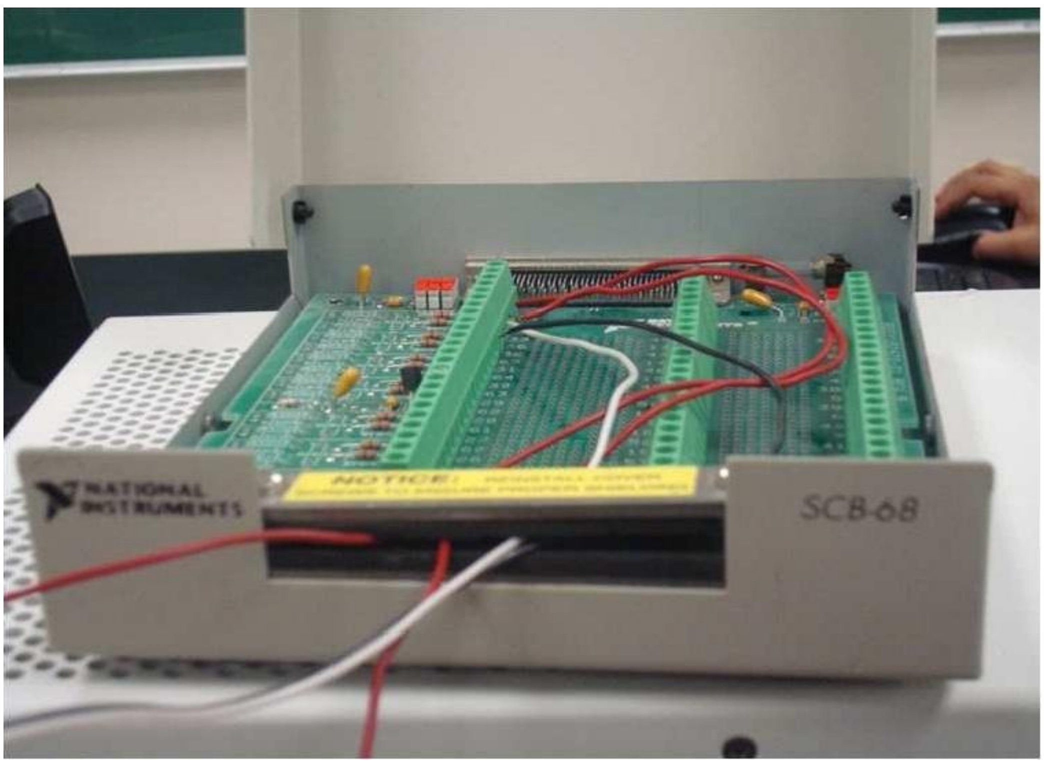

Figure 3.3: SCB-68 Connector box.

3.1.3 Data Acquisition (DAQ) Board

The DAQ board converts the analog signal into digital form, so the computer can process the EMG and force data. Two 6024E DAQ boards were used in this experimental setup, one for the force and the other for the EMG.

3.2 EMG Signal Sensing

Delsys has 4, 8 and 16 channel models. For this work, a 16 channel EMG systems was used. The gain of the system can be adjusted manually according to the requirements. Figure 3.4 shows the Bagnoli-16 EMG system.

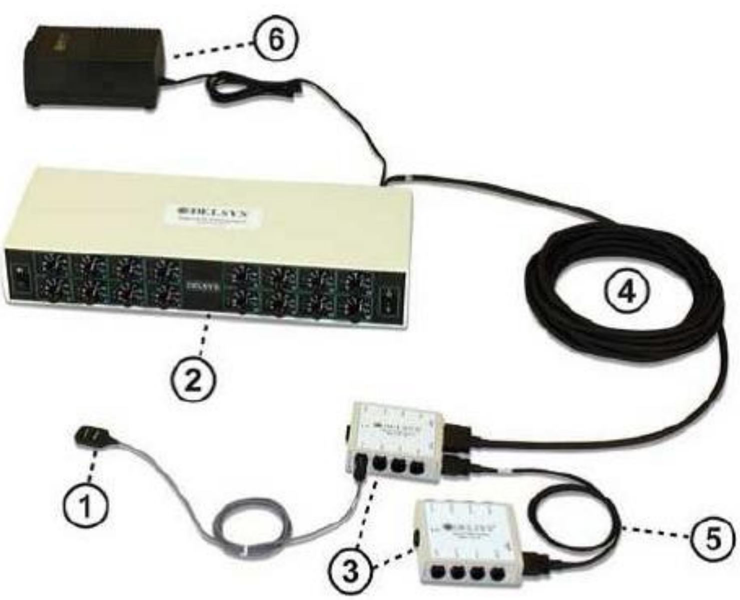

Figure 3.4: Bagnoli -16 EMG system [37].

In the above figure

(1) Differential surface electrodes

(2) Main amplifier unit

(3) Input modules

(4) Input cable

(5) Extension cable for input module

(6) Power supply

3.2.1 Main Amplifier Unit

Shown in Figure 3.5 is the Main Amplifier Unit (MAU). This unit conditions the detected signal and supplies the power to the sensor. The gain of the channels (16 channels) is variable depending upon the requirements; the gain can be adjusted to 100, 1000 or 10K. For the experiments in this work, the gain was set to 100. The filtering bandwidth of the MAU varies between 20Hz to 450 Hz.

Figure 3.5: Main Amplifier Unit [37].

3.2.2 DE-2.1 Single Differential Surface EMG Sensor

DE2.1 EMG sensors were used in this thesis work. These sensors can be placed directly on the skin using adhesive tapes. In addition to this, a reference electrode is placed on a neutral point i.e.; on the elbow. The EMG sensor measures the electric potential with respect to the reference electrode. The DE 2.1 EMG sensor is shown in Figure 3.6. It has two parallel silver bars (electrodes). It subtracts the EMG potential detected at these bars.

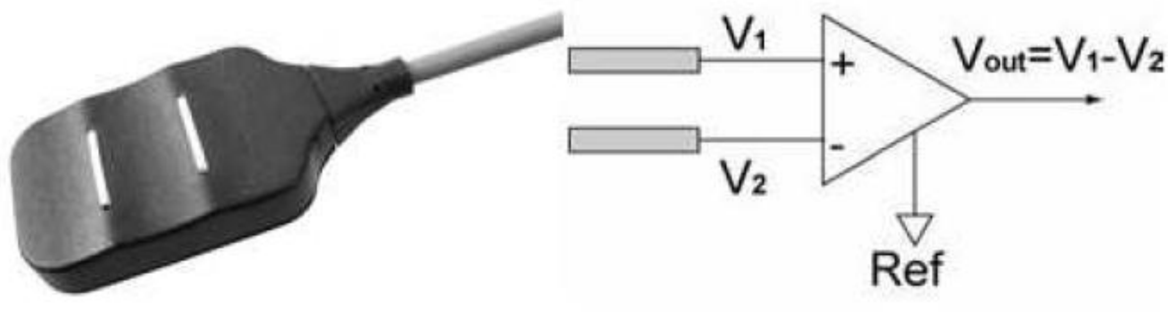

Figure 3.6: DE 2.1 single Differential Surface EMG sensor [37].

As shown in the above Figure 3.6, the sEMG (Vout) is the differential output between V1 and V2. The EMG sensors are designed in such a way that the most of the ambient electrical noise will be filtered out. The dimensions of these contact bars (electrodes) are 10 mm long, 1mm in thickness, spaced 10 mm apart. Figure 3.7 shows the geometry of the sensors.

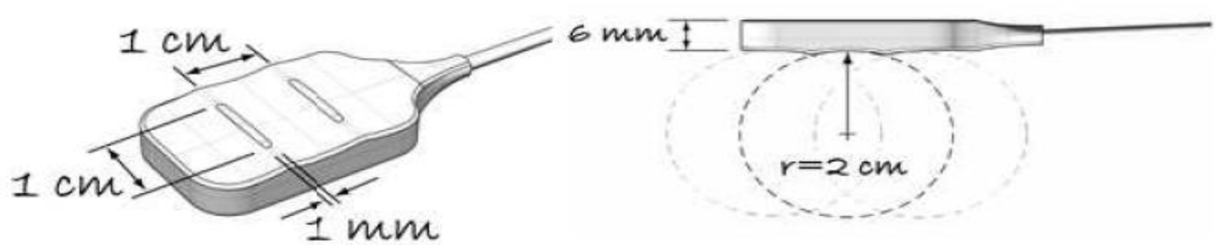

Figure 3.7: Geometry of the EMG sensor [37].

3.2.3 EMG Accessory Kit

An EMG accessory kit was supplied with the Bagnoli Delsys system. It consists of the following list of items:

- Adhesive Sensor Interfaces
- Reference Electrodes
- Reference Electrode Cable, seen in Figure 3.8.

Figure 3.8: EMG Accessory kit including adhesive tapes [37].

3.2.4 Input Modules

Shown in Figure 3.9 are the input modules. The Input module acts as an interface between the EMG sensors and the MAU. Hence they transmit the signals from sensors to the MAU and at the same time they supply power to the sensors.

Figure 3.9: Input Modules [37].

3.2.5 Input Cable

The input cable connects the MAU and the input module. The input cable transmits signals from the input module to the MAU and provides power to the EMG sensors.

3.2.6 Power Supply

The Medical Grade Power Supply, corresponding to IEC 60601-1 safety standards. It comes as a part of Bagnoli EMG systems package. The EMG power supply is suitable for 115 or 230 VAC, at 50 or 60 Hz.

3.3 Force Sensors

This section gives a brief description of the force sensors used in this work. These sensors are used to measure the force signal generated by the subject's finger motion.

There is a wide range of force sensors used for force measurement, depending on the user requirements. Two types of force sensors are used in this work.

- Circular force sensors.
- Rectangular force sensors.

3.3.1 Circular FSR

This circular force sensing resistors (FSR) is manufactured by Interlink Electronics and depicted in Figure 3.10. These sensors are made up of polymer thick film (PTF). They consist of four layers: (1) an electrically insulating plastic layer; (2) an active area; (3) a Plastic spacer; (4) a flexible substrate. To operate the FSR, a small amount of force is required to break the initial resistance. The output of the sensor depends on the surface area of the sensor where the force was applied.

Figure 3.10: Circular Force Resistive Sensor [39].

FSR, have durability and require less maintenance than a strain-gauge. They are used in control applications involving human touch and are optimized for the same. However a strain gauge has higher accuracy than a FSR, [40].

3.3.2 Rectangular Sensor

Figure 3.11 shows the rectangular force sensor used in this work. This is the only FSR from Interline Electronics that can be cut to a desired length. These FSR's are more suitable for qualitative than precision measurement [40].

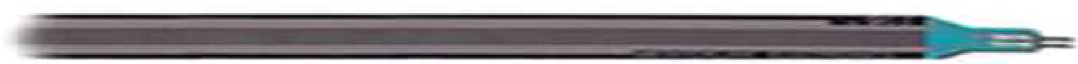

Figure 3.11: Rectangular force sensor [40].

3.3.3 Power Supply

Shown in the Figure 3.13 is the triple-Output DC power supply. This power supply used to perform the experiments. This unit is from Agilent and the model number is E3631A. It offers three independent outputs0-6V/ 5A and 0- ±25V/1A. To minimize the inference the 6 V output is electrically isolated from the ±25 V.

Figure 3.12: DC triple output power supply

3.4 Experimental set-up

The experimental set-up were implemented in this work was carried using DelsysBagnoli 16 System depicted in following Figure 3.13.

Using a wet probe point muscle stimulator (Rich-Mar Corporation, model number HV 1100) the motor points of the Flexor Digitorum Superficialis (FDS) were identified through the observed muscle action of the predominant movement of flexion of the first digit. The Flexor Digitorum Profundus (FDP) is also involved in the action of finger flexion, but it lies deeper than the FDS and hence the sEMG capturing includes both muscles in the finger motion. During a single episode of data collection, for each subject, the subject was asked to move only the index finger while fingers III-V were kept stationary. The primary sEMG sensor was placed on the motor point and the other two sensors placed adjacent to the motor point on the skin surface of test subject's dominant side at a distance of 1.5 cm on the either side of the sensor on the motor point

Using a Delsys®, Bagnoli-16 channel EMG, DS-160, S/N-1116 system, the EMG data from the skin surface is captured. This acquisition system has an internal amplification gain of 1000 and a bandwidth of 20 - 450 Hz and line voltage isolation of 6000 VDC, 4200 VAC (RMS). Pronged DE 2.1 differential surface electrodes and a reference electrode which is placed on the subject's elbow are used to acquire the sEMG signals, [41]**.** A model 402 single zone Force Sensitive Resistor (FSR) optimized for human touch control of electronic devices is used to acquire the skeletal muscle force. It has a 46.7 mm^2 active diameter area with a force sensitivity range of 0.1-100 N, force repeatability of ±6% and a continuous force resolution, [42].

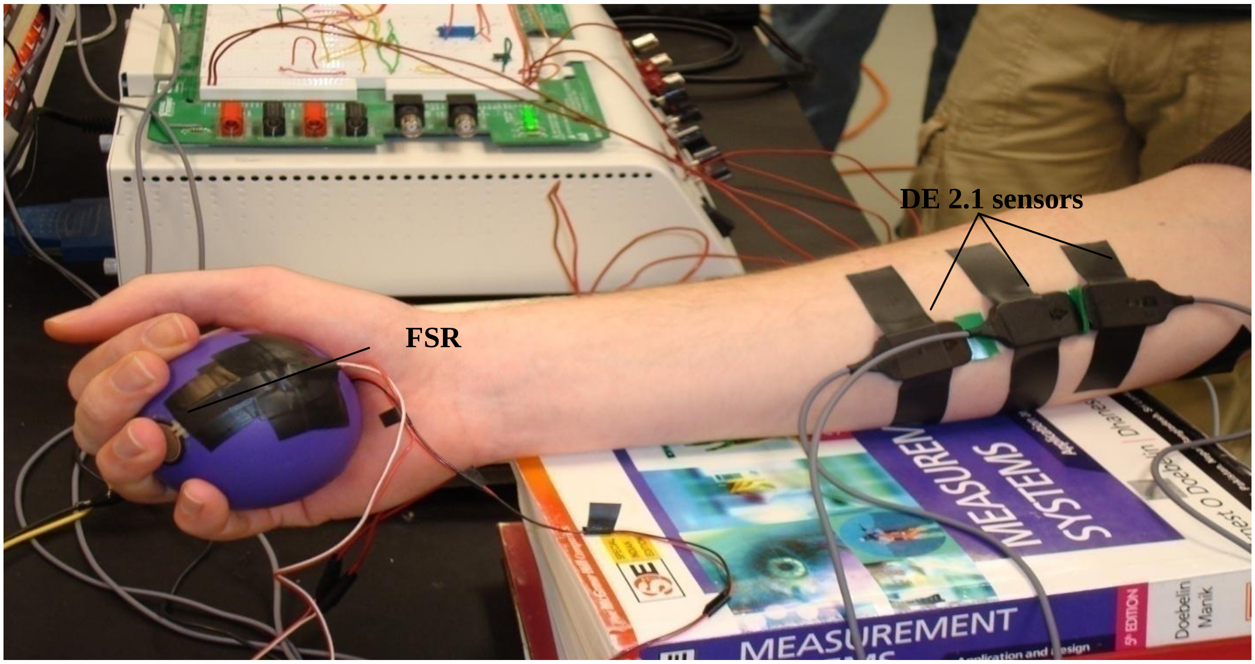

Figure 3.13: Experimental set-up using Delsys Bagnoli 16

During the experiment each subject is made to perform a random grasping action (index finger flexion and extension) for 9-10 seconds using a stress ball for added resistance. While doing so, the random grasping action finger force is applied on the FSR, which is mounted on the stress ball. Both the sEMG and the corresponding skeletal muscle force are synchronized and acquired using NI LabVIEW™ at a sampling rate of 2000 Hz. Since the content of the sEMG signal is in the range of 20-450 Hz, the sampling rate is adequately above the Nyquist frequency (to ensure ??).

Chapter 4: Signal Processing

Similar to the data acquisition process, signal processing plays also a major role in sEMG based prosthetic devices to remove noise from the desired signal. This chapter deals with the sEMG and its corresponding force signal processing techniques implemented in this work. The sEMG signal is the electrical potential generated by the muscle contraction and ranges from 0-10 mV i.e., -5 to +5 mV [45]. It contains noise since the signal will travel through various tissue layers. The acquired data signal is composed of sEMG data contaminated with artifacts originated at the skin-electrode interface and noise signals from the external sources. In all the applications that utilizes sEMG, only the positive values are analyzed. To make better use of the signal and reduce the noise, the signals need to undergo the processing stage comprising of rectification and filtration. So, for sEMG data a full wave rectification is preferable.

A filter can be defined as a system used to remove the unwanted components at a certain frequency from the signal. The employment of filtration leads to signal restoration and signal separation.

Signal Restoration: By using a particularly designed filter, the disturbed signal (due to noise or interference) can be restored. A good example for this is a speech signal.

Signal Separation: Usually, most of the measured signals contain external noise components. By using filters, the unwanted signal component can be separated from the desired portion of the signal. An example for this is an EMG signal which has some external noise from the power supply and equipment. By using the proper filter, those external noise signals can be reduced or eliminated.

The sEMG data can be used in various fields such as clinical applications, biomedical applications and human computer interaction. The raw sEMG signal will be filtered in different ways depending upon the application requirements. For example, in the diagnosis of the neuromuscular disorders, the motor unit action potentials (MUAP) firing rate provides a required information. Hence, the sEMG analysis will be achieved in those required terms [46]. For the past few decades, extensive research was conducted on the EMG filtration techniques to attain the accurate data based on the application requirements. With the advancements of technology in signal processing, there has been significant research done in sEMG analysis. Since this work is related to the prosthetic hand device, some of the analysis techniques that were implemented in this particular field are presented here.

4.1 Filtering

In general, band pass filters were implements on the raw sEMG signal to remove the low and high frequencies from the acquired signal. According to ISEK standards, a high-pass filter with a cutoff frequency 5 Hz and low-pass filter with a cutoff frequency of 500 Hz will remove the noise and attenuates the artifacts from the signal. High-pass filter reduces the artifacts, skin-electrode inference and the low-pass filter eliminates the noise from the external sources. In [47], it was stated that while using these filters, they also reduces the required information from the sEMG signal.

One of the main goals of our research work is to explore different filtering techniques. So, in my Master's thesis work, four different filtering techniques were implemented and compared. They are linear filters such as Butterworth, Chebyshev Type-II and non-linear filters such as Bayesian Exponential and Bayesian Half-Gaussian proposed by T.D. Sanger [48]. From the comparison results provides in [48] it was concluded that Bayesian Half-Gaussian filter is performing better compared to the other three filters. The Bayesian filters have the capability of recording the rapid changes in the signal along with the signal smoothening [49].But theses filters were compared using the sEMG data obtained from the single male test subject. To justify the results, this work was later extended and compared for 18 test subjects[50]. It also validates that out of the four filters, the Bayesian Half-Gaussian filter is giving a better performance compared to the other filters [50]. The Bayesian half-Gaussian filter is represented by the equation:

$$p(emg \mid x) = 2 \times \exp(-emg^2 \,/\, 2x^2) \,/\, (2\pi x^2)^{1/2}, \tag{4.1}$$

Where x - latent driving signal

$p(emg \mid x)$ - Conditional probability function.

Also, under close observation of EMG signals, the density function can be better approximated using a Laplacian density, which is given for a rectified EMG signal as follows:

$$p(emg \mid x) = \exp(-emg \,/\, x) \,/\, x. \tag{4.2}$$

Suppose the rectified EMG signal is given by $emg(t)$ at a given time *t,* the function $P[emg(t) \mid x(t)]$specifies the likelihood of each possible value of $x(t)$. Bayes rule gives the posterior density as

$$P[x(t) \mid emg(t)] = P[emg(t) \mid x(t) \times P[x(t) \mid emg(t)] \tag{4.3}$$

where, $P[x(t)]$ is the probability density for $x(t)$ immediately before the measurement of $emg(t)$. In general, the prior $P[x(t)]$ will depend on the entire past history of the measurements. Estimation of $P[x(t)]$ can be performed using a recursive algorithm based on discrete time measurements.

Using Bayes' rule we can write,

$$P[x(t) \mid emg(t), emg(t-1), ...] = P[emg(t) \mid x(t)] P[x(t) \mid emg(t-1), emg(t-2)..] \tag{4.4}$$

The recursive algorithm derived in [51] is utilized for the filtration of the recorded EMG signal. The mathematical form of the derived probability density function is given by:

$$\begin{aligned} &P(x, t-1) \approx \alpha P(x-\varepsilon, t-1) + (1-2\alpha) P(x, t-1) + \\ &\alpha P(x+\varepsilon, t-1) + \beta + (1-\beta) P(x, t-1) \end{aligned} \tag{4.5}$$

The recursive algorithm has the same steps as in [48]. But in the case of [48], the values of α and β are chosen empirically. Using an elitism based Genetic Algorithm (GA) (This is explained in detail in chapter 5), one can increase the probability of choosing the optimum values of α and β with the cost function in GA being the percentage of the model fits that are returned by the system identification model between the surface EMG and the force data.

Besides the better performance of the Bayesian Half-Gaussian, one main limitation of Half-Gaussian filter is that the latency requires a large buffer size which is difficult to implement in real-time.

Later, from the detailed review of Wavelet Transforms (WT) provided in [51] and their advantages in the field of biomedical signals, motivated by this work to implement WT and observe the results by comparing them with the existing filters employed in this work previously. M.B.I Reza et al., [46] also highlighted that the wavelet transforms is one of the capable mathematical tool to analyze the non-stationary and multi-component signals like EMG.

4.1.1 Wavelet Transforms

Wavelet Transforms (WT) is the most commonly used and popular tool for time-frequency transformations. In 1999, Englehart et al., [52] introduced wavelet packet transform for preprocessing the EMG signal and compared them with the time-frequency method. The results were promising in terms of better performance. Wavelet Transforms can mainly be classified into two types: Continuous Wavelet Transforms (CWT) and Discrete Wavelet Transforms (DWT). One major issue involved with the CWT is redundancy. It over samples the signal and generates many coefficients. It will be computationally expensive to implement on the biomedical signals. Because of the redundancy issues associated with the CWT, in case of signals such as EMG DWT are chosen since it doesn't have that aforementioned issue. According to [53, 54] Daubechies (db2, db8 anddb6) wavelets and the Orthogonal Meyer wavelet are the most commonly used wavelets for the signals that are similar to the EMG. Based on that, in [55], also WT db6 along with the threshold method are used for denoising the EMG signals collected from the forearm muscle.

A comprehensive study of 324 mother wavelets for sEMG signals was conducted in [51]. The results indicated superior performance of the Db 44 wavelet method for processing biomedical related signals [51]. The proposed hypotheses in [51] is put to the test by processing the acquired sEMG signal using wavelets and utilizing the processed signal for modeling the underlying skeletal muscle force generated by individual fingers of the human hand. So, in this work, a WT along with a Db 44 mother wavelet at 8 levels of decomposition is used in order to filter the acquired sEMG data. The single level of Discrete Wavelet Transform (DWT) is given as

$$u_{fi}[n] = \left(u_{ufi} * g_i\right)[n] = \sum_{k=-\infty}^{\infty} u_{ufi}[k]\, g_i[n-k], \tag{4.6}$$

$$u_{fi_{low}}[n] = \sum_{k=-\infty}^{\infty} u_{ufi}[k]\, g_i[2n-k] \tag{4.7}$$

$$u_{fi_{high}}[n] = \sum_{k=-\infty}^{\infty} u_{ufi}[k]\, h_i[2n-k] \tag{4.8}$$

Where i - corresponding sensor,

u_{ufi} -unfiltered sEMG signal,

u_{fi} - Filtered sEMG signal,

g_i - Co-efficient of the low-pass filter,

h_i - Co-efficient of the high pass filter.

g_i and h_i are chosen based on the International Society of Electrophysiology and Kinesiology (ISEK) standards to eliminate any noise in the sEMG signal.

4.2 Data Modeling

After the filtration, the next step in the analysis process depends upon the objectives of the work. The main objective of this work is to identify the motor unit location using the proposed algorithms. The acquired sEMG and the corresponding muscle force signals are analyzed by assuming that there is a linear association between the sEMG and the muscle force signals. The sEMG-force relationship investigation was started in 1952 by Lippold [56] and it was reported that there is a linear relationship between these two signals. From then it's been an ongoing research and debate about the EMG-Force relationship. Some researchers [56-58] reported that it's a linear relationship and while others reported that it is a non-linear relationship [59-61].

In 1981, Pery and Becky [62], did extensive study and a review on the relationship between the processed sEMG and its corresponding skeletal muscle force signals. Based on that, an investigation was done by [63] to observe the sEMG-force relationship and its variability for different muscle groups. They made some interesting conclusions and the one which we want to consider here is that the sEMG-force relationship is mainly decided by the muscle under investigation.

In [64], it was proposed that force estimation based on sEMG measurements is one of the best substitutions to the commercially available force measuring sensors. Several different methodologies were proposed to address the sEMG based skeletal muscle force estimation. A method for force estimation was introduced by combining a motor unit twitch model with motor unit pulse trains obtained from the multi-channel surface electromyogram and artificial neural networks [65, 66]. This type of force estimation uses the sEMG signals obtained from the upper arm muscle and elbow joint angular position velocity to predict the relationship between the EMG and the generated force. The EMG-to-torque relationship was narrowed down to a linear least squares problem in which a study of a few estimator processors such as single/multiple-channel un-whitened/whitened/adaptively-whitened was used to classify the EMG-torque relationship [67]. It concludes that the joint torque estimation can be improved with higher fidelity EMG amplitude processing. Another interesting algorithm based on the instrumental variable principle was proposed to obtain the dynamic relationship between the electrical and mechanical activity of the muscle [68]. It states that the least-squares, generalized least-squares and maximum likelihood estimators failed because of the nature of the noise assumptions.

As mentioned previously, in this work we are assuming that the sEMG-Force relationship is linear. Any system can be analyzed and controlled by using a mathematical model of the particular system. This model can be generated by two means. One is by using, physical, chemical or biological phenomena. The other is from the obtained experimental data *"The process of constructing models from the experimental data is called system identification*" [69]. In 2004, J. T. Bingham and M. P. Schoen [70] proposed a method of estimating the finger joint angles from sEMG data.

In this work also, we used System Identification (SI) techniques to infer the mathematical models based on the measured sEMG and its corresponding force data. The roots of SI are from statistical methods such as maximum likelihood and least squares. The SI technique is highly recommended when the mathematical model cannot be predicted by the physical laws. In these kinds of scenario, black-box modeling is implemented to predict the model structure from the observed/measured data.

There are 2 types of models. They are

(1.) Parametric models.

(2.) Non-parametric models.

Models where all the parameters are in finite-dimensional parameter spaces are called parametric models whereas in non-parametric models consists of infinite number of parameters. Some of the parametric models are the General-linear model, the Auto Regression (AR) model, the Autoregressive with (ARX) model, the Auto regressive moving average (ARMAX) model, the Box-Jenkins model, the Output-Error model, the Transfer Function model, and the State-Space model.

In general, the linear difference equation for any given input and output of a system is represented by:

$$y(t)+a_1y(t-1)+...+a_ny(t-n)=b_1u(t-1)+...b_mu(t-m) \tag{4.9}$$

Rewriting the above equation

$$y(t)=\varphi(t)\theta. \tag{4.10}$$

Where $\varphi(t)=[-y(t-1)...-y(t-n)u(t-1)..u(t-m)]^T$ and

$\theta=[a_1,...,a_nb_1,...b_m]^T$

In this work, we are motivated to use SI technique in order to infer the relationship between sEMG and its corresponding force from the results provided in [70]. In this work, they utilized Output Error (OE) Model of SI method to build the mathematical model that correlated the myoelectric signal with its matching hand motion.

In this work, initially we started with the linear parametric models from the SI toolbox in the Matlab(R) were used, which were explained below.

4.2.1 Output-error model

Output-Error (OE) model structure describes the system dynamics separately. The equation for OE model is given below:

$$M_i\equiv\hat{Y}(t)=\frac{B(q)}{F(q)}u(t-nk)+e(t) \tag{4.11}$$

$$B(q)=b_1+b_2q^{-1}+...+b_{n_b}q^{-n_b+1} \tag{4.12}$$

$$F(q)=1+f_1q^{-1}+\dots f_{n_f}q^{-n_f} \tag{4.13}$$

Where $\hat{y}(t)$ - the output at time t

$u(t-n_k)$ - Input data(sEMG)

$e(t)$ - Error at time t

q - Back shift operator.

The block diagram representation of the output error model is given by

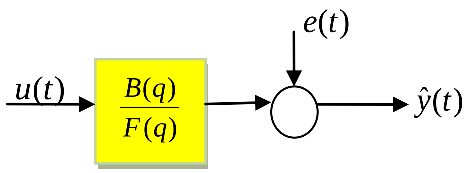

Figure 4.1: Block diagram representation of the Output-Error (OE) Model

4.2.2 ARX (Auto Regressive Model)

The mathematical representation of the ARX model is given as:

$$A(q)y(t)=B(q)u(t-n_k)+e(t)$$

(4.14)

$$A(q)=1+a_1q^{-1}+\dots+a_{n_a}q^{-n_a}\ ,\ B(q)=b_1+b_2q^{-1}+\dots+b_{n_b}q^{-n_b+1}$$

The block diagram representation is given as:

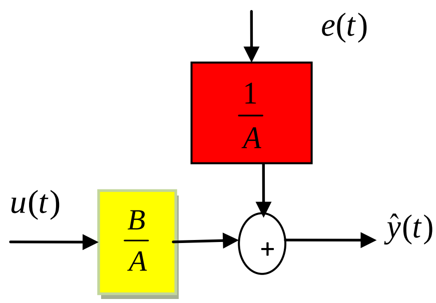

Figure 4.2: Block diagram representation of the Auto-Regressive (ARX) Model

4.2.3 ARMAX (Auto Regressive Moving Average Model)

The mathematical representation of the ARX model is given as:

$$A(q)y(t) = B(q)u(t-n_k) + C(q)e(t)$$

(4.15)

$$A(q) = 1 + a_1 q^{-1} + ... + a_{n_a} q^{-n_a} \text{ ,}$$

$$B(q) = b_1 + b_2 q^{-1} + ... + b_{n_b} q^{-n_b+1} \text{ and } C(q) = 1 + c_1 q^{-1} + ... + c_{n_c} q^{-n_c}$$

The block diagram representation of ARMAX model is as follows

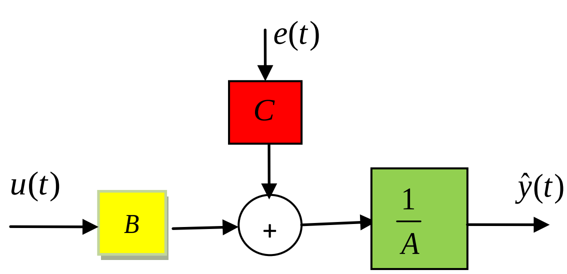

Figure 4.3: Block diagram representation of the Auto-Regressive Moving Average (ARMAX) Model

4.2.4 Box-Jenkins Model

The mathematical representation of the Box-Jenkins model is given as:

$$y(t) = \sum_{i=1}^{nu} \frac{B_i(q)}{F_i(q)} u_i(t - nk_i) + \frac{C(q)}{D(q)} e(t) \tag{4.16}$$

$$B(q) = b_1 + b_2 q^{-1} + ... + b_{n_b} q^{-n_b+1} \ , \ C(q) = 1 + c_1 q^{-1} + ... + c_{n_c} q^{-n_c}$$

$D(q) = 1 + d_1 q^{-1} + ... + d_{n_c} q^{-nd}$ and $F(q) = 1 + f_1 q^{-1} + ... + c_{nf} q^{-n_f}$

nu - Number of input channels

The block diagram representation of ARMAX model is as follows

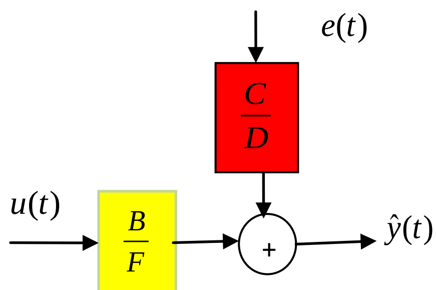

Figure 4.4: Block diagram representation of the Box-Jenkins (BJ) Model

In this present work, all the above mentioned parametric models were implemented to compute the dynamic relationship between acquired sEMG (input) and its corresponding Force (output) data. Out of all the models, for the available data, the OE models results are very promising compared to the other models. The results are provided and explained in detail in Chapter 7 (Results and Discussion).

Chapter 5: Methodology

5.1 Background

The identification of the motor point location is very important .The spatial locations of the sEMG sensors are fixed due to the prosthetic socket contact fittings. However, the daily use of upper extremity prosthetics causes relative motion between the skin and the prosthetic sockets. These motions result in a degeneration of functionality over the time, due to a mismatch of motor points location and sEMG sensor placement.

In spite of the extensive research done in the area of sEMG signals and its applications in various fields including biomechanics, rehabilitation and medical, there is very limited information available about the placement of the electrodes for sEMG acquisition [71].Everyone has their own standards. In 1992, Zipp projected an algorithm based on the body dimensions to determine the electrode placement location [72]. In his work, he proposed a set of requirements that need to be satisfied and implemented. In 2007 Henryk K , et al., have advocated the work proposed by Zipp and discussed about the effects of the electrode position on EMG recording in pectorials major[73]. In the recent study done by Massimilaino G et al., they proposed a method of motor point identification techniques for quadriceps and gastrocnemii muscle in the lower extremity.

As aforementioned, the objective of this dissertation work is to identify the motor point location automatically from the acquired sEMG and its corresponding force signals from the upper extremities. This chapter discusses the Dempster Shafer theory concept, which is utilized in this work, the novel proposed technique based on the Dempster Shafer Theory and its application to determine the motor point location.

5.2 Dempster Shafer Theory of Evidence

The Dempster Shafer Theory (DST) can also be called the theory of belief functions and it got its name from the combination of the two theories developed by Arthur P. Dempster in 1968 and Glenn Shafer in 1970 [74]. The theory gained attention during 1980 is in the field of Artificial Intelligence (AI). The main advantage of the DST is that it can make the uncertain judgments in case of available information as well as in case of limited information. The DST is the generalization of the Bayesian theory of subjective probabilities.

In 1986, Lotfi A. Zadeh [75] presented a simple view of DST theory and its implication for the rule of combination. In this dissertation work we are also using the sample examples provided by Lotfi in [75] to give better understanding of the DST concept before going in detail of its applications. For example, consider Table 5.1 with five employees whose age is not provided directly but the age within particular intervals was given such that it satisfies the criteria $Age(i) \in Q$.Where i is the assigned number to the employee and Q is the interval [30, 35]. i.e., the employee's age lies within the given interval with a lower probability of 30 and upper probability of 35.

Table 5.1: Employee and the age interval information

Employee Number	Age interval
1	[32, 36]
2	[30, 32]

3	[40, 45]
4	[30,32]
5	[38,40]

Now we need to determine what fraction of employee satisfy the given age criteria and lies within the age of [30, 35]. Here, there are three possibilities for each employee. They are

(i) Possible (*P*)

(ii) Certain (*C*)

(iii) Not possible (*NP*)

Applying the above three cases to the five employees and determining their case will give us the following Table 5.2.

Table 5.2: Employee, age interval ate the test analysis information

Employee Number	Age interval	Test Analysis
1	[32, 36]	*P*
2	[30, 32]	*C*
3	[40, 45]	*NP*
4	[30,32]	*C*
5	[38,40]	*NP*

The analysis was done depending on their lower and upper probability values. As given in [75] the representation of the Table 5.2 in Equation form is

$$Resp(Q) = ((N(Q); \Pi(Q)), \tag{5.1}$$

Where $Resp(Q)$ - Response of Q

$N(Q)$ - Certainty of Q

$\Pi(Q)$ - Possibility of Q

The numerical interpretation of Equation 5.1

$$Resp[30,35] = (N[30,35] = 2/5; \Pi[30,35]) = 3/5),$$

To interpret Equation 5.1 from DST perceptive, Lotif in [75] stated that the first term in the $Resp(Q)$ is the measure of belief (B) and the second term represents the measure of Plausibility (Pl) which are explained in the section below. This [75] is highly recommended for better understanding of the DST concept.

The Dempster Shafer theory generalizes the probability theory. The DST is a two-fold concept. The initial step, the masses need to be assigned and then the combining factor comes into representation. For any given space Ω, the probabilities are assigned for all the possible subsets of the given set and called as power set which is represented by 2^{Ω}. For example, let the given set have three elements a, b and c, then the power set 2^{Ω} is given by

$$2^{\Omega} = \{\{a\},\{b\},\{c\},\{a,b\},\{a,c\},\{a,c\},\{a,b,c\},\phi\} \tag{5.2}$$

All the assigned masses will sum up to 1. The next step is the rule of combination, in this scenario is given as

$$m(D) = \begin{cases} 0 & , if \;\; D = \phi \\ \dfrac{\sum_{A \cap B \cap C = D} m_1(A) m_2(B) m_3(C)}{1 - \sum_{A \cap B \cap C = \phi} m_1(A) m_2(B) m_3(C)} & \text{Otherwise} \end{cases} \tag{5.3}$$

Where $m_1\{A\}$ - Prior mass distribution based on evidence A

$m_2\{B\}$ - Prior mass distribution based on evidence B

$m_3\{C\}$ -Prior mass distribution based on evidence C

ϕ - Null set

The numerator is called the belief function and the denominator is called the plausibility function. For better understanding of the DST concept, a simple numerical example is provided below adapted from the work provided in [76].

A car was stolen from the apartment's parking lot. We know that the robbery was done by one of three steals Tim, Tom and Tori. Now we have a set of hypotheses given by

$$\Theta = \{Tim, Tom, Tori\}$$

With the evidence theory, the probability allocation is not limited to the members of the set $\{\{Tim\}, \{Tom\}, \{Tori\}\}$. It makes a mass assignment function denoted by $m(.)$ .Where $m : 2^{\Theta} \rightarrow [0,1]$ assigns probability to any set which is a member of the given power set Θ .

Thus the set of probabilities for this example is given by

$2^{\Theta} = \{\{Tom, Tim, Tori\}, \{Tom, Tim\}, \{Tim, Tori\}, \{Tom, Tori\}, \{Tom\}, \{Tim\}, \{Tori\}, \phi\}$ with the following conditions:

$$\sum_{p \in 2^{\Theta}} m(p) = 1$$

$$m(\phi) = 0$$

In the case, we have two evidences. The first evidence we have is that the thief leaving the parking lot with the car is 80% likely to be man. Therefore we know that $p(man) = 0.8$. If we apply probability theory here

$$p(\neg man) = p(Tori) = 1 - 0.8 = 0.2$$

Rewriting the probabilities in terms of mass assignments, we get $p(Man) = 0.8 \Rightarrow m(\{Tom, Tim\}) = 0.8$ and the remaining probability of unknown information is represented by $m(\{Tim, Tom, Tori\}) = 0.2$.Table 5.3 gives the available evidence I in terms of mass assignments.

Table 5.3: Evidence I represented in mass function

$\{Tom, Tim\}$	$\{Tom, Tim, Tori\}$
0.8	0.2

Similarly, consider the second evidence reporting with confidence 60% that Tom left when the theft happened. So, we write in terms of mass assignments, we get $m'(\{Tim, Tori\}) = 0.6$ and the remaining probability is $m'(\{Tom, Tim, Tori\}) = 0.4$. The tabular representation of Evidence II is shown in Table 5.4

Table 5.4 : Evidence II represented in mass functions

$\{Tim, Tori\}$	$\{Tim, Tom, Tori\}$
0.6	0.4

Now we have two different evidences for the same incident with a conflict. If we apply a Dempster rule by combining two evidences using Equation 5.3 will give a new mass assignment. In order to obtain that, we need to calculate the belief and plausibility for the Equation. The belief function can be computed by the product of the mass assignments from the two evidences which were provided in Table 5.5.

Table 5.5 : Belief Function from two evidences

	$\{Tim, Tori\}$ 0.6	$\{Tim, Tom, Tori\}$ 0.4
$\{Tom, Tim\}$ 0.6	$\{Tim\}$ 0.48	$\{Tom, Tim\}$ 0.12
$\{Tim, Tom, Tori\}$ 0.2	$\{Tim, Tori\}$ 0.32	$\{Tim, Tom, Tori\}$ 0.08

Once we have the final mass assignments, belief and plausibility can be easily assessed as follows

$$Bel(X) = \sum_{Y \subset X} m(Y) \quad , \quad Pl(X) = \sum_{X \cap Y \neq \phi} m(Y)$$

Both belief and plausibility are related to one another and calculated by

$$Bel(X) = 1 - Pl(\neg X) \quad , \quad Pl(X) = 1 - Bel(\neg X)$$

Thus we can compute the belief and plausibility functions and obtain the probabilities from different evidences with conflict.

Before going into details of the proposed technique based on the DST, the following section will discuss some of the applications of the DST in various different fields. It can be used for data fusion as well as the uncertainty analysis.

5.3 DST Applications

DST has been used in different fields for various applications. Few to mention are: medical diagnosis, image processing, satellite sensor data fusion, etc. Compared to the probability approaches, DST is renowned for its safety and reliable modeling [77]. In medical diagnosis, uncertainty is the main characteristic of the information. In general, a medical practitioner relies on the empirical knowledge which is a superficial relationship between the symptom and associated disease. The results can be inaccurate and unreliable. To address this issue, the medical practitioners diagnose the data from different sources and combine them to make a decision. In recent years, DST based fusion procedure has become widely in use.

For an example, a DST based fusion technique was implemented to predict breast cancer tumors [78]. The two sources are from gene-expression patterns in peripheral blood cells and Fine-Needle Aspirate Cytology (FNAC) data. The belief functions and uncertain classifiers were computed and then fused using the DST combination rule. It claims that this approach is good especially for healthcare applications where it requires handling the robust data from uncertain classifiers. Another medical application that it was highly used is in medical data mining [79, 80]. In [79], DST was employed for data mining of the medical data in order to predict the disease. In their work, they carried the experiments on breast cancer and dermatology data. The input was fed into three different classifiers, they are: K nearest neighbor (KNN), Bayesian and Decision Tree classifier.

The outputs from the classifiers are considered as evidences and combined using the DST to achieve the final diagnosis.

Apart from the medical applications, DST can also be used for anomaly detection. In [81], DST was utilized in the process of email anomaly identification i.e., email worm detection. The threshold values were computed and the mass assignments were done. The next step was sending the mass to the DST combination component. The overall mass with determine whether the data is normal or abnormal. Another area where DST was vastly used is in the area of image processing applications [82-87]. The image can either be a medical image or a radar image.

Ben Chaabane, S et al., [82, 83] used a color image segmentation approach based on DS evidence theory. In their work, they combined the information from three different sources for the same image. The proposed method was tested on the cell images and concluded that the DST outperformed in handling the uncertain, imprecise and incomplete information.

According to Ali Naseri and Omid Azmoon [88], radar network functionality strongly depends on data fusion algorithms. Radar networks have various applications in the military and civil fields such as air traffic control, defense etc. They stressed that there is a lot of ambiguity associated with radar backscatter; therefore, probability of detection is an important factor for choosing the optimization algorithm. In their work, they investigated on three different fusion algorithms: classic, Bayesian and Dempster-Shafer theory.

The proposed three algorithms were simulated and evaluated from the radar data information. From the results, they declared that the DST is best for two-cell and four cell networks.

Similarly, in [89], they presented a multi-scale image fusion technique based on Dempster-Shafer evidence Theory. By implementing this they were able to see the improvement in the land cover map which is rich in spatial and spectral information.

The next section which discusses about the proposed technique based on DST for motor point identification

5.4 Proposed Technique

As presented in Section 5.3, the concept behind the DST is given by the combination of evidences obtained from different sources. Using these evidences, DST models the conflict between the obtained information. The DST approach requires that at least two evidences are extracted from the given data. The main advantage of the DST is that it does not require any prior knowledge, which is potentially suitable for the present work, if implemented real-time.

For this work, the sources of evidences are chosen from the Kullback Information Criterion (KIC) and a Fuzzy inference system (FIS). The KIC is obtained from identifying the dynamical relationship between the sEMG signals and its corresponding finger forces of the prosthetic device. The fuzzy logic inference system also uses the sEMG signal and corresponding force signals as input and output, and the membership functions are chosen from the sEMG entropy, relative error and the correlation between the sEMG and force signals. The following block diagram in Figure 5.1 gives the brief overview of the proposed algorithm for the determination of the motor point location.

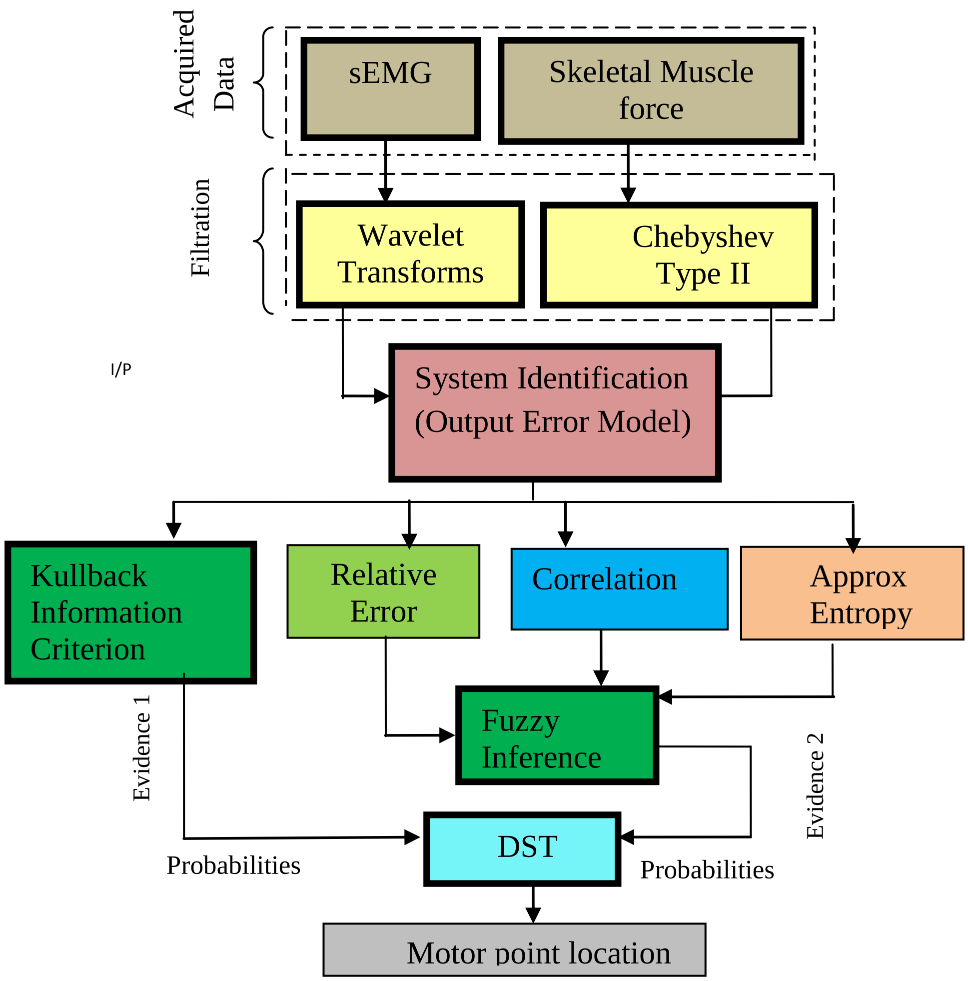

Figure 5.1 : Block diagram representation of the overall proposed work

5.4.1 Kullback Information Criterion

In the field of scientific research, statistical modeling is an important tool. Models are used to estimate the future behavior of the system based on the present data. Statistical modeling is used in various applications to understand the behavior of a particular system, to determine and control the complex systems, etc. The objective of the statistical modeling is to present the information of the system in the statistical model form and to evaluate various forms of the system such as prediction, control, information, extraction, knowledge discovery, validation, risk evaluation, and decision making. So, complex systems can be more easily evaluated by choosing the right statistical model of the system.

A statistical model can be defined as a probability distribution obtained by using observed data and approximating the true distribution of probabilistic events. Figure 5.2 illustrates the estimation of the true structure by using the observed data.

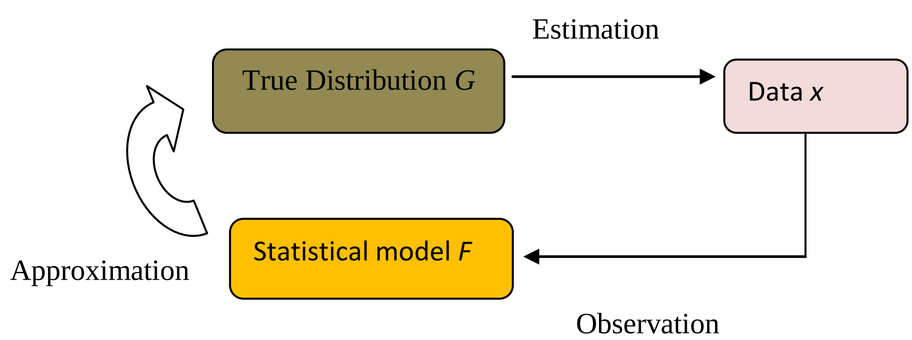

Figure 5.2: True structure estimation based on statistical modeling [90].

According to Akaike[90], the object of statistical modeling is to estimate the future data based on the observed data as accurately as possible. This can be referred as the predictive point of view. In the case of infinite data sets, there will not be much difference between predictive point of view and making a prediction. Conversely for a finite data set, the difference can be seen prominently because of variation in the optimal model for prediction and the true model estimated by the predictive point inference. According to the information criteria, sometimes simple models can give better information than the models obtained from true structures. The statistical modeling in the predictive point of view is shown in Figure 5.3.

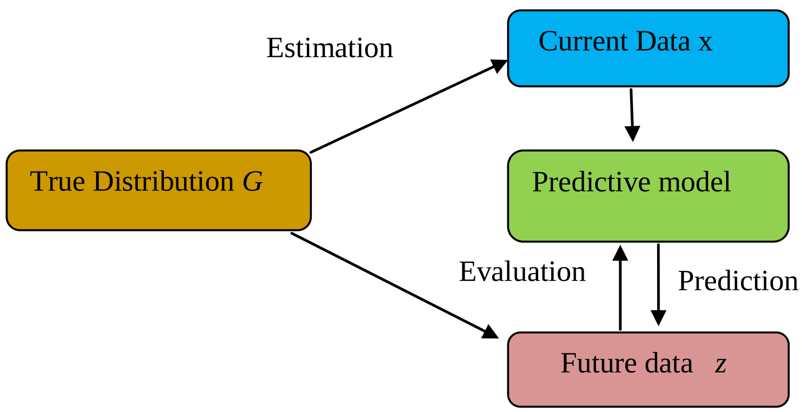

Figure 5.3: Statistical modeling in the predictive point of view [90].

Figure 5.4 represents the extraction of information from the model. A model can be obtained from the prior information and the observed data.

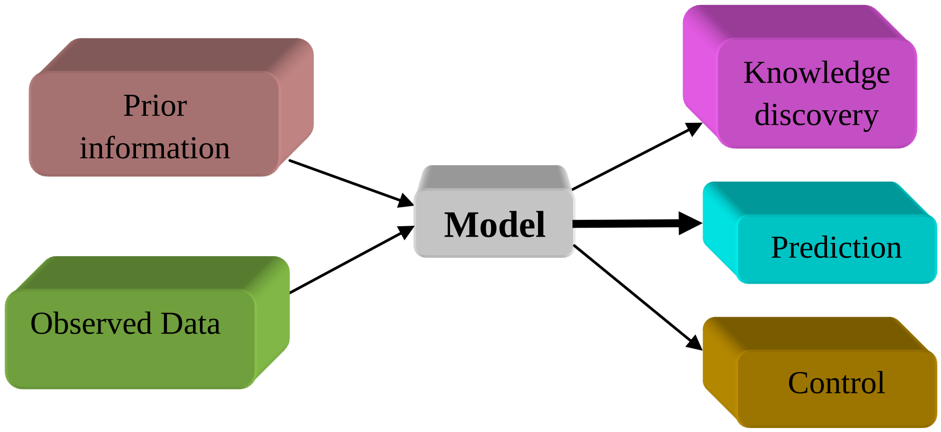

Figure 5.4: Extraction of information from the model [90].

From a practical point of view, a statistical model can be defined as the model obtained from prior information, and observed data. It also depends on the reason for the analysis. Therefore the aim of statistical modeling is to get a good model which is useful for extraction of information based on the required analysis. In order to judge the effectiveness of the statistical model, Akaike [90] proposed that the closeness between the predictive distributions obtained from the model and the true distribution should be measured, rather than minimizing the predictive error. Later he also proposed a method of evaluating the statistical model in terms of the Kullback-Leibler information (divergence). The model evaluation criterion based on Kullback-Leibler information is known as the information criterion [90].

The three basic concepts from which this information criterion was derived are:

(1) A prediction –based viewpoint of modeling.

(2) Evaluation of prediction accuracy in terms of distributions.

(3) Evaluation of the closeness of distributions in terms of Kullback-Leibler information.

Kullback's Information Criterion (KIC) is an asymmetric measure [91]. The measure of the models dissimilarity can be obtained by the sum of two directed divergences, known as Kullback's symmetric or J-divergence [74] as given by the Equation 5.4.

$$KIC(p_i) = \frac{n}{2}\log R_i + \frac{(p_i+1)n}{n-p_i-2} - n\psi\left(\frac{n-p_i}{2}\right) + g(n) \qquad (5.4)$$

where n - Number of data points in the set

p_i - Order of the Model i.e., the output-error model from SI technique

R_i - Residual square norm

ψ - digamma function

$g(n) = n * \log(n/2)$

After obtaining the estimated models using SI techniques, the probabilities were calculated by using the following steps I - III:

(I) Identify models M_1, M_2, …, M_k using acquired data input(u) and output(Y), for k number of sensors collecting data simultaneously.

(II) Compute the residual square norm $R_i = \| Y - \Phi_i \hat{\theta}_i \|^2 = \|Y - \hat{Y}\|$, where $\hat{\theta}_i = \left\{\Phi_i^T \Phi_i\right\}^{-1} \Phi_i^T Y$,

and $\vec{\Phi} = \begin{bmatrix} Y_p^T & u_p^T & Y_{p-1}^T & \cdots & u_1^T \\ Y_{p+1}^T & u_{p+1}^T & Y_p^T & \cdots & u_2^T \\ \vdots & \vdots & \vdots & \ddots & \vdots \\ Y_{n-1}^T & u_{n-1}^T & Y_{n-2}^T & \cdots & u_{n-p}^T \end{bmatrix}$,

(III) Calculate the probability by using KIC Equation 5.4.

(IV) Compute the probability of each sensor by using

$$p(M_i \mid z) = \frac{e^{-l_i}}{\sum_{j=1}^{k} e^{-l_j}}$$

where k- number of sensors

For this work, the input is chosen as sEMG from the subject and output is the corresponding skeletal muscle force signal for the three sensors that are mounted on the surface of the skin as shown in Figure 3.2. The models M_1, M_2 and M_3 were obtained by employing the system identification technique i.e., step 1. After that residual square norms were computed for the each model and finally the KIC based probabilities were obtains for the three sensors. The same steps were implements on the 10 test subjects and the probability values are provided and discussed in the Chapter 7.

5.4.2 Fuzzy logic (FL)

Fuzzy logic is a concept introduced by Lotif A. Zadeh, a professor at University of California at Berkley in 1965. It mainly deals with the approximate reasoning rather than fixed value. It provided a simple solution based on ambiguous, vague information. Fuzzy logic have various application ranging from simple, small to complex, networked system and perhaps easy to implement. Fuzzy sets give the mathematical definition based on the degrees of membership functions. In [92], advantages were very well listed of using FL and its unique features which are provided below:

- It is a smooth output function regardless of the wide range of inputs and also a robust system, because it doesn't require a specific set of inputs.
- Since the FIS is based on user-defined rules, it can be altered and modified easily to improvise the system performance.
- Any sensor data that provides some information of a system's inputs and outputs is adequate. This allows the sensors to be inexpensive and imprecise, therefore keeping the overall system cost and complexity low.
- Because of the rule-based operation, there will not be any limitations to the number of inputs to be processed and the number of outputs to be generated. The complexity of the system depends on the inputs and outputs. So, it is advisable to break the system into smaller FL systems.
- FL can control systems that would be complicated or unfeasible to model mathematically.

Consider a classic (crisp) set R of real numbers larger than 35 which can be written as

$$R = \{a \mid a < 35\}.$$

In this case, 35 is the boundary number. If a is smaller than this number, then a belongs to the set R; otherwise a does not belong to the set R. Let a and R be a temperature in centigrade and cool, respectively. If temperature (a) is 34.99, which is smaller than 35 and belongs to the set R, then people consider the weather is cool (R); however if temperature is 35.01, which is larger than 35 and does not belong to the set R. In this scenario, humans think the weather is not cold.

In contrast to a classical set, a fuzzy set is a set without the crisp boundaries i.e., the transition from "belongs to set" to "doesn't belongs to set" will be smooth and characterized by the defined membership functions. It defines the degree to which the element belongs to a given set.

For example, if a belongs to a set R, then the fuzzy set A is defined by:

$$A = \{(a, \mu_A(a)) \mid a \in R\},$$

where $\mu_A(a)$ is the membership function of the fuzzy set A. The membership function will map each element of a to a membership value between 0 and 1. In case, if the value of the membership function $\mu_A(a)$ is either 0 or 1, then the fuzzy set will become a classic set and $\mu_A(a)$ will be a characteristic function of A. Figure 5.5 gives a picture of the distinction between the classic set and the fuzzy set.

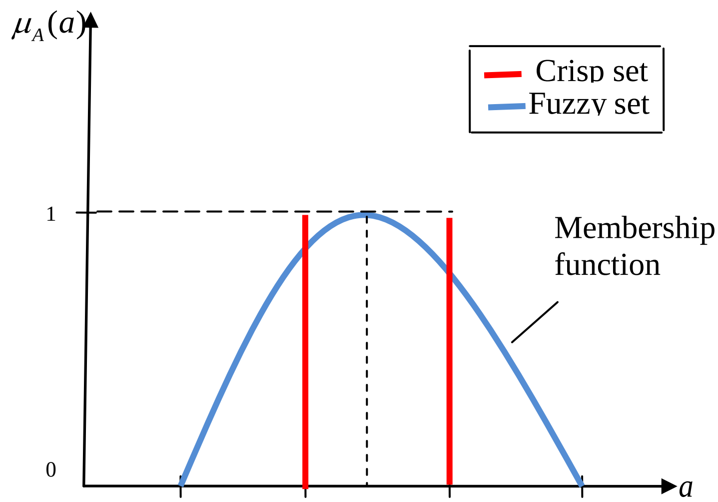

Figure 5.5: Crisp set Vs Fuzzy set

5.4.2.1 Membership Function

As mentioned earlier, a membership function is the criterion of the fuzzy set. The fuzziness of a fuzzy set is determined by the membership function. The shape of the membership functions is very important, since it has an impact on the fuzzy inference system. For the better knowledge of the fuzzy inference system, here we discuss different shapes of the membership functions. In particular following five types are listed and explained:

(a) Triangular membership function

(b) Trapezoidal membership function

(c) Gaussian membership function

(d) Bell membership function

(e) Sigmoidal membership function

Triangular Membership Function

A triangular member function is defined by three parameters $\{a,b,c\}$ and given as

$$triangle(x',a,b,c)=\begin{cases}0, & x<a.\\ \dfrac{x-a}{b-a}, & a\le x\le b.\\ \dfrac{c-x}{c-b}, & b\le x\le c.\\ 0, & c\le x.\end{cases}$$

The alternative way of representing the above equation is by using *min* and *max* functions which can be written as

$$triangle(x',a,b,c)=\max\left(\min\left(\frac{x-a}{b-a},\frac{c-x}{c-b}\right),0\right)$$

The parameters $\{a,b,c\}$ define the x coordinates of the triangular membership function.

Trapezoidal Membership Function

A trapezoidal membership function is defined by four parameters $\{a,b,c,d\}$ and given as

$$Trapezoid(x',a,b,c,d)=\begin{cases}0, & x<a.\\ \dfrac{x-a}{b-a}, & a\le x\le b.\\ \dfrac{d-x}{d-c}, & c\le x\le d.\\ 0, & d\le x\end{cases}$$

Alternate representation using min and max is given as

$$trapeziod(x', a, b, c) = \max\left(\min\left(\frac{x-a}{b-a}, 1, \frac{d-x}{d-c} \right), 0 \right).$$

The parameters $\{a, b, c, d\}$ represents the x coordinates of the trapezoidal membership function.

Gaussian Membership Function

A Gaussian membership functions is defined by two parameters $\{c, \sigma\}$ and is given as

$$gaussian(x', c, \sigma) = e^{\frac{1}{2}\left(\frac{x-c}{\sigma}\right)^2}$$

where c - membership function center

σ - Membership function width

Bell Membership Function

A Bell membership function is specified by three parameters $\{a, b, c\}$ and is given as

$$bell(x', a, b, c) = \frac{1}{1 + \left| \frac{x-c}{a} \right|^{2b}}$$

Here b is a positive and can also be called as Cauchy membership function.

Sigmoidal Membership Function

A sigmoidal membership function is defined by two parameters and is given as

$$sig\left(x',a,c\right)=\frac{1}{1+\exp\left[-a(x-c)\right]}$$

Here, a controls the slope at the crossover point $a=c$.

Fuzzy Inference System

A Fuzzy Inference System (FIS) uses the fuzzy logic concept to map inputs to outputs. FIS uses the set of fuzzy membership functions and rules. The fuzzy system follows four steps to make a conclusion. They are Fuzzification, Fuzzy inference, Defuzzification. The block diagram representation of FIS system is given in Figure 5.6.

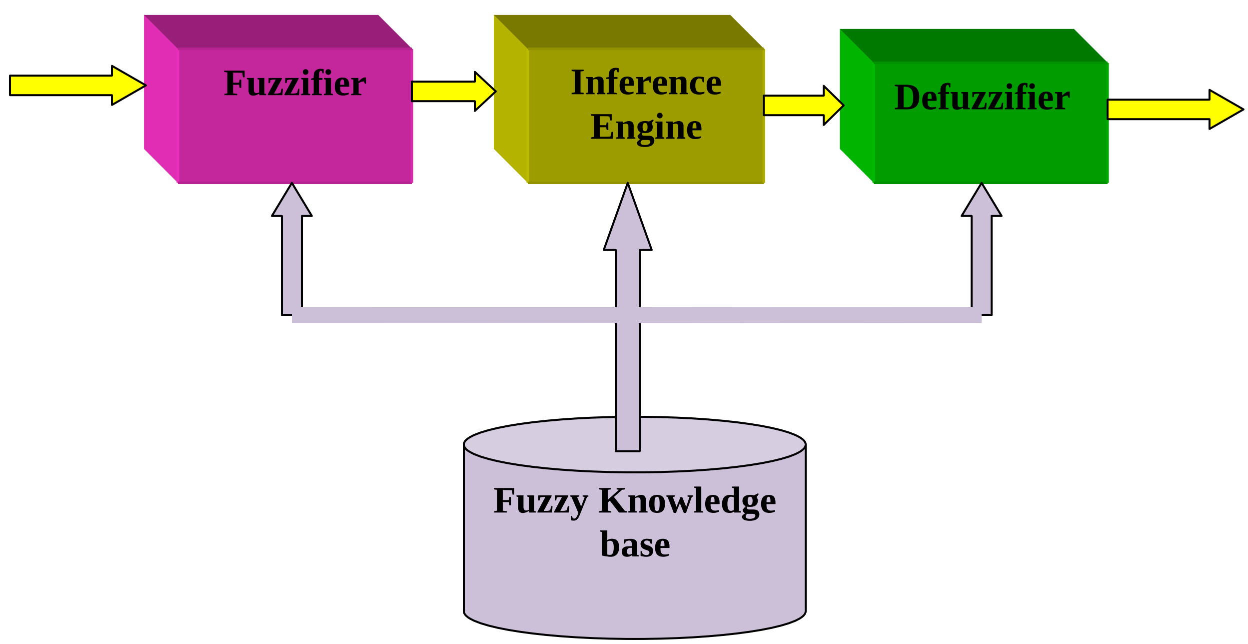

Figure 5.6 : Block diagram representation of Fuzzy Inference Systems (FIS)

To get a better understanding of the FL concept and FIS, we will explain with a simple and very commonly used tipping example[1].

A person goes to a restaurant and would like to tip based on the service and the quality of the food. In this case, we apply FL inference considering service represented by bad, good and best on the scale of 0 to 100 (100 as best) and quality of food represented by rancid and delicious on the scale 0 to 100 (100 being delicious) as inputs variables. The output variable, tip will be decided as either generous or average or cheap based on the defined rules. In this example, we define three rules and they are

- IF service is bad or food is rancid, THEN tip is cheap (5%)

-IF service is good, THEN tip is average (15%)

-IF service is best or food is delicious, THEN tip is generous (25%)

Based on the above defined fuzzy rules, the tip percentage can be determined.

Similar to the above example, in this work, 3 inputs were considered that were obtained from

The system identification models of sEMG and force signals. They were:

1.) Relative error

2.) Correlation

3.) Approximate entropy

[1] http://www.mathworks.com/help/fuzzy/an-introductory-example-fuzzy-versus-nonfuzzy-logic.

Based on these inputs, the sensor probabilities are found based on FIS. The following block diagram in Figure 5.7 shows fuzzy logic inputs, membership's functions chosen for this work.

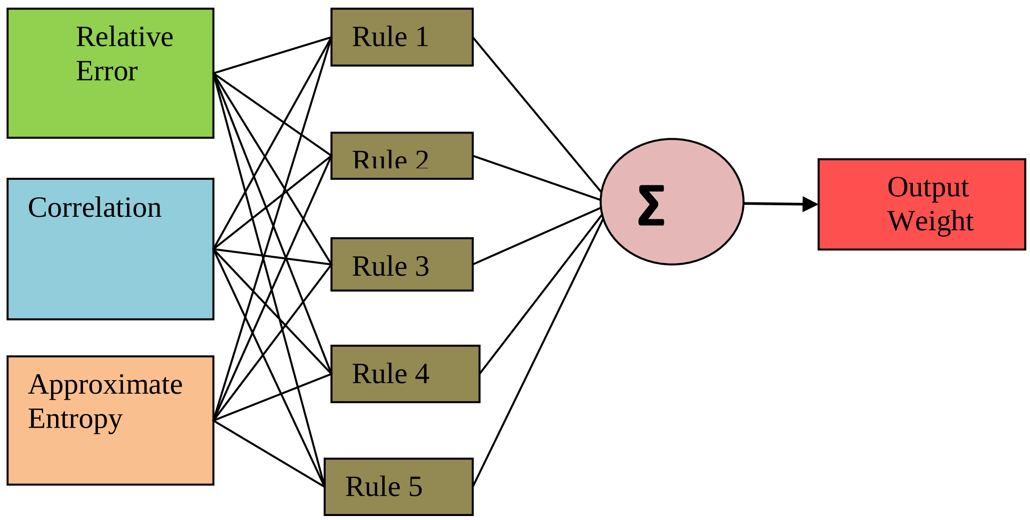

Figure 5.7: Fuzzy inference system with Relative error, Correlation and Approximate Entropy as inputs

The following steps 1 to 9 are implemented to compute the FL based probabilities for the 3 sensors.

Step 1: Compute entropy, from a time series of data $\hat{y}_i(1), \hat{y}_i(2), \ldots \hat{y}_i(N)$ where N - number of data points

Step 2: Fix m, an integer, and r, a positive real number. The value of m represents the length of compared run of data, and r specifies a filtering level.

Step 3: Form a sequence of vectors $x(1), x(2), \ldots x(N-m+1)$ in R^m defined by the discrete sequence of the input sEMG data $x(k) = [u(k), u(k+1), \ldots u(k+m-1)]$.

Step 4: Use the sequence $x(1), x(2), \ldots x(N-m+1)$ to construct, for each k, $1 \le k \le N-m+1$ $C_k^m(r) =$ (Number of $x(j)$ such that $d\left[x(k), x(j)\right] < r) / (N-m+1)$

$d\left[x, x^*\right]$ is defined as $d\left[x, x^*\right] = \max\limits_a \left|u(a) - u^*(a)\right|$,

Where $u(a)$ - m scalar components of x

d - represents the distance between the vectors $x(k)$ and $x(j)$.

***Step 5*:** Define $\Phi^m(r) = (N-m+1)^{-1} \sum_{i=1}^{N-m+1} C_i^m(r)$.

The quantity $C_i^m(r)$ is the fraction of patterns of length □ that resemble the pattern of the same length that begins at interval□, we define $\Phi^m(r)$ as the mean of these $C_i^m(r)$ values

Step 6: Define approximate entropy (E) as

$$E_i = \log(\Phi^m(r)) - \log(\Phi^{m+1}(r)).$$

Where $\log$ is the natural logarithm, for m and r fixed as in Step 2.

Step 7: Compute Relative Error (RE) between actual forces

(y) and the individual WH model estimated force ($\hat{y}$)

$$\eta = \frac{\delta y}{\hat{y}_i},$$

where $\delta y = y - \hat{y}$

y - Actual force from FSR

$\hat{y}$ - Individual WH model estimated force

Step 8: Compute Correlation coefficient as

$$\rho_i = \frac{\operatorname{cov}(y,\hat{y})}{\sigma_y \sigma_{\hat{y}}} = \frac{E\left[(y-\mu_y)(\hat{y}-\mu_{\hat{y}})\right]}{\sigma_y \sigma_{\hat{y}}}$$

where μ - mean, σ - Standard Deviation

***Step 9**:* Define the fuzzy inference system,

$$F^z = \text{If } E_i A_1^z \text{ or } \rho_i B_1^z \text{ or } \eta_i C_1^z \text{ then } W^z \text{ is } D_1^z$$

where $F^z (I = 1, 2, ..., l)$ denotes the I^{th} fuzzy rule, $E_i (i = 1, 2, ..., M_i)$, $\rho_i (i = 1, 2, ...M_i)$, $\eta_i (i = 1, 2, ..., M_i)$ are the entropy, correlation and relative error inputs for the □□h model □□is the output weight of the fuzzy rule F^z ,and $A_I^z (I = 1, 2, ..., l)$ is the Gaussian fuzzy membership function $B_1^z (I = 1, 2, ..., l)$ $C_1^z (I = 1, 2, ..., l)$ $D_1^z (I = 1, 2, ..., l)$ are triangular fuzzy membership functions respectively.

After obtaining the evidences from the two sources, substituting them in the Equation 5.3 which will give the weights of each sensor. Based on the obtained masses, belief and plausibility functions will be computed. By substituting them in the DST Equation i.e., 5.3, will give the probabilities of each sensor based on the rule of combination. The results are discussed in detail in Chapter 7.

Chapter 6: Data Fusion

The previous chapter discussed about the Dempster Shafer Theory concept, its applications, the use of the DST for the motor unit identification based on the evidenced obtained from KIC and FL. This chapter addresses the concept of data fusion and implementation of data fusion algorithm for the SEMG sensor data.

6.1 Data Fusion Literature

In general, the sEMG signals are acquired by placing a single bipolar electrode on the muscle belly [93] which limits their accuracy. The sensor array will address that issue. While using the multiple electrodes, the orientation of the electrodes also plays an important role because of the motor point location approximation. The misalignment of the electrodes leads to the sEMG amplitude reduction [94]. The sEMG sensors are aligned perpendicular to the superficial musculature (flexor digitorum superficialis). The goal of proposing a sensor data fusion method is to improve the accuracy of the skeletal muscle force estimation. Data fusion is a process of combining the data sets from different sources to gain more information. It can be achieved in three different ways: Data-level fusion, feature -level fusion, and decision-level fusion. Data level fusion is the combination of data from the sources; feature-level fusion is merging the features of the sources, and decision-level fusion is the combination of the results from the sources. In this work, decision-level fusion is used to combine the data from the three sensors. The information extracted from the three sEMG sensors is fused with a proposed fusion algorithm to improve the skeletal muscle force estimation. The proposed fusion algorithm is developed for an arbitrary number of sensors.

The field of multi-sensor data fusion was recently recognized as a specialized field of research. It is a subject which draws from different areas such as statistical estimation, signal processing, computer science, artificial intelligence, weapon systems, etc. The overall goal of data fusion is to make inferences concerning a certain state of nature using multiple data sources [95].

Many practical problems arising in monitoring can be modeled with the aid of parametric models. In general, multiple sensors are used in order to reduce uncertainty and obtain more complete knowledge of the state to be measured. Multi sensor data fusion is a multilevel, multifaceted process dealing with the automatic detection, association, correlation, estimation, and combination of data from single and multiple information sources. Hence, we find a number of relevant contributions in the literature. Sebastian Bitzer et al., 2006[96], present the techniques for decomposing surface electromyography signals into the constituent motor unit action potential trains. A surface sensor array is used to collect data from four channels of differentially amplified EMG signals. This technique consists of identifying action potentials in the EMG signals and assigning them to specific motor units by classifying shapes and amplitudes of the action potentials. The assignments are made based on template matching and firing of the individual motor units. The decomposition is achieved by a set of algorithms that uses an Artificial Intelligence (AI) framework. The accuracy is reported to be 97% for 30-s duration. The accuracy was verified by comparing the EMG signals detected simultaneously. In Carlo J.De Luca et. al, 2006[97], a method based on support vector machines is introduced. It is capable of detecting the opening and closing actions of the human thumb, index finger, and other fingers based on recorded surface EMG. This method is ideally suited for the control of an active prosthesis with a high number of active degrees of freedom. Some of the properties and problems of recorded signals are addressed in [97].They are:

d.) The amplitude of the sEMG signal varies depending on the size of the muscle that is measured and its position relative to the electrode.

e.) Due to muscle fatigue, a subjective change in the perception of the force produced during a finger action, or due to external influences related to electromagnetic pollution, and amplitude changes.

f.) The most challenging property of surface based EMG signal measurement with respect to a robust classification is that it changes with arm posture. This is because the underlying muscles, especially towards the wrist, change their position relative to the electrodes on the skin when the hand is rotated.

In Lapatki et.al, 2003 [98], the sEMG technique has been extended with the design of linear and two-dimensional electrode arrays and grids. These arrays or grids are capable of covering a larger part of the muscle and hence obtaining some spatial information. By using the electrode grid with small electrode sizes and inter-electrode spacing, it is possible to decompose the sEMG interference pattern for single MU analysis and the determination of firing events of individual MUs. This sensor technique was applied for the facial musculature. The rectangular grid consisted of seven columns each having each 13 electrodes (the diameter of each electrode is 1.9 mm). To facilitate the skin attachment, perforations of 1.2 mm in diameter were made between four electrodes. On the basis of the spatial version of the Nyquist sampling criterion, the inter-electrode distance was chosen as 4 mm center-to-center. This grid can be cut to any desired sizes and shapes. The electrode to skin resistance is very low (below 300kΩ) [98]. S.H.Roy et.al, 2007[99] used the data fusion model which is applicable to the field of car safety and driver-assistance applications. There are different data fusion models. A rather popular model is the Joint Directors of Laboratories (JDL) model. The overall JDL data fusion process consists of six separate levels of processing [99].

Level 0 (Data Alignment): Responsible for removing redundant information acquired by different sensors or to filter out the wideband noise.

Level 1 (Object Refinement): Performs a correct association between sensor data and multiple entities, estimates the parameters that are most significant for particular applications, depending upon the basis of an extracted feature entity.

Level 2 (Situation Refinement): The output results of Level 1 processing are used to extract useful information about the relationships between multiple entities located in the same environment.

Level 3(Threat Refinement): Possible threats are predicted based on the current situation.

Level 4 (Process Refinement/ Resources Management): controls the overall data fusion process to improve the real-time performances.

Level 5 (Cognitive Refinement): The fused data will be transformed into a form that can easily be interpreted by the users. This JDL model is too theoretical to be implemented in practice.

David Macii et al, 2008 [100] give details about the performance of sEMG sensors for various conditions affecting the electro-mechanical stability between the sensor and its contact. Two different tests were conducted, one is an adhesive peel test and the other is a mechanical disturbance test. It was found that by adding a highly adhesive double-sided tape the effect of shielding the electrical contact between electrodes and skin was increased. Two types of peel force responses were observed. The first response was recorded by the gradual loss of electrode contact with the skin using a low peel force (by slowly increasing the amplitude). The second response was given by the rapid loss of electrode contact with the skin (occurring at a high peel force by an abrupt increase in signal amplitude). In order to determine the input of the central nervous system to a muscle, sEMG parameters like root mean square (RMS) and median power frequency (FMED) were mostly used. These RMS and median signals are not only influenced by the central nervous system, but also by the peripheral muscle actions i.e., the action potential of the motor unit firing per second. Macii et al were mainly concentrating on deriving the relation between the sEMG and the force with fatigue and comparing to RMS and FMED. Multi-channel sEMG can be used to estimate the motor unit action potential rate (MR). The main objective was to know the performance of estimated MR by comparing it to the number of motor units and their firing rates. According to this paper[100], even though the motor units action potential (MUAPs) is not that accurate, it compares the estimated MR and actual MR and their independence of the muscle properties to determine the input from the central nervous system to the muscle, in case of lower muscle contractions. By using the bipolar electrodes, the EMG signal extraction is not the exact one related to the particular muscle. This is because of the large number of motor units' involvement which results in more cross-talk. This can be overcome to some extent by using multiple array sensors, which can measure the individual motor unit potential.

Regarding decomposition of surface EMG signals [101], found the existence of a continuous increasing relationship between the estimated MR signal and the active motor units' firing rate. At lower muscle contraction, estimated MR is apt to study the input from the central nervous system to the muscle. This paper discusses about the decomposition of the surface EMG signals into individual motor unit action potential trains. An Artificial intelligence (AI) based algorithm was used for the decomposition of the EMG signal. An EMG sensor array with four electrodes was used to collect the sEMG signal. The accuracy was tested by measuring the EMG signal with both a surface EMG sensor array and with needle electrodes and comparing this with EMG signal obtained from needle electrodes. The accuracy varies from 75% to 91% in the automatic mode. In order to increase the accuracy, the interactive mode was used. This gives an accuracy of around 97%. In particular for the i^{th} decomposable motor unit, the decomposition accuracy *A(i)* is given by the equation

$$A(i) = \frac{N_{FIR}(i) - N_{FN}(i) - N_{FP}(i)}{N_{FIR}(i)} \times 100\% , \quad (6.1)$$

Where, $N_{FIR}(i)$ – number of true firings of the motor unit.

$N_{FN}(i)$, $N_{FP}(i)$ - number of false negatives and false positives given by the decomposition algorithm for that particular motor unit.

For *N* decomposable motor units, the total decomposition accuracy *A* is given by

$$A = \frac{1}{N}\sum_{i=1}^{N} A(i) \tag{6.2}$$

The paper concludes that the behavior of the motor units can be studied in detail by using this technique when compared to the needle electrodes [101].

So far, we discussed about the data fusion concept and literature about different fusion algorithms. Based on this [102], in our previous preliminary work (thesis) we explored fusion algorithm based on Akakike Information Criterion (AIC), Bayesian Information Criterion (BIC) and Kullback Information Criterion (KIC) [103]. KIC was detailed explained in previous Chapter 5, Section 5.3.Similarly AIC is given by

$$AIC(p_i) = \frac{n}{2}\log R_i + \frac{(p_i+1)n}{n-p_i-2} \tag{6.3}$$

and BIC is given by

$$BIC(p_i) = \frac{n}{2}\log R_i + \frac{p_i+1}{2}\log n \tag{6.4}$$

Of all the three proposed fusion algorithms, KIC based fusion algorithm out-performed when compared to the AIC and BIC. In this dissertation work, we explored another statistical model based fusion algorithm i.e, Minimum Description Length (MDL) criterion (explained in section 6.2). The proposed fusion algorithm was tested on 10 test subjects' data to validate the results which were provided in Chapter 7.

6.2 Minimum Description Length (MDL) Criterion

In 1978, the Minimum Description Length (MDL) concept was introduced by Jorma Rissanen [104]. The fundamental idea behind the MDL principle is based on the algorithmic complexity of Solomonoff, Kolmogorov and Chaitin [105]. MDL is closely coupled to the Bayesian inference, but it neglect the interpretation difficulties associated with the Bayesian inference. In this work, we are inspired by [102] and used the Minimum Description Length criterion to fuse the estimated models obtained by using SI technique. It is given by

$$MDL(p_i) = \frac{n}{2}\log(\hat{\sigma}_i^2) + \frac{p_i + 1}{2}\log F_i + L_i \tag{6.5}$$

Where $F_i = (Y^T Y - R_i)/)(p_i \hat{\sigma}_i^2)$, $L_i = \frac{1}{2}\log\left(\frac{n - p_i}{p^3{}_i}\right)$

To fuse the data from the three sensors, we implemented the steps I to IV provided in the Chapter 5, section 5.3. In step III, KIC equation is replaced with Equation 6.5.

After achieving the individual probabilities for three sensors, the fusion step was computed by the Equation 6.6, given below.

$$\hat{y}_f = \sum_{i=1}^{k} p(M_i \mid z)\hat{y}_i \tag{6.6}$$

The results are formatted in table and discussed in Chapter 7.

According to the literature, for Equations 5.3, 6.3, 6.4 and 6.5, the standard number of data points, n is set to 30. However, there appears to be no investigation on what the optimum value is for achieving a good fusion output. In this work, we are interested in finding an optimum value for n with regard to the identification and fusion results applied to finger force data and sEMG data. We utilize a Genetic Algorithm (GA) based optimization on the number of data points to be used for the computation of the KIC coefficient. In particular, the search for an optimum value is also limited – in order to preserve the computational efficiency – to a range of $15 \le n \le 160$.

6.3 Genetic Algorithm (GA)

GA is a heuristic search which imitates the natural selection process and includes steps of inheritance, mutation, selection and crossover. It has many applications is various fields like engineering , biology, economics, chemistry, mathematics and many other fields. Now-a-days GA is a very popular and most commonly used method for optimization.

The objective function is used in an elitism based continuous number genetic algorithm. Genetic algorithms are evolutionary algorithms that simulate Darwin's survival of the fittest principle. The initial population of the candidate solutions is randomly generated and represented as chromosomes (where the genes are formed as each parameter of the solution). These chromosomes are evaluated based on an objective function and ranked in terms of its fitness. A subset of the next generation of candidate solutions is selected based on their performance with the objective function. The remaining set of the new generation is produced by a mating process, where the best performing candidate solutions comprise the subset of the parents. In addition to the mating process, a mutation rate is also imbedded in the generation of the new population. The mutation rate enables the search for the optimum solution to overcome local minimums and locate the global minimum/optimum. This process of selection, mating, and mutation is repeated a number of times until the best performing candidate solution converges to some stationary value. The flow chart representation of the genetic algorithm is shown in Figure 6.1.

The objective function for the optimization of the number of data points used in the KIC fusion based algorithm is formulated by the squared accumulative absolute value of the error between the estimated and measured muscle force data and the corresponding correlation between the resulting estimated force $\hat{y}_f$ and the actual force y . In particular, the cost function is given by

$$J = \lambda \sum_{i=1}^{n} \left| y(t-i) - \hat{y}_f(t-i) \right|^2 + \nu \left(corr\left[y, \hat{y}_f \right] \right) \tag{6.7}$$

where, λ and ν are weighting coefficients and *corr(.)* is the correlation function

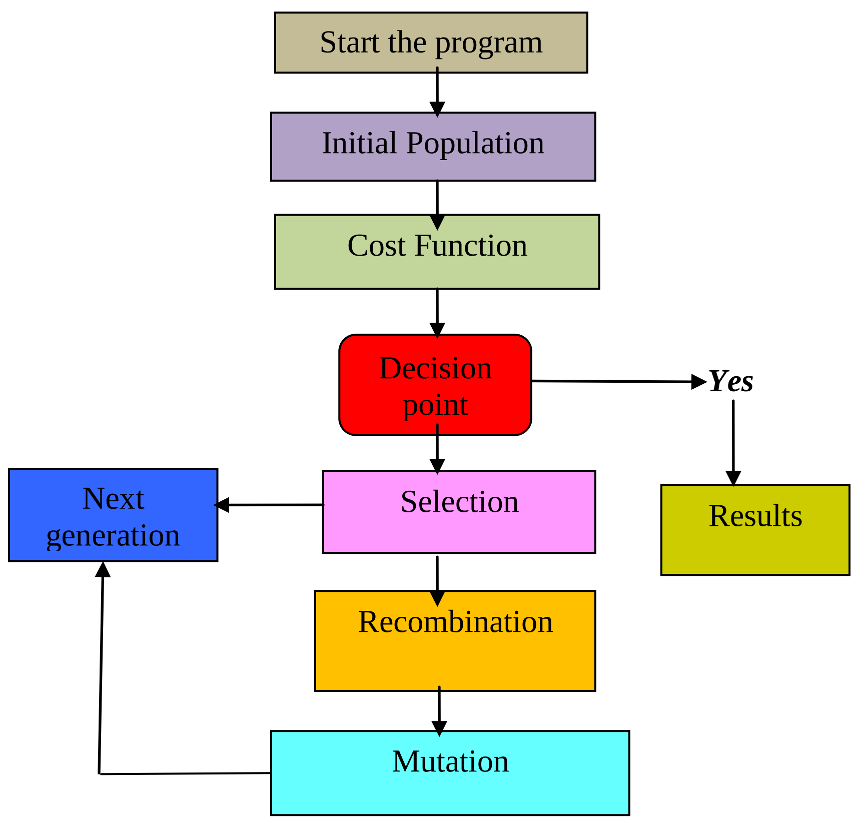

Figure 6.1 : Flow chart representation of Genetic Algorithm

To summarize, from chapter 1 to Chapter 6, we discussed about the Prosthetics literature, human hand anatomy, experimental design, data acquisition implemented in this work, filtering techniques, and proposed techniques. The next Chapter 7 i.e., Results and Discussion highlights the results obtained in this work and the discussion.

Chapter 7: Results and Discussion

This chapter is organized as four sub-sections: Filtration results, System Modeling results, data fusion results, and proposed technique i.e., DST application results.

7.1 Filtration Results

In this section, we will discuss about application of the two filtering techniques i.e., Half-Gaussian filter and Wavelet Transform based filter that are used to process the sEMG signals which are acquired at the sampling rate of 2000 samples/sec. Figure 7.1 shows the unfiltered sEMG signal from sensor 2 (s_2) and filtered signal using Half-Gaussian filter.

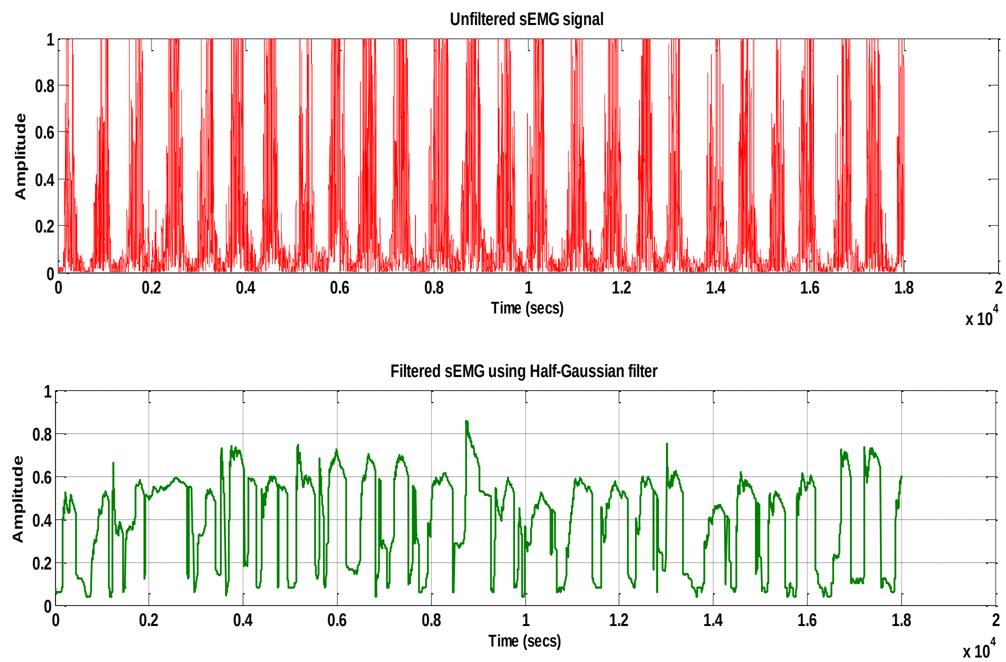

Figure 7.1 : Unfiltered and Filtered sEMG signal using Half-Gaussian filter

The latency variable x in Equation 4.5 requires a large buffer size which makes the real-time implementation impossible. Because of the limitations associated with the Half-Gaussian filter, we explored new sEMG filtration with a Discrete Wavelet Transforms (DWT) that has the capacity to be implemented in real-time. Figure 7.2 shows the unfiltered and filtered sEMG signal from sensor 2 (s_2) using WT db 44.

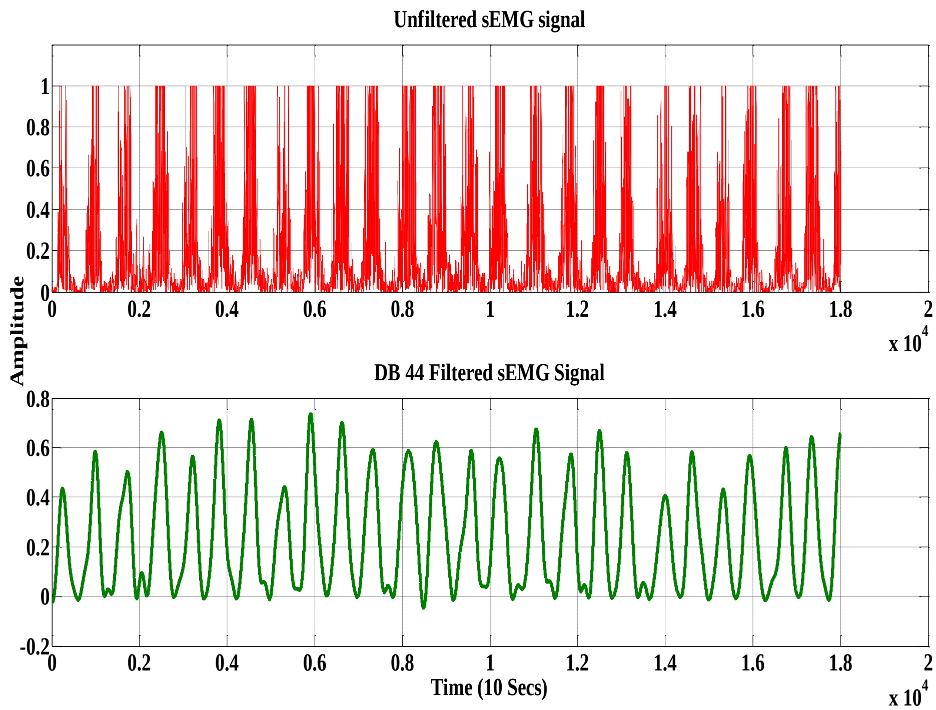

Figure 7.2 : Filtered and unfiltered sEMG using Wavelet DB 44

Figure 7.3 shows the WT based Db 44 sEMG filtered data, and the x-axis shows the sEMG data points for 9 seconds duration. Figure 7.3a shows the unfiltered and filtered (using the Db 44 wavelet) sEMG signals. Figure 7.3b shows the decomposition coefficients of the sEMG signal at each level and Figure 7.3c depicts the reconstructed approximation of the sEMG signal based on the decomposition coefficients at each level.

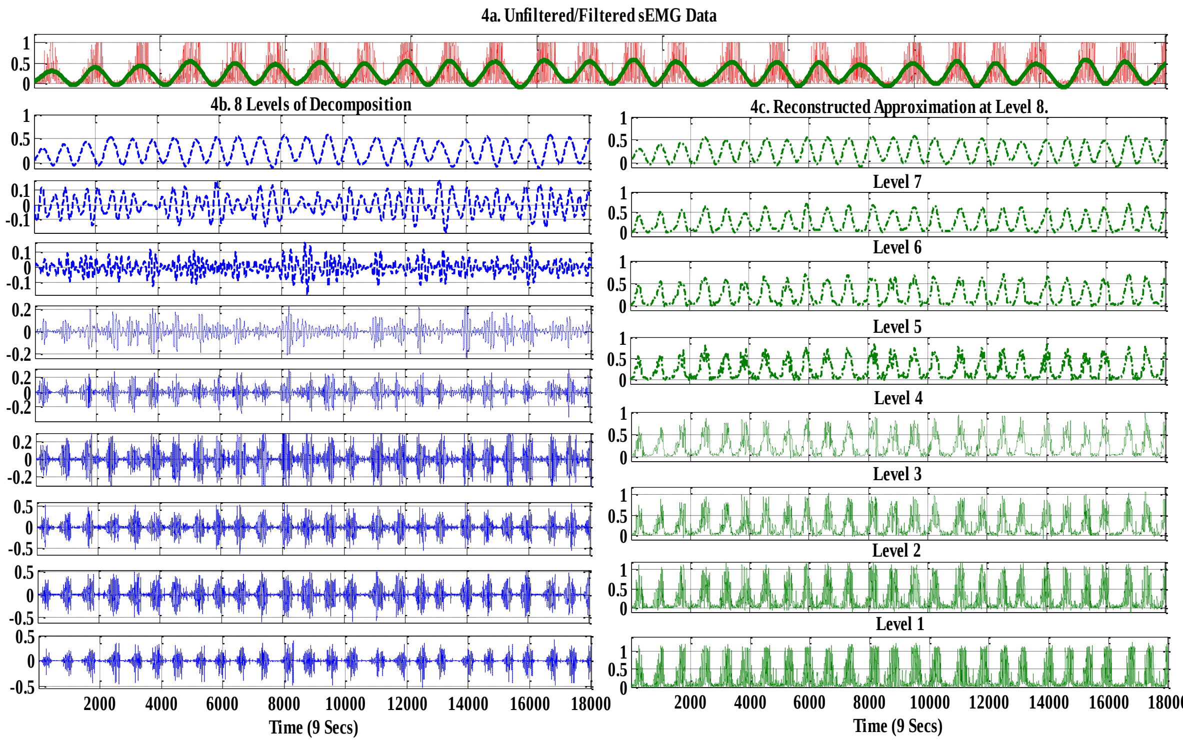

Figure 7.3: (a). Filtered and unfiltered sEMG signal using wavelets Daubechies 44 filter. (b.) 7 levels of decomposition co-efficient for the sEMG signal using wavelet Daubechies 44 filter, (c.) Reconstructed approximation of sEMG signal at each level using wavelet Daubechies 44 filter.

Similarly, DWT db 44 is used for the sEMG signals filtration acquired at a sampling rate of 2000 samples/sec from 10 test subjects. The force signal is filtered using Chebyshev type -II filter and Figure 7.4 depicts the filtered and unfiltered force signal.

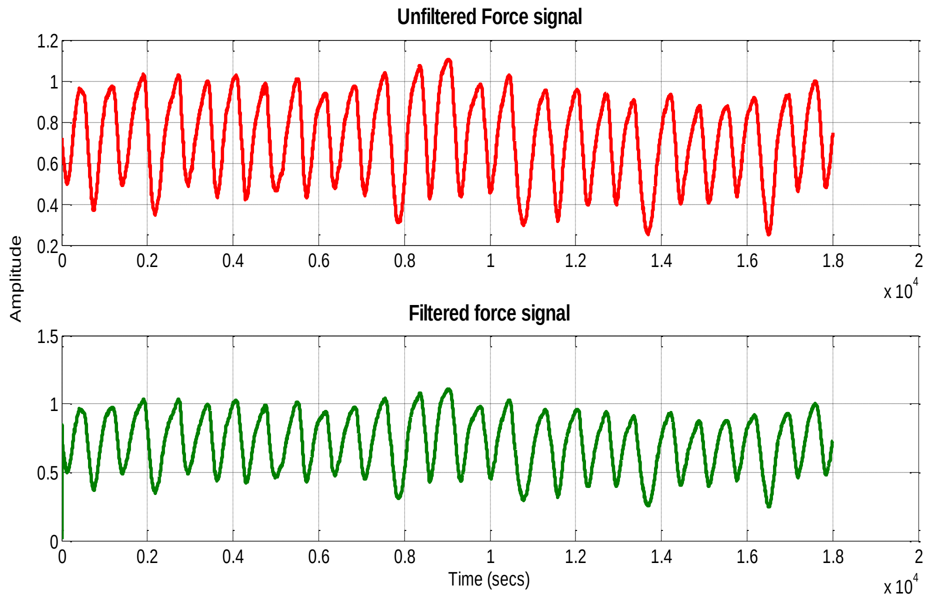

Figure 7.4: Unfiltered and filtered force signal using Chebyshev type-II

7.2 sEMG/Force Modeling

After pre-processing the data, sEMG data $u_1(t), u_2(t)$ and $u_3(t)$ from the three sEMG sensors and their corresponding skeletal force signal $Y(t)$ the data is used to identify the dynamic relationship between them by utilizing the SI technique. Four linear SI models – – ARX, ARMAX, OE and BJ are investigated to model the dynamics of the sEMG signal and the corresponding skeletal muscle force.

The modeling of linear dynamics of the sEMG signal and the corresponding skeletal muscle force are achieved by using the model structures which are shown in Figures 4.1, 4.2, 4.3, and 4.4. Table 7.1 shows the correlation coefficients for the four model structures.

Table 7.1: Percentage correlation coefficients for linear SI models

	M_1	M_2	M_3
ARX	42.48	**54.29**	45.54
ARMAX	42.11	**56.21**	51.03
OE	56.43	**72.08**	64.33
BJ	46.27	**65.32**	59.01

M_2 is the model identified from the sEMG sensor data $u_2(t)$ located on the motor unit. In all cases, the model inferred from this sensor provides a better correlation between the sEMG and the skeletal muscle force data when compared to the models M_1 and M_3 which are identified from the sensor data $u_1(t)$ and $u_3(t)$ respectively. The OE model is yielding the better performance in approximating the dynamics between the sEMG and skeletal muscle force signals and yielding a correlation of 72.08% than to the other models. Hence, for the rest of the work the OE model is utilized for all the subjects to perform the study. The following Table 7.2 provides the correlation coefficients obtained for the models for each of the 10 test subjects and each sensor combination.

Table 7.2: Percentage Correlation Coefficients using OE model structure for 10 test subjects

Subject	M_1	M_2	M_3
1	56.4	73.0	68.3
2	54.2	72.9	67.0
3	65.0	70.2	69.7

4	61.2	69.2	66.5
5	58.8	70.0	68.2
6	60.2	71.1	66.5
7	65.6	70.5	68.0
8	59.8	70.2	66.1
9	60.0	70.2	64.3
10	59.9	70.6	67.0

7.3 Proposed Methodology Results

This section discusses about the results obtained from KIC based probabilities i.e., Evidence I and Fuzzy inference based probabilities i.e., Evidence II and then will discuss about the proposed methodology results i.e., DST for motor point identification results for 10 different test subjects.

7.3.1 Kullback Information Criterion Results

After modeling the dynamics relating sEMG and finger force data, linear OE models are utilized to determine the probability of each sensor using the Kullback information Criterion (KIC), discussed in Chapter 5, Section 5.4.1.

For the given subject, a sensor array of three sEMG sensors is used. Hence, for the proposed approach, three model sets are identified accordingly as discussed in section 7.2. These models are M_1, M_2 and M_3 utilizing the three sets of sEMG data u_1, u_2 and u_3 and corresponding skeletal muscle force data Y .The individual probabilities associated for the three sensor set $\Omega = \{\{s_1\},\{s_2\},\{s_3\}\}$ are computed according to the proposed utilization of the KIC . Evidence I probabilities for the three sensors are obtained by executing the steps I to IV from Chapter 5, Section 5.4.1 and are provided in Table 7.3. for each test subject.

Table 7.3 : Evidence I from Kullback Information Criterion (KIC)

$\{s_1\}$	$\{s_2\}$	$\{s_3\}$
0.2	0.5	0.3

From Table 7.3, exhibits the probabilities normalized between 0 and 1 for convenience to be used in DST application. It is also evident that sensor 2 i.e., $\{s_2\}$ has the highest likelihood with probability of 0.5 being the location at motor point M_2 , compared to the other two sensors $\{s_1\}$ and $\{s_3\}$ located on either side of the motor point respectively.

Similarly, the probabilities for 3 sensors for a set of 10 subjects were computed and normalized between 0 and 1. Table 7.4 provides the individual KIC based probabilities.

Table 7.4: Evidence I from Kullback Information Criterion (KIC) for 10 test subjects

Subject	$\{s_1\}$	$\{s_2\}$	$\{s_3\}$
1	0.2	0.5	0.3
2	0.1	0.6	0.3
3	0.3	0.4	0.3

4	0.2	0.5	0.3
5	0.1	0.7	0.2
6	0.2	0.5	0.3
7	0.3	0.6	0.2
8	0.1	0.5	0.4
9	0.3	0.4	0.3
10	0.1	0.5	0.4

7.3.2 Fuzzy Logic Results

A second set of evidence is required for DST and are obtained from the fuzzy inference system. The three inputs for the FIS are entropy(η), correlation(ρ) and relative error(e). These are computed by executing the steps V to VIII from Chapter 5, Section 5.4.2. Table 7.5 provides the entropy, correlation, and relative error for M_1, M_2 and M_3 obtained for three sensors sEMG and their corresponding force signals using OE based SI technique.

Table 7.5 : Entropy, Correlation and Relative Error for the three models obtained from OE models

S	M_1			M_2			M_3		
	η	ρ	e	η	ρ	e	η	ρ	e
1	30.67	56.46	0.31	27.4	73.05	0.17	41.93	68.32	0.52
2	32.48	54.27	0.40	26.09	72.92	0.13	41.43	67.05	0.47

3	32.21	65.03	0.23	28.71	70.28	0.19	39.08	69.73	0.58
4	31.67	61.25	0.29	27.98	69.24	0.20	40.35	66.57	0.51
5	39.53	58.84	0.55	29.55	70.06	0.18	30.92	68.26	0.27
6	32.67	60.27	0.57	27.60	71.12	0.19	39.73	66.58	0.24
7	33.56	65.60	0.21	28.39	70.50	0.19	38.05	68.09	0.60
8	30.12	59.81	0.21	26.05	70.23	0.15	43.83	66.11	0.64
9	42.29	60.08	0.61	26.11	70.25	0.13	31.60	64.32	0.26
10	33.23	59.90	0.25	28.92	70.61	0.17	37.85	67.06	0.55

Considering the Entropy, Correlation and Relative error as inputs, the following set of rules are defined for the FL inference system:

(1.) If Entropy is low or Correlation is low or Relative error is high then weight is VLW

(2.) If Entropy is Low or Correlation is Medium or Relative error is Medium then weight is MLW

(3.) If Entropy is low or Correlation is High or Relative error is Low then weight is LW

(4.) If Entropy is Medium or Correlation is Medium or Relative error is Medium then weight is LMW

(5.) If Entropy is Medium or Correlation is High or Relative error is Low then weight is MW

(6.) If Entropy is Medium or Correlation is High or Relative error is Low then weight is MHW

(7.) If Entropy is High or Correlation is High or Relative error is Low then weight is LHW

(8.) If Entropy is High or Correlation is High or Relative error is Low then weight is HW

(9.) If Entropy is High or Correlation is Medium or Relative error is Medium then weight is MHW

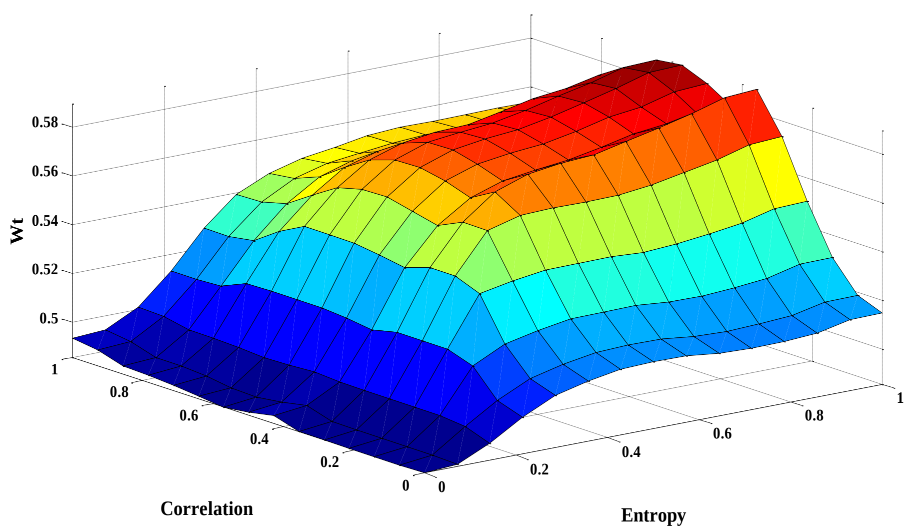

Figure 7.5 : Surface plot for the entropy, correlation coefficients and the corresponding weights for each sensor

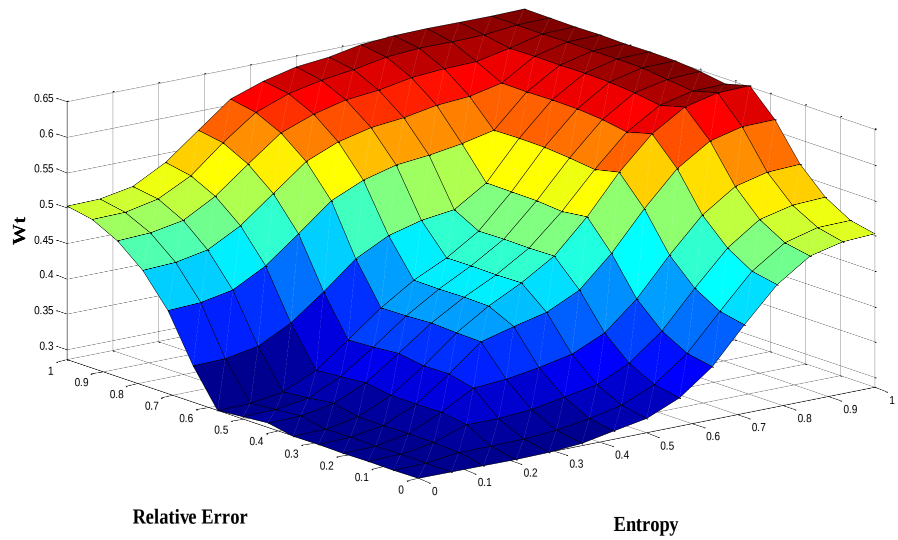

Figure 7.6: Surface plot for the entropy, RE and the corresponding weights for each sensor

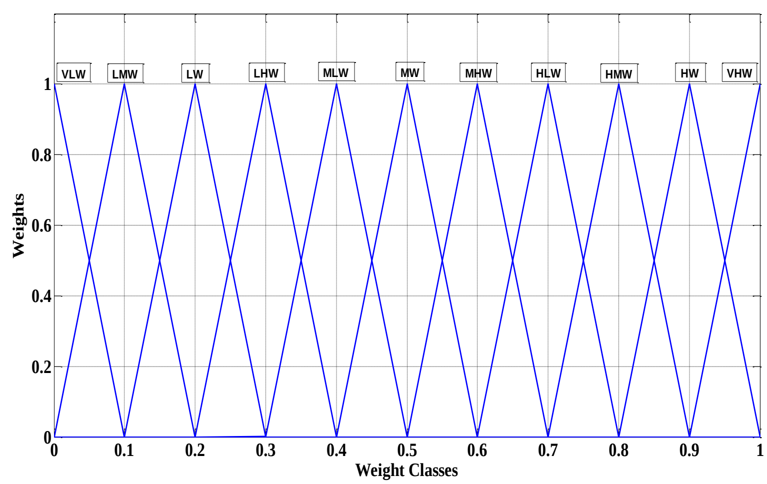

Figure 7.7 : Weight classes for the fuzzy inference system

Figures 7.5 and 7.6 show the fuzzy inference system surface plots based on entropy, RE and the correlation coefficient for each sensor. Figure 7.7 shows the triangular defuzzification for the output weights of the fuzzy inference system, where VLW, LMW, LW LHW, MLW, MW, MHW, HLW, HMW, HW and VHW represents weights of the models based on Entropy (η), Relative Error (e) and the correlation(ρ).

The fuzzy inference system assigns the probabilities to the possible sets of the three sensors i.e., $\{\{s_1\},\{s_2\},\{s_3\},\{s_1,s_2\},\{s_2,s_3\},\{s_1,s_2,s_3\}\}$ and the obtained probabilities are normalized between 0 and 1. Table 7.6 provides the normalized probabilities for each sensor and the combinations of the sensors for one test subject

Table 7.6: Evidence II from Fuzzy Inference

$\{s_1\}$	$\{s_2\}$	$\{s_3\}$	$\{s_1,s_2\}$	$\{s_2,s_3\}$	$\{s_1,s_2,s_3\}$
0.1	0.3	0.1	0.2	0.1	0.2

Similarly, the second evidence set for 10 test subjects weights are obtained by the use of the propose of Fuzzy logic concept. Table 7.7 provides the normalized sensor probabilities for 10 test subjects.

Table 7.7: Evidence from Fuzzy inference for 10 test subjects

Subject	$\{s_1\}$	$\{s_2\}$	$\{s_3\}$	$\{s_1,s_2\}$	$\{s_2,s_3\}$	$\{s_1,s_2,s_3\}$
1	0.1	0.3	0.1	0.2	0.1	0.2
2	0.1	0.2	0.1	0.1	0.2	0.3
3	0.1	0.1	0.1	0.2	0.3	0.3
4	0.1	0.1	0.1	0.3	0.3	0.2
5	0.1	0.2	0.2	0.1	0.2	0.2
6	0.2	0.3	0.1	0.1	0.1	0.2

7	0.1	0.2	0.2	0.1	0.2	0.2
8	0.1	0.2	0.1	0.2	0.1	0.3
9	0.1	0.2	0.1	0.2	0.1	0.3
10	0.1	0.1	0.1	0.2	0.2	0.2

7.3.3 Dempster Shafer Theory Results

From Tables 7.3 and 7.7, it is apparent that probability assignments from two evidences differ from each other. Based on the obtained evidences, the DST concept will be applied and determine the motor point location.

Using these evidences, DST models the conflict between the obtained information. Table 7.8 provides the masses (probabilities) that are the union of the two evidences to evaluate the belief and plausibility functions as given by Equation (5.2).

By substitution of the belief and plausibility in Equation 5.2, and using the proposed DST rules of combination, the resulting probabilities are computed and provided in Table 7.9 for one test subject.

Table 7.8 : Masses for believe and plausibility functions

	$\{s_1\}$ 0.2	$\{s_2\}$ 0.5	$\{s_3\}$ 0.3
$\{s_1\}$ 0.1	0.02	0	0
$\{s_2\}$ 0.3	0	0.15	0
$\{s_3\}$ 0.1	0	0	0.03
$\{s_1, s_2\}$ 0.2	0.04	0.1	0
$\{s_2, s_3\}$ 0.1	0	0.05	0.03
$\{s_1, s_2, s_3\}$ 0.2	0.04	0.10	0.06

Table 7.9 : DST results for the three sensors

$\{s_1\}$	$\{s_2\}$	$\{s_3\}$
0.20	0.51	0.24

From Table 7.9, one can infer that sensor s_2 has a probability of 0.51 of being the sensor on the motor point when compared to the other two sensors closest to the corresponding motor point. Similarly DST was applied to 10 test subjects to determine the probability of each sensor. Table 7.10 provides the individual probabilities for three sensors $\{s_1\}$, $\{s_2\}$, $\{s_3\}$ of 10 test subjects.

Table 7.10 : Probabilities of three sensors obtained by using KIC and FL as evidences to DST

Subject	$\{s_1\}$	$\{s_2\}$	$\{s_3\}$
1	0.20	0.51	0.24
2	0.25	0.62	0.33
3	0.31	0.59	0.45
4	0.32	0.64	0.41
5	0.12	0.66	0.30
6	0.18	0.54	0.21
7	0.14	0.55	0.26
8	0.12	0.40	0.31
9	0.20	0.47	0.33
10	0.11	0.56	0.33

7.4 Data Fusion Results

As mentioned in Chapter 6, in our previous work we explored three different fusion algorithms based on Akaike Information Criterion, Bayesian Information Criterion and Kullback Information Criterion. In this work we investigate another fusion algorithm based on Minimum Description Length Criterion as well. For statistical comparison purpose, we compute the four different criterion based fusion algorithms for 10 test subjects in this work.

Before computing the fusion algorithm, the n value in all the equations 5.4, 6.3, 6.4 and 6.5 is optimized by an elitism based GA.

The literature addressing the use of the criterions for the purpose of data fusion, the number of data points used has been set to some small number, i.e. quite often one finds $n = 30$. However, there is no analysis existing to support this selection. Using the proposed GA and objective function as defined in Equation 6.6, and the two model structures to characterize the sEMG relationship to skeletal muscle force, the resulting quality of the extracted OE models is rather insensitive to the number of data points used to compute the criterion. In this work, the search area has been confined to a range of 145 data points and the conclusions are to be made only for this range. The extended range has not been a topic of this investigation and may hold improved results. However, the computational cost increases substantially with larger numbers of data point for the computation of the probability based criterions, which is reflected in longer computation times, and is unpractical for modelling sEMG signals of muscle forces.

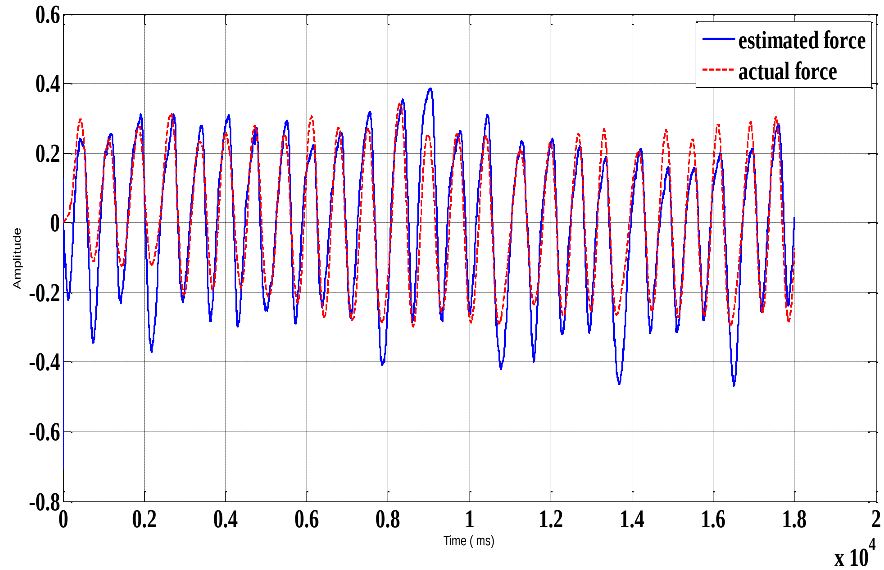

Figure 7.8. : Measured force vs. estimated force using Output Error Models.

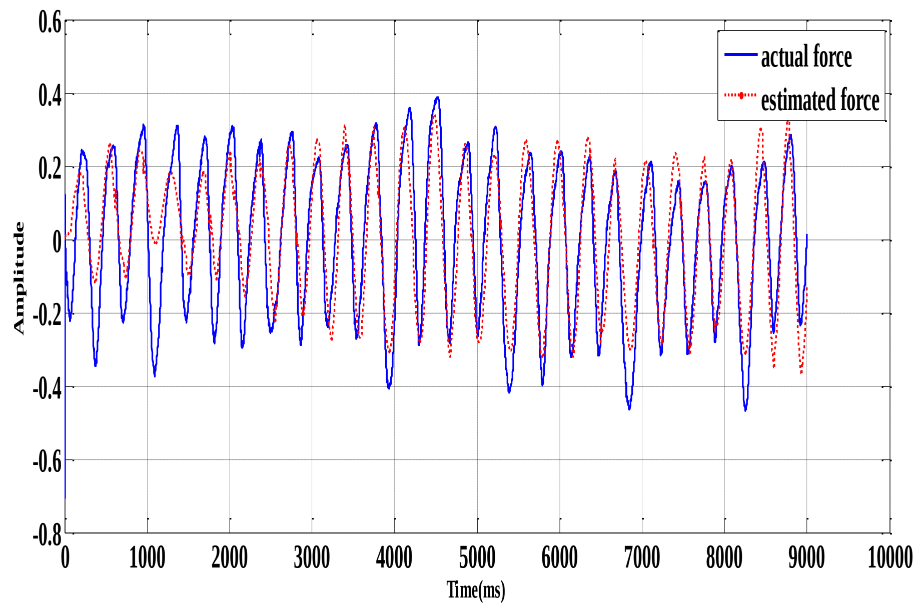

Figure 7.9: Measured force vs. estimated force for down sampled data using Output Error Models.

.

Figures 7.8 and 7.9 shows the actual force and estimated force for the linear OE models, the correlation between the actual force and the estimated force is independent of the sampling rate and is 85% for both cases, 1000 Hz and 2000 Hz.

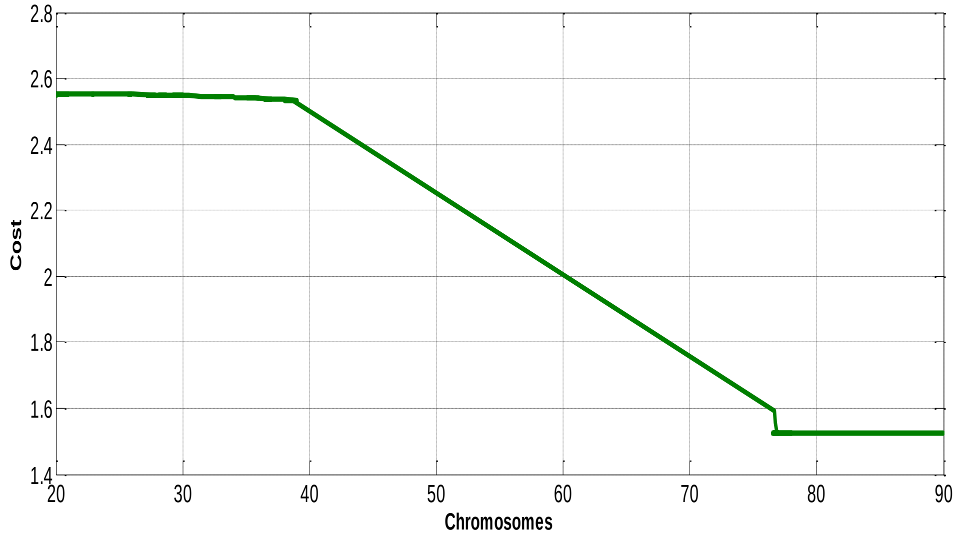

Figure 7.10: Minimum cost for GA using 100 generations.

The minimum cost as defined by Equation 6.6 for a GA using 100 generations is shown for each iteration in the Fig. 7.10.

Table 7.11 : Comparison of Model Probability for three sensors

n	$pmz1$	$pmz2$	$pmz3$	Corr
30	0.35	0.62	0.49	0.8651
50	0.46	0.62	0.37	0.8653
75	0.31	0.68	0.43	0.8655
100	0.48	0.59	0.38	0.8656

For Table 7.10 $pmz1$, $pmz2$ and $pmz3$ - are the individual probabilities of the models M_1, M_2 and M_3 , corr- stands for the correlation between actual force and estimated force.

From Table 7.11, we can infer that the highest correlation is at the optimum value. However, the sensitivity with respect to the number of data points '*n*' used in the fusion algorithm is minimal. This implies that the selection of the number of data points '*n*' has little influence on the fusion algorithm and can be chosen small in order to preserve computational efficiency.

Table 7.12: Fusion algorithm comparison of percentage mean correlation coefficients for OE models for 10 test subjects

Subjects	M_1	M_2	M_3	**AIC**	**BIC**	**KIC**	**MDL**
1	56.4	73.0	68.3	78.5	73.6	86.0	72.8
2	54.2	72.9	67.0	77.3	74.0	86.7	73.6
3	65.0	70.2	69.7	76.3	74.1	86.3	73.0
4	61.2	69.2	66.5	76.9	73.6	85.1	72.5
5	58.8	70.0	68.2	76.2	74.7	87.2	73.3
6	60.2	71.1	66.5	78.7	73.9	86.7	73.1
7	65.6	70.5	68.0	77.2	74.5	86.0	73.8
8	59.8	70.2	66.1	77.4	73.6	85.9	72.0
9	60.0	70.2	64.3	78.6	74.5	85.2	72.6
10	59.9	70.6	67.0	77.2	72.6	86.7	72.2

Table 7.12 gives the individual estimated model correlation values M_1, M_2 and M_3 of the three sensors and also gives the overall fused force correlation values for the linear parametric OE models. The fusion models are computed by using the probability based criterions - AIC, BIC, KIC and MDL. In all the cases, the values are high for M_2 which is the estimated model output for the sensor placed on the motor unit when compared with other models M_1 and M_3. Therefore, it can be inferred that the sensor located directly on the motor point is giving data that is more suitable to extract useful information when compared with the other sensory data.

It can also be inferred from Table 7.12, M_3 is yielding the next best performance when compared with M_1. But in case of subject 3, 4, and 8, the individual correlations of the three sensors are very close to each other. This could be due to motor point location in reference to sensor alignment and crosstalk and noise interference. Although better individual models can be inferred by using SI technique, fusion algorithm improves the estimated force output consistently. All the three models are fused by using the probability based proposed criterions- AIC, BIC, KIC and MDL based fusion algorithm. Even thought, the fusion algorithms shows improvement in the overall correlation value in the all cases, KIC based fusion algorithm worked best for the linear Output Error (OE) models for 10 subjects when compared to AIC, BIC and MDL. Since KIC is an asymmetric measure of the models dissimilarity it would work better for the bio-medical signals when compared to AIC, BIC and MDL.

Chapter 8: Conclusion and Future Work

8.1 Conclusion

Determination of motor point locations on a forearm allows for proper sEMG sensor placement. In addition, utilizing a sensor array, as proposed in earlier works by the authors, the operation and control of myoelectric based prosthetic devices can be enhanced. Currently, there is no algorithm available to determine these locations without electrical stimulation. The common method employed is by using an external electrical stimulator, testing various region of the forearm, until a corresponding joint motion occurs. This procedure is time consuming, and uncomfortable for the patient. For prosthetic device users, once the EMG sensor is placed at the identified location, movement due to the use of the prosthetic device usually results in a mismatch of the sEMG sensor and motor point location. Regardless of the matching objective, i.e. on a motor point or distinctly away from a motor point, relative movements between the motor point and the sensor may negate this objective and lead to greatly reduced performance of the device. The proposed algorithm along with a sensor array, allows for automatic assignment of motor point locations, with the resolution of the sensor arrays special dimension. The experimental results presented in this work are preliminary and will be extended in the near future to a statistical investigation. However, along with simulation results, the proposed algorithm shows promise to allow for detecting sensor allocation with motor point location, as well as motor point identification. As an extension of this work, utilizing a dense sensor array, in terms of spatial dimensions, a tracking algorithm can be developed based on the proposed algorithm identifying which sensor is closest to the corresponding motor point.

8.2 Future Work

Research has shown that the adaptation of the prosthetic arm is conditional to a system that provides distally referred sensations of touch and joint movements [106]. It is postulated that to achieve greater dexterity and performance, prostheses without a sensory feedback system will be obsolete, [107-109]. It was assumed for a long time that the replacement of a natural arm with intelligent prosthetic arm is an impossible task. The main discrepancy lied in the insufficient analysis of the concept of sensory feedback and by not taking into account the knowledge of physiology of kinesthesis [110]. However with the passage of time, and as the technology matured, these factors were taken into account and later formed the base for a modern prosthetic hand.. By using the sensory feedback, natural ambiences can be provided to the prosthetic hand users. It will help the user to have more control on the hand and can be fully embedded into the work as a normal person without any disability [111].

Sensory feedback can be obtained by the use of different implantable electrodes, such as needle or cuff electrodes. For robotic hands, [112] used this principle to excite the responsible nerves directly. They implanted the electrodes in fascicles of the nerves of amputees. The stimulation through these electrodes gives the feedback information on grip strength and position of the limb. This is not a closed-loop system and has some limitations in terms of optimization.

External sensors and switches are usually used in controlling functional neuromuscular simulation systems (FNS). They pose problems such as donning, and calibration. For implementation artificial sensors are difficult to build and are insufficiently bio compatible. Now-a-days with the advancement of electrical interfacing with nerves and muscles, natural sensors are being considered as an alternative source of feedback and command signals for FNS. For high-level control natural or artificial sensors can equally perform for decision making methods. Surface electromyography (sEMG) signals are being 1000 times larger than electro neuro organs are easier to measure, but have not provided reliable indicators so far. Characteristics like muscle fatigue are not indicated by these which are in FNS systems [113]. Andrew et.al, [114] explained about the electrocutaneous stimulation for sensory communication in rehabilitation engineering. Some procedures for implementing electro tactile displace and generating reliable, pain free sensations with a useful communication bandwidth. This paper presents an overview of what technologies have been developed in recent years and tries to forecast the direction of future research based on the current state of knowledge for advancing sensory feedback based prosthetic hands.

Some efforts have been made in recent years to address sensory feedback for the prosthetic users, [115]. The sensory feedback system interacting with the prosthetic and sensory cortex needs to be capable of communicating with both systems simultaneously, avoid issues of fatigue, assimilation, as well as be capable of sensing through the mechanical hand various types of signals, such as pressure, texture, temperature, shear forces, and surface conditions. In the following, we present a brief review of the inner workings of sensation through healthy human skin. There are numerous afferent receptors in the human skin to sense different sensation ranging from touch to temperature. In particular, there are cutaneous mechanoreceptors, thermoreceptors, nociceptors, bulboid corpuscles and chemoreceptors.

Cutaneous Mechanoreceptors are free nerve endings, sensing touch, pressure, and stretch. They are classified into four main types in the human skin:

1. Ruffini’s end organs detect touch, pressure and tension deep in the skin. They are located all over the skin and are rather slowly adapting nerve endings and sensitive to skin stretch. Ruffini’s end organs are mainly helpful with sense of and control of finger position and movement; they are also useful for detecting slippage of objects along the surface of the skin. Hence they help control grip force.
2. Meissner’s corpuscle (or tactile corpuscle) is a mechanoreceptor (nerve ending). The location of Meissner’s corpuscles is the glabrous skin. They detect changes in texture (most sensitive if vibration occurs below or around 50 Hz), are receptive to light touch sensation. Meissner’s corpuscles are dynamic in nature, which results into rapid adaptation to external stimuli.
3. Pacinian corpuscles are fewer in number compared to Meissner and Merkel’s discs, but adapt very rapidly. The location of Pacinian corpuscles are in subcutaneous tissue, interosseous membranes. Pacinian corpuscles detect rapid vibrations (about 200-300 Hz). They are nerve endings in the skin which are sensitive to pain and deep pressure (poking), and are also dynamic (adapt to stimuli).

4. Merkel’s discs are located in all of the human skin and in hair follicles. Merkel’s disc detects sustained touch and pressure and can distinguish shapes and textures. These

receptors are good for touch and pressure. Their adaptation rate is rather slow as they are static in nature.

The location of the four mechanoreceptors is shown in Figure 2.7.

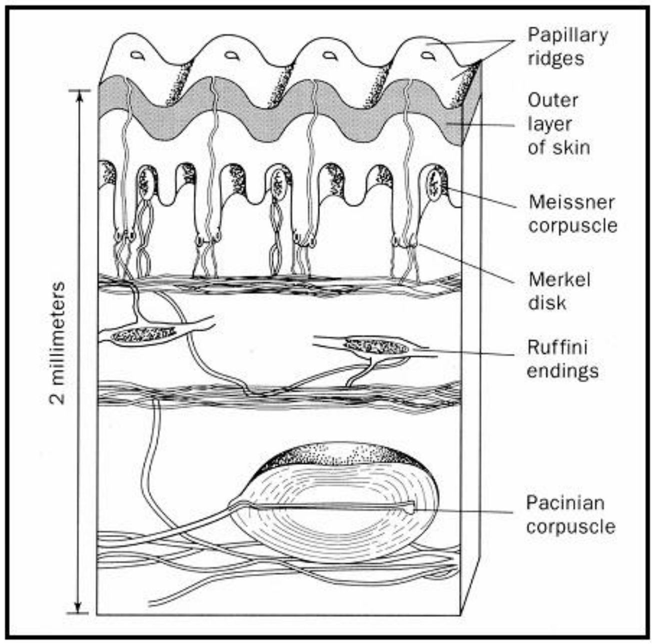

Figure 8.1: Mechanoreceptors location in human skin [116].

Thermoreceptors: are sensory neurons that sense changes in temperature. Heat is sensed through unmyelinated C-fibers, which possess a low conduction velocity. This result into the transmission of sensed information transmitted to the brain within a few seconds. Cold is sensed using C-fibers and thinly myelinated A-delta fibers, which conduct the information to the brain faster (within one second) [112]. For warm receptors, the warming effect is translated into an increase in action potential discharge rate, while cooling results in a decrease of the discharge rate. For cold receptors this is inverted, where the action potential firing rate is increased when cooling occurs and decreased when warming occurs. There is some literature [117]which notes that above 45^{o}C, some cold receptors also respond with an action potential discharge due to the increased temperature (paradoxical response to heat).

Cutaneous Nociceptors: is a skin receptor responsible of detecting damaging stimuli and alarming the system by creating the perception of pain. There are also thermal nociceptors which generate heat pain for temperatures above 42^{o}C.

While healthy subjects have access to all the information gathered by these receptors, individuals with amputations have to relearn how to collect information about an object they touch with the prosthetic. Recent research has shown that sensory feedback of contact information from the prosthetic with its surroundings improves the user's ability to control and adapt to the prosthetic [118]. Currently, most work addressing the inclusion of feedback for the prosthetic user addresses only very basic elements such as tactile feedback about finger pressure.

Holmes, [118] addressed the mental representation for sensory inputs of the human body within the brain. This input from the periphery has a strong effect on the perceptual awareness of body parts, natural or appended prosthesis for identifying its own body and for identifying artificial limbs. With sensory inputs, control and handling of the prostheses are improved. Some efforts have been made in recent years to address sensory feedback for the prosthetic users. For example, [119] used electrical stimulation to communicate pressure or position of the prosthesis in order to provide a closed- loop control of the hand. The most successful methods for communicating peripheral inputs were Electrical Surface Simulation (ESS) and Mechanical Surface Simulation (MSS), [120, 121]. Research shows that electro-tactile stimulators allow the distinction of 59 different sensations; the mechanical vibrator is able to transmit 16 different sensations, [122].

Tactile sensors can be split into two types: active and passive. In the general scenario, tactile sensory user interfaces passive touch i.e., stimulation is made passively on the surface of the skin. In some instances, in which when an object needs to be identified active touch comes into picture. This active touch utilizes distinct shapes and texture and encodes this sensory information which helps to identify the object without visual contact. In the active touch scenario shape encoding is very important, [123]. The tactile sensors can be used with electrical, pneumatic, and electro-mechanical devices. In the following sections the two most prevailing sensory feedback systems are discussed.

8.2.1 Mechanical Stimulation

In the case of electro-mechanical (vibro tactile) devices, a mechanical vibration or touch is produced and super-positioned onto a healthy skin area with functional mechano-receptors. The vibro tactile displays are classified into two basic types. They are pins and large point contact stimulators, [124].

The pin type vibro tactile displays based on piezoelectric bimorph pins are convenient and simple to use. They are non-invasive with good two point discrimination. These pin types are very good in presenting fine cues for surface texture edge and line detection when used as an array, [125]. In contrast, large contact point stimulators are very simple vibrators that are pressed against the skin surface. They yield much lower resolution when compared to the pin type. But the advantage with these types of simulators is that they can be distributed over large section of the body. Therefore multiple simultaneous cues for surface texture, edge and line detections [126] can be produced.

The mechanical stimulation uses pneumatic devices such as bladders or pockets which can be inflated or deflated, [127]. Hence they create a pulsing sensation that the user can easily feel. These devices can either be attached directly or to other devices that are used to complete the tasks. The main advantages of these pneumatic devices (bladders) – when compared to vibrotactile displays – are localization i.e., they have significantly low interference with the nearby bladders, the pump mechanism can be mounted remotely such that the control devices will require a minor modification. A variety of sensory information of the stimulus can be generated by altering the configuration or shape of these bladders [127,128].

A number of studies have been conducted using the mechanical vibrator as basis [46, 50, 129, and 130]. This approach generally leads to a higher acceptance rate by the user as well as an increased users' performance (time and efficiency of use). However, there are some limitations with mechanical stimulation, mechanical vibration is limited to 16 sensations when used as a source of sensory feedback, they are bulkier and hard to control, and the pneumatic tactile displays include leak control, and air compressibility issues.

8.2.2 Electrical stimulation

In order to design better prostheses with vibro-tactile feedback, electrical stimulation of the muscles is necessary. By applying the electrical currents paralyzed muscles can be made to contract. These electrically elicited muscle contractions are controlled in such a way that the prosthesis acquires its full functionality. This technique is called “functional electrical stimulation”. There is a lot of ongoing research on FES systems to restore the functionality of the upper and lower extremity prosthesis [131]. *Kajimotoet. al*,[132] used an electrode array with a particular distribution of the electrode’s charge to communicate with the user, the sensation of pressure at the fingertips. Their smart touch prototype consists of optical sensors to capture an image and convert that into tactile information and displays through electrical stimulation. Using an electro-tactile system makes it possible to access seven (7) different classes of mechanoreceptors, two (2) classes of thermo receptors, four (4) classes of nocioceptors, and three (3) classes of proprioceptors within the human skin, [133-138]. To utilize the possible 59 sensations from electrical stimulations, Szeto et. al [137] used electro-tactile stimulations by changing frequency and intensity of the feedback. In [139], the authors used interferential stimulation to transit spatial movement of the hand. Electrical stimulation is described in literature by using voltage-regulated stimulation, [139]. Voltage-regulated systems are sensitive to changes in the amputee’s skin impedance. In reference [140], this problem was addressed by creating a voltage-regulated stimulator with a high frequency biphasic waveform. This approach lead to the avoidance of sensitivity (ability to discriminate objects) drop off. Array sensors have been used successfully for different purposes [141, 142]. As above mentioned, work presented in [133] utilize an electrode array. A rather large array was used by [143], where 144 electrodes are used on a blind person’s tongue in order to provide some spatial awareness of his/her surroundings. Electrode arrays for feedback have numerous advantages and can help tailor the sensory feedback system to the skin area chosen.

References

[1] Amputee Coalition of America (ACA) National Limb Information Center Limb Loss Facts in the United States

[2] Causalities in Afghanistan & Iraq. www.unknownnews.net. June 5. 2006

[3] Ziegler-Graham K, MacKenzie EJ, Ephraim PL, Travison TG, Brookmeyer R."Estimating the prevalence of limb loss in the United States: 2005 to 2050". Arch Phys Med Rehabil. 2008 Mar;89(3):422-9.

[4] A. Esquenaziand Robert HM., "Rehabilitation in limb deficiency and amputation", Arch. Phys. Med. Rehabil. 1996 Marc :7(3):18-28.

[5] Merrill DR, Lockhart J, Troyk PR, Weir RF, Hankin DL. Development of an implantable myoelectric sensor for advanced prosthesis control. Artif Organs.2011 Mar;35(3):249-52.

[6] Biddiss EA, Chau TT. Upper limb prosthesis use and abandonment: a survey of the last 25 years. Prosthet Orthot Int. 2007 Sep;31(3):236-57.

[7] Kyberd PJ, Hill W. Survey of upper limb prosthesis users in Sweden, the United Kingdom and Canada. Prosthet Orthot Int. 2011 Jun;35(2):234-41

[8] http://www.aboutonehandtyping.com/statistics.html

[9] http://www.limbless-association.org/wp-content/uploads/2010/09/Types-of Amputation.pdf

[10] E.F. Murphy and A.B. Wilson, Limb Prosthetics and orthotics, In M. Clynes and J.H. Milsum , editors, Biomedical Engineering Systems, pp 489-549, Mcgraw-Hill, New York, NY, 1970.

[11] http://www.amputee-coalition.org/military-instep/prosthetic-devices-upper.html

[12] http://www.nist.gov/tip/wp/pswp/upload/239_limb_prosthetics_services_devices.pdf

[13] D.S. Naidu and C.H. Chen, " Control strategies for Smart Prosthetic Hand Technologies: An Overview,", Book Chapter 14, Distributed Diagnosis and Home Healthcare (D2H2), vol 2, American Scientific Publishers, CA, January 2011.

[14] Arendt-Nielsen L, Zwarts M. Measurement of muscle fiber conduction velocity inhumans: techniques and applications. J Clin Neurophysiol. 1989 Apr;6(2):173-90.

[15] Naumann M, Reiners K. Diagnostic value of in situ muscle fiber conduction velocity measurements in myopathies. ActaNeurol Scand. 1996 Feb-Mar;93(2-3):193-7.

[16] Van der Hoeven JH, Zwarts MJ, Van Weerden TW. Muscle fiber conduction velocity in amyotrophic lateral sclerosis and traumatic lesions of the plexus brachialis. Electroencephalogr Clin Neurophysiol. 1993 Oct;89(5):304-10.

[17] Farina D, Fortunato E, Merletti R. Noninvasive estimation of motor unit conduction velocity distribution using linear electrode arrays. IEEE Trans Biomed Eng. 2000 Mar;47(3):380-8.

[18] De Luca CJ. Physiology and mathematics of myoelectric signals. IEEE Trans Biomed Eng. 1979 Jun;26(6):313-25.

[19] . Stulen FB, DeLuca CJ. Frequency parameters of the myoelectric signal as a measure of muscle conduction velocity. IEEE Trans Biomed Eng. 1981 Jul;28(7):515-23.

[20] Rau G, Disselhorst-Klug C. Principles of high-spatial-resolution surface EMG(HSR-EMG): single motor unit detection and application in the diagnosis of neuromuscular disorders. J Electromyogr Kinesiol. 1997 Dec;7(4):233-239.

[21] Carlo J. De Luca, Alexander Adam, R Wotiz, D Gilmore, S. Hamid, Decomposition of surface EMG signals, J. Neurophysiology, 2006 ; 96: 1646-1657.

[22] Chauvet E, Fokapu O, Hogrel JY, Gamet D, Duchêne J. Automatic identification of motor unit action potential trains from electromyographic signals using fuzzy techniques. Med Biol Eng Comput. 2003 Nov;41(6):646-53.

[23] Holobar A, Minetto MA, Botter A, Negro F, Farina D. Experimental analysis of accuracy in the identification of motor unit spike trains from high-density surface EMG. IEEE Trans Neural Syst Rehabil Eng. 2010 Jun;18(3):221-9.

[24] Glaser V, Holobar A, Zazula D. Real-time motor unit identification from high-density surface EMG. IEEE Trans Neural Syst Rehabil Eng. 2013 Nov;21(6):949-58.

[25] Rojas-Martínez M, Mañanas MA, Alonso JF, Merletti R. Identification of isometric contractions based on High Density EMG maps. J Electromyogr Kinesiol. 2013 Feb;23(1):33-42.

[26] Katsis CD, Goletsis Y, Likas A, Fotiadis DI, Sarmas I. A novel method for automated EMG decomposition and MUAP classification. Artif Intell Med. 2006 May;37(1):55-64.

[27] Zarei, E. Maghooli, K. Firoozabadi, S.M.P.A new approach for EMG Decomposition Based on Overlaps solution, IEEE Digital Signal Processing, pp. 119-122, 2007.

[28] Zhu X, Zhang Y. High-density surface EMG decomposition based on a convolutive blind source separation approach. Conf Proc IEEE Eng Med Biol Soc. 2012; 2012:609-12.

[29] www.wikipedia.org

[30] http://www.britannica.com/EBchecked/topic/448388/pectoral-girdle

[31] http://www.getbodysmart.com/ap/skeletalsystem/skeleton/appendicular/upperlimbs/menu/menu.html

[32] A. Sheri. “Skeletal System.” The Upper Limb (Arm). Exploring Nature Resource2005-2009.August2,2009..http://exploringnature.org/db/detail.php?dbID=24&detID=31

[33] http://www4.nau.edu/biology/bio201/skeletal_muscle_system_and_upper.htm

[34] http://www.revolutionarytennis.com/Serve/body_UP_Contact/wrist_and_hand_terms_copy.jpg

[35] http://patientsites.com/media/img/380/hand_anatomy_nerves01.jpg

[36] http://www.tekyard.com/DesktopDefault.aspx?tabid=456&inventoryID=41311

[37] http://www.tekyard.com/DesktopDefault.aspx?tabid=456&InventoryID=41311Gallagher, Martin . "Driver Fatigue Detection Project." 07042009. National University of Ireland, Galway . 07 Apr 2009 <http://ohm.nuigalway.ie/0607/03gallagher/report.html

[38] http://www.dotmed.com/listing/muscle-stimulator/richmar/hv-1000/778680

[39] J.S. Wilson, Sensor Technology Handbook, Newnes, Elsevier Inc.,USA.

[40] http://www.robotshop.ca/interlink-05-circular-fsr-3.html.

[41] http://www.delsys.com/Products/Bagnoli_Desktop.html

[42] http://www.trossenrobotics.com/productsdocs/2010-10-26-DataSheet-FSR402-Layout2.pfd

[43] http://www.isek-online.org/standards_emg.thml

[44] A. Urfer, J. Creelman, P. Kumar, A. Sebastian, M. Anugolu and M.P. Schoen, The development of a Functional Amputation Residuum measurement of the Upper extremity for Potential Myoelectric Prosthetic.

[45] Stashuk D. EMG signal decomposition: how can it be accomplished and used? J Electromyogr Kinesiol. 2001 Jun;11(3):151-73.

[46] Raez MB, Hussain MS, Mohd-Yasin F. Techniques of EMG signal analysis:detection, processing, classification and applications. Biol Proced Online.2006;8:11-35. Epub 2006 Mar 23. Erratum in: Biol Proced Online. 2006;8():163.

[47] Zecca M, Micera S, Carrozza MC, Dario P. Control of multifunctional prosthetic hands by processing the electromyographic signal. Crit Rev Biomed Eng.2002;30(4-6):459-85.

[48] Sanger TD. Bayesian filtering of myoelectric signals. J Neurophysiol. 2007 Feb;97(2):1839-45. Epub 2006 Dec 20.

[49] De Luca CJ, Gilmore LD, Kuznetsov M, Roy SH. Filtering the surface EMG signal: Movement artifact and baseline noise contamination. J Biomech. 2010 May 28;43(8):1573-9.

[50] Potluri C, Anugolu M, Schoen MP, Subbaram Naidu D, Urfer A, Chiu S. Hybrid fusion of linear, non-linear and spectral models for the dynamic modeling of

sEMG and skeletal muscle force: an application to upper extremity amputation. Comput Biol Med. 2013 Nov;43(11):1815-26.

[51] J. Rafiee, M.A. Rafiee, N. Prause, Schoen M.P. Wavelet basis functions in biomedical signal processing, Expert Systems with App. 2010; 38: 6190-6201.

[52] Englehart K, Hudgins B, Parker PA. A wavelet-based continuous classification scheme for multifunction myoelectric control. IEEE Trans Biomed Eng. 2001 Mar;48(3):302-11.

[53] T. David Mewette, N. Homer, J. R. Karen, ―Removing Power Line Noise from Recorded EMG‖, Proceedings of the 23rd annual international conference, pp 2190- 2193, Oct 25-28, Istanbul, Turkey.

[54] Wachowiak MP, Rash GS, Quesada PM, Desoky AH. Wavelet-based noise removal for biomechanical signals: a comparative study. IEEE Trans Biomed Eng. 2000 Mar;47(3):360-8.

[55] N.M. Sobahi. Denoising of EMG signals based on Wavelet Transform. Asian Trans on Eng. 2011 Nov; 01: 2221-4267.

[56] LIPPOLD OC. The relation between integrated action potentials in a human muscle and its isometric tension. J Physiol. 1952 Aug;117(4):492-9.

[57] Moritani T, deVries HA. Reexamination of the relationship between the surface integrated electromyogram (IEMG) and force of isometric contraction. Am J Phys Med. 1978 Dec;57(6):263-77.

[58] Milner-Brown HS, and R B. Stein .The relation between the surface electromyogram and muscular force. J. Physiol. London. 1975 ; 246 (3): 549-569.

[59] Bouisset,S. EMG and muscular force in normal motor activities. In: New developments In EMG and Clinical Neurophysiology, edited by J. E. Desmedt. Basel, Switzerland: Karger, 1973; 1: 547-583.

[60] Komi PV, Buskirk ER. Reproducibility of electromyographic measurements with inserted wire electrodes and surface electrodes. Electromyography. 1970 Nov-Dec;10(4):357-67.

[61] Vredenbreg, J., and G. Rau. Surface electromyography in re-lation to force, muscle length and endurance. In: New Developments in EMG and Clinical Neurophysiology, edited by J. E. Desmedt. Basel, Switzerland: Karger, 1973; I: 607-622.

[62] Perry J, Bekey GA. EMG-force relationships in skeletal muscle. Crit Rev Biomed Eng. 1981;7(1):1-22.

[63] Lawrence JH, De Luca CJ. Myoelectric signal versus force relationship in different human muscles. J Appl Physiol Respir Environ Exerc Physiol. 1983 Jun;54(6):1653-9.

[64] Hashemi J, Hashtrudi-Zaad K, Morin E, Mousavi P. Dynamic modeling of EMG-force relationship using parallel cascade identification. Conf Proc IEEE Eng Med Biol Soc. 2010;2010:1328-31.

[65] R. Istenic, A. Holobar, R. Merletti, and D. Zazula, EMG based muscle force estimation using motor unit twitch model and convolution kernel compensation, 11th Mediterranean Conference on Medical and Biomedical Engineering and Computers, IFMBE Proceedings, vol.16, pp. 114-117, 2007.

[66] F. Mobasser and K. Hashtrudi-Zaad, Rowing stroke force estimation with EMG signal using artificial neural networks, IEEE conference on Control Applications, pp.825-830, 2005.

[67] E.A. Clancy, N. Hogan, Relating Agonist-Antagonist Elentromyograms to joint torque during Isometric, Quasi-Isotonic, non-fatiguing contractions, IEEE Transactions on biomedical engineering, vol.44, no.10, pp.1024-1028, 1997

[68] P.J. Lago and N.B. Jones, Parameter estimation of system dynamics with modulation-type nosie- application to the modeling of the dynamic relationship between the EMG and force transients in muscle, IEEE Proceedings on Control theory and Applications, vol. 131, no.6, pp. 221-228, 1984.

[69] http://wikis.controltheorypro.com/index.php?title=Introduction_to_System_Identification

[70] J.T. Bingham and M.P. Schoen, Characterization of Myoelectric signals using System Identification Techniques, Proceedings of IMECE, Anaheim, California, Nov 13-19, 2004.

[71] Deluca, C. J. 1997, The use of surface electromyography in biomechanics. Journal of Applied Biomechanics, 13(3), 135-163

[72] Zipp P, 1982 Recoomendations for the standardization of lead postions in surface electromyography. Eur J. applPhysiol, 50: 41-54.

[73] HenrykKrol, grzerozSobata, AntoniNawarat, Effect of Electrode position on EMG recording in pectorials major, Journal of Human Kinetics vol 17, 2007 , pp: 105-112.

[74] http://fitelson.org/topics/shafer.pdf

[75] http://citeseerx.ist.psu.edu/viewdoc/download?rep=rep1&type=pdf&doi=10.1.1.98.6349

[76] Simon Parsons and E.H. Mandani, " Qualitative Dempster-Shafer Theory", Proceedings of the III Imacs International workshop on Qualitative Reasoning and Decision Technologies, Barcelona, June 1993.

[77] Rakowsky Uwe Kay, "Fundamentals of the Dempster-Shafer theory and its applications to system safety and reliability modeling", RTA#3-4,2007, December, special issue.

[78] Mansoor Raza, Iqbal Gondal, David Green and Ross L. Coppel, Fusion of FNA-cyology and Gene-expression Data Using Dempster- Shafer Theory of Evidence to predict Breast Cancer Tumors", Bioinformation by biomedical infrmatics publishing group.

[79] http://cse.uta.edu/research/publications/Downloads/CSE-2003-23.pdf

[80] IoanDumitrache, IoanaMihu, Monica C. Voinescu, " An advanced Decision Support System for Medical Diagnosis, Proceedings of the 17th World Congress, The international Federation of Automation Control , Seoul, Korea, July 6-11, 2008.

[81] http://arxiv.org/ftp/arxiv/papers/0803/0803.1568.pdf

[82] Chaabane S. Ben, Sayadi M, Fnaiech F., Brassart E., "Dempster-Shafer Evidence Theory for Image segmentation: Application in cell Images, International Journal of Signal Processing , 2009, vol .5 Issue 2., p 126.

[83] Same as ref 82

[84] M. Rombaut, Y Min Xhu, Study of Dempster-Shafer Theory for image segmentation applications, Elsevier 2002.

[85] F Rottensteiner, J Trinder, S clode, K Kubik, "Using the dempster-Shafer method for the fusion of LIDAR data and multi-spectral images for building detection. Elsevier 2005.

[86] S Foucher , M germain, JM Boucher, Multisource classification using ICM and Dempster Shafer theory, IEEE transactions

[87] TC Lin, Partition belief median filter based on Dempster-Shafer Theory for image processing, 2008 Elsevier

[88] Ali Naseri , Omid Azmoon, " evaluation of data fusion in radars network and determination of optimum algorithm, International journal of UbiComp (IJU) , Vol.2, No.4, Oct 2011

[89] Bouakache, A., Khedam R., Abbas. N, AitAbdesselam, " Multi-scale Satellite Images Fusion using Dempster Shafer Theory, 3rd IEEE international conference on Information and Communication Technologies, 7-11, Apr 2008.

[90] Sadanori Konishi, Genshiro Kitagawa, " Information criteria and Statistical Modeling, International statistical Review, vol.76, 2008

[91] Abd-Krim Seghouane, Maiza Bekara, Gilles Fleury, "A small Sample Model Selection Criterion Based on Kullback's symmetric Divergence," IEEE Transactions on Instrumentation and Measurement, vol. 52, no. 4, pp.1009-1020, 2003.

[92] http://www.doc.ic.ac.uk/~nd/surprise_96/journal/vol1/sbaa/article1.html

[93] D. Staudenmann, I. Kingma, A. Daffertshofer, D. F. Stegeman, J. H. Van Dieen, Improving EMG-Based Muscle Force Estimation by Using a High-Density EMG Grid and Principal Component Analysis, IEEE transactions on Biomedical Engineering, Vol. 53, No. 4, pp. 712-719, (2006).

[94] R. Merletti, L. Lo Conte, E. Avignone, and P. Guglielminotti, Modeling of surface myoelectric signals. I. Model implementation, IEEE transactions on Biomedical Engineering, vol. 46, No.7, pp. 810-820, (1999).

[95] " Information criteria and Statistical Modeling", Sadanori Konishi Genshiro Kitagawa

[96] Sebastian Bitzer, Patrick van der Smagt , 2006 IEEE International conference on Robotics and Automation page 2820-2825

[97] Carlo J. De Luca, Alexander Adam, Robert Wotiz, L. Donald Gilmore and S. 96:1646-1657, 2006. doi:10.1152/jn.00009.2006

[98] Articles in press. J Appl physiology (September 12, 2003). 10.1152/japplphysiol.00521.2003 "A thin, flexible multi-electrode grid for high-density surface EMG" , Lapatki B.G. , Van Dijk J.P., jonas I.E., Zwarts M.J. , Stegeman, D.F.

[99] Med Bio Eng Comput(2007) ' Electro-Mechanical stability of surface EMg sensors'. S.H.Roy, G.De Luca, M.S.Cheng, A.Johansson, L.D.gilmore, C.J. De Luca.

[100] David Macii,Andre Boni ,Mariolino De Cecco, and Dario Petri, IEEE Instrumentation and Measurement Magazine ,vol II, no.3 June 2008, Tutorial 14:Multisensor Data Fusion,

[101] Carlo J. De Luca, Alexander Adam, Robert Wotiz, L. Donald Gilmore and S. Hamid Nawab, "Decomposition of Surface EMG signals". J Neurophysiol 96: 1646-1657, 2006;

[102] Madhavi Anugolu, Anish Sebastian, Parmod Kumar, Marco P. Schoen, Alex Urfer, and D. Subbaram Naidu, "*Surface EMG Array Sensor Based Model Fusion*

Using Bayesian Approaches For Prosthetic Hands," 2009 ASME Dynamic Systems and Control Conference, Hollywood, California, USA, Oct. 12-14, 2009.

[103] Madhavi Anugolu, Time Domain Surface EMG Sensor Fusion for Estimating Finger Force, Thesis Submitted in Fall 2010 at Idaho State University

[104] J. Rissanen (1978) Modeling by the shortest data description. Automatica 14, 465-471

[105] http://www.scholarpedia.org/article/Minimum_description_length

[106] Estimating the Prevalence of Limb Loss in the United States- 2005 to 2050 Kathryn Ziegler-Graham, PhD, et al, Archives of Physical Medicine and Rehabilitation 89(3):422-429, 2008.

[107] Horch, K. W., & Dhillon, G. (2006). Towards a neuroprosthetic arm. Proceedings of the First IEEE/RAS-EMBS International Conference on Biomedical Robotics and Biomechatronics, 1639243, 1125-8.

[108] J. N. Billock, "Prosthetic management of complete hand and arm deficiencies," in:J.M. Hunter, E.J. MacKin and A.D. Callahan(Eds.),Rehabilitation of the Hand: Surgery and Therapy, St. Louis: Mosby-Year Book,1189-1201, 1995.

[109] S. Hubbard, "Myoprosthetic management of the upper limb amputee," in:J.M. Hunter, E.J. MacKinandA.D. Callahan(Eds.),Rehabilitation of the Hand: Surgery and Therapy, St. Louis: Mosby-Year Book,1241-1252, 1995.

[110] G. Lundborg, B. Rosen, K. Lindstrom and S. Lindberg, "Artificial sensibility based on the use of piezo resistive sensors:preliminary observations," J.Hand Surg.Br., 23:620-626, 1998.

[111] P. Herberts, L. Korner, “Ideas on Sensory feedback in hand prostheses”, ProsthetOrthotInt, December 1979, vol 3. No. 3 157-162.

[112] http://www.research.gov/researchportal/appmanager/base/desktop;jsessionid=5JSnNMdMdnn5n4vhVrCp32VWlvjJnLsmfdc19DcYbkJd5jrwSQMt!1821093771!1028386895?_nfpb=true&_windowLabel=awardSummary_1&_urlType=action&awardSummary_1_action=selectAwardDetail&awardSummary_1_id=%2FresearchGov%2FAwardHighlight%2FPublicAffairs%2F16782_SensoryFeedbackfromaProstheticHand.html

[113] Christian Antfolk, Christian Balkenius, et al., “A tactile Display system for Hand prostheses to discriminate pressure and individual finger localization”

[114] Dhillon, G. S., and Horch K. W., IEEE Trans. Neural Systems and Rehabilitation Engineering, “Direct neural sensory feedback and control of a prosthetic arm,” 13(4), pp. 468-472, 2005.

[115] Szeto, A. Y. J., Riso, R., 1990, “Sensory Feedback using Electrical Stimulation of the Tactile Sense”, in R.V. Smith and J.H. Leslie, Jr. (Eds.), Rehabilitation Engineering, Boca Raton, CRC Press, pp. 29-78.

[116] Cipriani, C. Zaccone, F., Micera. S., Carrozza, M. C., 2008, “On the Shared Control of an EMG Controlled Prosthetic Hand: Analysis of User-Prosthetics Interaction,” IEEE Trans. Robotics, 24(1), pp. 170-184.

[117] http://www.sensorprod.com/news/whitepapers/2006_tsa/index.php

[118] Darian-Smith, Ian; Johnson KO, LaMotte C, Shigenaga Y, Kenins P, Champness P (1979). "Warm fibers innervating palmar and digital skin of the

monkey: responses to thermal stimuli.".Journal of Neurophysiology42 (5): 1297–1315.

[119] Holmes, N. P., Spence, C., Cogn. Process,“The body schema and multisensory representation(s) of peripersonal space,” 5, 94-105, 2004.

[120] Pylatiuk, C., Kargov, A., Schulz, S., Journal of Prosthetics and Orthotics, “Design and Evaluation of a Low-Cost Force Feedback System for Myoelectric Prosthetic Hands,”, 18(2), pp. 57-61. 2006a.

[121] G.F. Shannon, “A comparison of alternative means of providing sensory feedback on upper limbProstheses”, Med Biol Eng. 1976 May; 14(3), 289-294.

[122] Geldard, F.A. (1957) Adventures in tactile literacy. Am psycho 115-24.

[123] Kaczmarek, K. A., Webster, J. G., Bach-y-Rita, P., Tompkins, W. J., IEEE Trans. Biomedical Engineering,“Electro-tictile and vibrotactile display for sensory substitution systems,” 38, pp. 1-15, 1991.

[124] M. Akamatsu, I.S. MacKenzie, and T. Hasbrouc, “A Comparison of Tactile, Auditory, and Visual Feedback in a Pointing Task Using a Mouse-Type Device,” Ergonomics 38, pp. 816-827, 1995.

[125] S. Brewster and L.M. Brown, “Tactons: Structured Tactile Messages for Non-Visual Information Display,” Proc. 5th Australasian User Interface Conference (AUIC2004), Dunedin, pp. 15-23, 2004.

[126] J.C. Bliss, M.H. Katcher, C.H. Rogers, R.P. Sheppard, “Optical-to-tactile image conversion for the blind,” IEEE Trans. Man-Machine Systems, MMS-11(1), pp. 58-65, 1970.

[127] M. Schrope, “Simply Sensational,” New Scientist, pp. 30-33, June 2, 2001.

[128] M. Enriquez, O. Afonin, B. Yager, and K. Maclean, “A Pneumatic Tactile Alerting System for the Driving Environment,” PUI 2001, Workshop on Perceptual/Perceptive User Interfaces, Orlando, FL, November 15-16, 2001.

[129] Lilly Spirkovska, “Summary on Tactile Interfaces techniques and Systems, NASA Ames Research Center, September 22, 2004.

[130] Pylatiuk, C., Doederlein, L, Orthopade, “Bionic Arm prostheses. State of the art in research and development,”, 35(11), pp. 1169-1170, 2006b.

[131] Schulz, A. E., Marasco, P. D., Kuiken, T. A., Brain Research, “Vibrotactile detection thresholds for chest skin of amputees following targeted reinnervation surgery,“, 1251, pp. 121-129, 2008.

[132] P. Hunter pecham, Jayme S. Knutson, “Functional electrical simulation for neuromuscular applications”, Annu. Rev. Biomed.Eng, March 23, 2005.

[133] Kajimoto, H., Kawakami, N., Maeda, T., Inami, M., IEEE Computer Graphics and Applications,” Emerging Technologies, “SmartTouch: Electric Skin to Touch the Untouchable”, 24(1), pp. 36-43, 2004.

[134] Kaczmarek, K. A., Webster, J. G., Bach-y-Rita, P., Tompkins, W. J., IEEE Trans. Biomedical Engineering,“Electro-tictile and vibrotactile display for sensory substitution systems,” 38, pp. 1-15, 1991.

[135] Kajimoto, H., Kawakami, N., Maeda, T., Tachi, S., Electronics and Communications in Japan, “Electrocutaneous Display with Receptor Selective Stimulations”, Part 2, 85(6), pp. 40-49, 2002.

[136] Kajimoto, H., Kawakami, N., Inami, M., Tachi, S., Proceedings of the Annual Conference on Artificial Reality and Tele existence ICAT 99, Virtual Reality Soc.

of Japan, “Tactile feeling Display using Functional Electrical Stimulation” pp. 107-114, 1999.

[137] Szeto, A. Y. J., Riso, R., in R.V. Smith and J.H. Leslie, Jr. (Eds.), Rehabilitation Engineering, Boca Raton, CRC Press, “Sensory Feedback using Electrical Stimulation of the Tactile Sense”, pp. 29-78, 1990.

[138] Asamura, N., Yokoyama, N., Shinoda, H., Proceedings IEEE Virtual Reality Conference, “A Method of Selective Stimulation to Epidermal Skin Receptrots for Realistic Touch Feedback”, pp. 274-281, 1999.

[139] Navarro, X., Krueger, T., Lago, N., Micera, S., Stieglitz, T., Dario, P., Journal of the Peripheral Nervous System, “A critical review of interfaces with the peripheral nervous system for the control of neuroprostheses and hybrid bionic systems”, 10(3), pp. 229-258. 2005.

[140] Hernandez, A., Yokoi, H., Ohnishi, T., a Arai, T., Proceedings of the 9th Int. Conf. On Intelligent Autonomous Systems, IOS Press, Tokyo, Japan, “An f-MRI study of an EMG prosthetic hand biofeedback system”, pp. 921-929, 2006.

[141] Chandrasekhar Potluri, Parmod Kumar, Madhavi Anugolu, Alex Urfer, Steve Chiu, D. Subbaram Naidu, and Marco P. Schoen, “Frequency Domain Surface EMG Sensor Fusion for Estimating Finger Forces,” 32nd Annual International Conference of the IEEE Engineering in Medicine and Biology Society, Buenos Aires, Argentina, Aug. 31 – Sept. 4, 2010.

[142] Madhavi Anugolu, Anish Sebastian, Parmod Kumar, Marco P. Schoen, Alex Urfer, and D. Subbaram Naidu, “Surface EMG Array Sensor Based Model Fusion using Bayesian Approaches for Prosthetic Hands,” Proceedings of the

Dynamic Systems and Control Conference (DSCC), Hollywood, CA, October 2009.

[143] Paul Bach-y-Rita, Stephen W. Kercel, Sensort substitution and the human-machine interface, Trends in Cognitive Sciences, Volume 7, Issue 12, December 2003, Pages 541-546.

[144] Chandrasekhar Potluri, Parmod Kumar, Madhavi Anugolu, Steve Chiu, Alex Urfer, Marco P. Schoen, and D. Subbaram Naidu, "sEMG Based Fuzzy Control Strategy with ANFIS Path Planning For Prosthetic Hand," 3rd IEEE RAS &EMBS International Conference on Biomedical Robotics and Biomechatronics, Tokyo, Sept 26-30, 2010

[145] Potluri C, Yimesker Y, P Kumar, J Molitor, Steve C. Chiu, D. Subbaram Naidu, Fellow, IEEE, S.H. Mousavinezhad, "sEMG Based Real-Time Embedded Force Control Strategy for a Prosthetic Hand Prototype" IEEE International Conference on Electro/Information Technology, Mankato, Minnesota, USA, May 15-17, 2011

LIST OF PUBLICATIONS

JOURNALS

1. Chandrasekhar Potluri, Madhavi Anugolu, Marco P. Schoen, D. Subbaram Naidu, Alex Urfer and Steve Chiu, "*Hybrid Fusion of Linear, Non-linear and Spectral Models for the Dynamic Modeling of sEMG and Skeletal Muscle Force: An application to Upper Extremity Amputation*", Elsevier Computers in Biology and Medicine, Vol. 43(11), November 2013,pp1815-1826.

REFERRED CONFERENCES PUBLICATIONS

1. Madhavi Anugolu, Anish Sebastian, Parmod Kumar, Marco P. Schoen, Alex Urfer, and D. Subbaram Naidu, "*Surface EMG Array Sensor Based Model Fusion Using Bayesian Approaches For Prosthetic Hands*," 2009 ASME Dynamic Systems and Control Conference, Hollywood, California, USA, Oct. 12-14, 2009.
2. Madhavi Anugolu, Chandrasekhar Potluri, AdananIlyas, Parmod Kumar, Steve Chiu, Nancy Devine, Alex Urfer, and Marco Schoen, "*A Review on Sensory Feedback For sEMG Based Prosthetic Hands,"* ICAI'11 - The 2011 International Conference on Artificial Intelligence, Las Vegas, Nevada, USA, July 18-21, 2011.

3. Madhavi Anugolu, Chandrasekhar Potluri, Steve Chiu, Alex Urfer, Jim Creelman and Marco Schoen, "*A sEMG- Skeletal Musclen Based on Minimum Description Length Criterion,"* ICAI'11 - The 2012 International Conference on Artificial Intelligence, Las Vegas, Nevada, USA, July 16-19, 2012.

4. Madhavi Anugolu, Chandrasekhar Potluri,Parmod Kumar, Alex Urfer, Jim Creelman, Marco P. Schoen, "*Genetic Algorithm Based Optimization of Kullback Information Criterion: Improved System Identification of Skeletal Muscle Force and sEMG Signals"* , 2012 IEEE International Instrumentation and Measurement Technology Conference, May 13-16 2012, Graz, Austria.

5. Chandrasekhar Potluri, Madhavi Anugolu, YimeskerYihun, Parmod Kumar, Steve Chiu, *Member, IEEE*, Marco P. Schoen, *Senior Member, IEEE*, D. Subbaram Naidu, *Fellow, IEEE "Implementation of sEMG-Based Real-Time Embedded Adaptive Finger Force Control for a Prosthetic Hand",* IEEE Conference on Decision and Control and European Control Conference (IEEE CDC-ECC), Orlando, Florida, USA, December 12-15, 2011.

6. Chandrasekhar Potluri, Parmod Kumar, Madhavi Anugolu, Alex Urfer, Steve Chiu, D. Subbaram Naidu, and Marco P. Schoen, *"Frequency Domain Surface EMG Sensor Fusion for Estimating Finger Forces,"* 32nd Annual International Conference of the IEEE Engineering in Medicine and Biology Society, Buenos Aires, Argentina, Aug. 31 – Sept. 4, 2010.

7. Chandrasekhar Potluri, Parmod Kumar, Jeff Moliter, Madhavi Anugolu, Jensen Alex, Kenyon Hart, and Steve Chiu, *"Multi-Level Embedded Motor Control for Prosthesis," International Conference on Embedded Systems and Applications*, ESA'2010, Las Vegas, Nevada, USA, July 12-15, 2010.

8. Chandrasekhar Potluri, Parmod Kumar, Madhavi Anugolu, Steve Chiu, Alex Urfer, Marco P. Schoen, and D. Subbaram Naidu, "*sEMG Based Fuzzy Control*

Strategy with ANFIS Path Planning For Prosthetic Hand," 3rd IEEE RAS &EMBS International Conference on Biomedical Robotics and Biomechatronics, Tokyo, Sept 26-30, 2010.

9. Chandrasekhar Potluri, MadhaviAnugolu,YimeskerYihun,Alex Jensen, Steve Chiu *Member, IEEE*, Marco P. Schoen, *Senior Member, IEEE*, and D. Subbaram Naidu, *Fellow, IEEE*. *"Optimal Tracking of a sEMG based Force Model for a Prosthetic Hand"*, 33rd Annual International Conference of the IEEE Engineering in Medicine and Biology Society, Boston, MA, USA, Aug 31- Sep 3, 2011

10. Chandrasekhar Potluri, Madhavi Anugolu, Parmod Kumar, Amir Fassih, YimeskerYihun, Steve Chiu, and Subbaram Naidu, "*Real-Time sEMG Acquisition and Processing Using a PIC 32 Microcontroller,"* ESA'11 - 9th Int'l Conference on Embedded Systems and Applications, Las Vegas, Nevada, USA, July 18-21, 2011.

11. Chandrasekhar Potluri, Madhavi Anugolu, Alex Jensen, Girish Sriram, Shiwei Liu, Steve Chiu, "*PIC 32 Microcontroller Based sEMG Acquisition System and Processing Using Wavelet Transforms,"* ESA'12 - 9th Int'l Conference on Embedded Systems and Applications, Las Vegas, Nevada, USA, July 16-19, 2012.

12. Chandrasekhar Potluri, Madhavi Anugolu, Steve Chiu, Alex Urfer, Alba Perez, Marco P. Schoen, D. Subbaram Naidu "Fusion of Spectral Models for Dynamic Modeling of sEMG and Skeletal Muscle Force" submitted to 34th Annual

International Conference of the IEEE Engineering in Medicine and Biology Society, San Diego, CA, USA, Aug 28-Sep 1, 2012.

13. Parmod Kumar, Chandrasekhar Potluri, Madhavi Anugolu, Anish Sebastian, Jim Creelman, Alex Urfer, Steve Chiu, D. Subbaram Naidu, and Marco P. Schoen, *"*A Hybrid Adaptive Data Fusion with Linear and Nonlinear Models for Skeletal Muscle Force Estimation*,"* 5th Cairo International Conference on Biomedical Engineering, Cairo, Egypt, Dec. 16-18, 2010.

14. Parmod Kumar, Chandrasekhar Potluri, Anish Sebastian, Steve Chiu, Alex Urfer, D. Subbaram Naidu, and Marco P. Schoen, *"An Adaptive Multi Sensor Data Fusion with Hybrid Nonlinear ARX and Wiener-Hammerstein Models for Skeletal Muscle Force Estimation,"* The 14th World Scientific and Engineering Academy and Society (WSEAS) International Conference on Systems, Corfu Island, Greece, July 22-24, 2010.

15. Parmod Kumar, Chandrasekhar Potluri, Anish Sebastian, YimeskerYihun, Adnan Ilyas, MadhaviAnugolu, Rohit Sharma, Steve Chiu, Jim Creelman, Alex Urfer, D. Subbaram Naidu, *Fellow IEEE,* and Marco P. Schoen, *Senior Member IEEE, "A Hybrid Adaptive Multi Sensor Data Fusion for Estimation of Skeletal Muscle Force for Prosthetic Hand Control" ICAI'11, Worldcomp 2011, LasVegas, USA, July 18-21, 2011.*

16. Parmod Kumar, Anish Sebastian, MadhaviAnugolu, Chandrasekhar Potluri, Amir Fassih, YimeskerYihun, Alex Jensen, Yi Tang, C. H. Chen, Steve Chiu, Ken Bosworth, Jim Creelman, Alex Urfer, D. S. Naidu and Marco P. Schoen. "*An*

Adaptive Hybrid Data Fusion Based Identification of Skeletal Muscle Force with ANFIS and Smoothing Spline Curve Fitting”, IEEE International Conference on Fuzzy Systems (FUZZ-IEEE), Taipai, Taiwan, June 27- 30, 2011.

17. Parmod Kumar, Anish Sebastian, Chandrasekhar Potluri, YimeskerYihun, Adnan Ilyas, Madhavi Anugolu, Rohit Sharma, Jim Creelman, Alex Urfer, D. Subbaram Naidu, *Fellow, IEEE*, and Marco P. Schoen, *Senior Member, IEEE “Spectral Analysis of sEMG Signals to Investigate Skeletal Muscle Fatigue”* IEEEConference on Decision and Control and European Control Conference (IEEE CDC-ECC), Orlando, Florida, USA, December 12-15, 2011.

18. Parmod Kumar, Anish Sebastian, Chandrasekhar Potluri, Adnan Ilyas, Madhavi Anugolu, Alex Urfer, and Marco Schoen, *“Adaptive Finger Angle Estimation from sEMG Data with Multiple Linear and Nonlinear Model Data Fusion,”* The 10th World Scientific and Engineering Academy and Society (WSEAS) International Conference on Dynamical Systems and Control, Iasi, Romania, July 1-3, 2011.

19. Chandrasekhar Potluri, Madhavi Anugolu, Steve chiu, D.Subbaram Naidu, Marco P. Schoen, “ *A sEMG-based Real-time Adaptive Joint angle Estimation and Control for a Prosthetic Hand Prototype*”, 12th WSEAS International Conference on Systems theory and Scientific computation , Istanbul, Turkey, August 21-23, 2012